UTILISATION DE LA SPECTROSCOPIE D'IMPÉDANCE ÉLECTROCHIMIQUE POUR ÉTUDIER LES BIOCAPTEURS ÉLECTROCHIMIQUES À BASE D'APTAMÈRE

USING ELECTROCHEMICAL IMPEDANCE SPECTROSCOPY TO STUDY ELECTROCHEMICAL APTAMER-BASED BIOSENSORS

par

Erfan Rahbarimehr

Mémoire présenté au Département de chimie en vue
de l'obtention du grade de maître ès sciences (M.Sc.)

FACULTÉ DES SCIENCES
UNIVERSITÉ DE SHERBROOKE

Sherbrooke, Québec, Canada, Juillet 2023

Le 5 Juillet 2023

le jury a accepté le mémoire de Monsieur Erfan Rahbarimehr dans sa version finale.

Membres du jury

Professeur Philippe Dauphin Ducharme
Directeur de recherche
Département de chimie

Professeur Pedro Alejandro Segura
Évaluateur interne
Département de chimie

Professeur Yves Dory
Président
Département de chimie

RÉSUMÉ

L’occurrence d'erreurs médicamenteuses pouvant entraîner des conséquences graves pour les patients (réactions indésirables aux médicaments, décès, etc.) demeure un enjeu de taille pour les soins de santé. Récemment, pour faire face à ce problème, la médecine personnalisée a émergé comme une alternative efficace afin d’améliorer l'efficacité des prescriptions de médicaments. Cette approche consiste à adapter les traitements aux besoins spécifiques d'un patient en fonction de sa génétique, de son environnement et de son mode de vie.

Toutefois, pour parvenir à une véritable médecine personnalisée, il est nécessaire de développer des méthodes analytiques capables de fournir un suivi en temps réel des molécules. À ce jour, les approches analytiques actuelles ne permettent au mieux qu'une seule mesure instantanée de l'état de santé et nécessitent des prélèvements veineux envoyés à des laboratoires externes où des professionnels qualifiés effectuent des analyses à l'aide d'instruments encombrants. En revanche, les biocapteurs peuvent fournir des mesures continues et précises de divers biomarqueurs et fournir des informations pour une intervention précoce. De plus, les biocapteurs peuvent être utilisés pour surveiller l'efficacité des traitements et ajuster les doses de médicaments en temps réel, ce qui peut conduire à de meilleurs résultats thérapeutiques. Le développement de la médecine personnalisée et de plateformes de surveillance en temps réel a le potentiel de révolutionner les soins de santé en améliorant la qualité et la qualité de résultats pour les patients.

Les biocapteurs électrochimiques à base d'aptamères (E-AB) ont émergé comme des candidats pour le développement d'outils de médecine personnalisée. Composés d'une courte séquence d'acide nucléique spécifique à une cible moléculaire (un aptamère) modifiée par un rapporteur rédox immobilisé sur une surface d'électrode, ces capteurs permettent des mesures en temps réel et continues de diverses espèces moléculaires telles que des protéines, des acides nucléiques et des petites molécules directement dans des matrices complexes non diluées. La flexibilité avec laquelle les aptamères peuvent être échangés dans cette plateforme de détection en fait une plateforme optimale pour la conception d'outils de médecine personnalisée pour diverses applications cliniques. Toutefois, la mise en œuvre des capteurs E-AB dans diverses applications a été entravée par la faible affinité des aptamères (dans la plage μM−mM), qui ne couvre pas l'ensemble de la plage de concentrations cliniquement pertinente sur laquelle les molécules doivent être quantifiées.

Dans la première partie de cette étude, nous avons examiné deux techniques d'interrogation électrochimiques, à savoir la voltampérométrie à onde carrée et la spectroscopie d'impédance électrochimique, pour mesurer les constantes de dissociation des capteurs E-AB. Les résultats ont révélé que, bien que la voltampérométrie à onde carrée soit la technique d'interrogation la plus couramment utilisée, elle produit des constantes de dissociation des aptamères plus élevées que celles mesurées pour le même aptamère avec d'autres techniques, ce qui, dans certains cas, empêche les capteurs E-AB de mesurer la concentration des molécules dans la plage clinique cible. Nous avons constaté que la spectroscopie d'impédance électrochimique, en revanche, s'est révélée être une technique supérieure en raison de sa capacité à déconvoluer les contributions résistives et capacitives interfaciales au courant mesuré et à quantifier les processus électrochimiques se produisant à différentes échelles de temps avec une résolution plus élevée. Lors de la comparaison des constantes de dissociation mesurées par spectroscopie d'impédance électrochimique avec la méthode de référence en caractérisation d'aptamères, le titrage calorimétrique isotherme, nous avons constaté que ces constantes étaient soit dans les limites des erreurs expérimentales, ou différenciées par un facteur de 2 à 3. Par conséquent, notre étude propose que la spectroscopie d'impédance électrochimique soit une technique électrochimique plus fiable et précise par rapport à la voltampérométrie à onde carrée pour l'interrogation des capteurs E-AB.

Dans la deuxième partie de cette étude, nous avons découvert un nouveau mécanisme de traduction du signal pour les capteurs E-AB, impliquant le rapporteur rédox largement utilisé, le bleu de méthylène, qui entre en compétition avec la liaison du ligand. Les résultats ont démontré que le bleu de méthylène replie l'aptamère que nous avons testé et déloge les ligands de sa poche de liaison. Par conséquent, les propriétés électrochimiques du bleu de méthylène changent, ce qui entraîne un signal mesurable. Étant donné la prévalence du bleu de méthylène dans les capteurs E-AB, cette découverte remet en question le mécanisme conventionnel largement accepté du "changement conformationnel" des capteurs E-AB et suggère un schéma alternatif de traduction du signal. Notre étude apporte des éclaircissements importants sur les propriétés physico-chimiques sous-jacentes à la surface des capteurs E-AB et leurs fondements.

SUMMARY

One of the significant challenges in the healthcare industry is medication errors, which can lead to severe consequences for patients, including adverse drug reactions and even death. Recently, to tackle this issue, personalized medicine solutions are emerging as potential alternatives to improve the efficiency with which drug dosing is achieved. Specifically, these approaches involve tailoring medical treatment to the specific needs of a patient based on their genetics, environments and lifestyles.

To achieve true personalized medicine requires the development of analytical methods capable of providing real-time monitoring of molecules. To date, however, current analytical approaches, at best, only provide a single snapshot of one's health and require venous draws that are sent to external laboratories where trained personnel perform analyses on cumbersome instrumentation. Biosensors, in contrast, can provide continuous and accurate measurements of various biomarkers and can allow for early detections providing information for early intervention. Additionally, biosensors can be used to monitor the efficacy of treatments and adjust medication dosages in real time, which can lead to better therapeutic outcomes. The development of personalized medicine and real-time monitoring sensing platforms has the potential to revolutionize the healthcare industry, providing better patient outcomes and improving the overall efficiency and quality of the healthcare system.

Electrochemical aptamer-based (E-AB) sensors have emerged as candidates to develop personalized medicine tools. Being comprised of a redox-reporter-modified short nucleic acid sequence (i.e., aptamer) immobilized on an electrode surface affords real-time and continuous measurements of diverse molecular species, such as proteins, nucleic acids, and small molecules directly in undiluted complex matrices. The flexibility with which aptamers can be swapped in this sensing platform makes them an optimal platform for designing personalized medicine tools for diverse clinical applications. The widespread implementation of E-AB sensors has been hampered by their restricted aptamer affinity (μM−mM range), which falls short of covering the entire range of clinically relevant concentrations at which molecules need to be assessed.

In the first part of this memoir, we investigated two electrochemical interrogation techniques, namely, square-wave voltammetry and electrochemical impedance spectroscopy, in measuring the dissociation constants of E-AB sensors. The results revealed that although square-wave voltammetry has been the most used interrogation technique, it systematically yields aptamers' dissociation constants higher than ones measured for the same aptamer with other techniques and thus in certain cases leaves E-AB sensors unable to measure the concentration of molecules in the target clinical range. We found that

electrochemical impedance spectroscopy, in contrast, proved to be a superior technique due to its ability to deconvolute interfacial resistive and capacitive contributions to the measured current and quantify electrochemical processes occurring on several time scales with higher resolution. When comparing dissociation constants measured via electrochemical impedance spectroscopy with the gold standard method in aptamer characterization isothermal titration calorimetry we found that these were either within experimental errors or only 2−3-fold apart. Therefore, our study proposes that electrochemical impedance spectroscopy is a more reliable and accurate electrochemical technique compared to square-wave voltammetry for interrogating E-AB sensors.

In the second part of this memoir, we discovered a new signal transduction mechanism for E-AB sensors which involves the widely used redox reporter methylene blue, which competes with ligand binding. The results demonstrated that methylene blue folds the aptamer we tested and dislodges ligands from its binding pocket. Consequently, the electrochemical properties of methylene blue change, leading to a measurable signal. Given the prevalence of methylene blue in E-AB sensors, this finding challenges the widely accepted conventional "conformational change" mechanism of E-AB sensors and suggests an alternative signal transduction scheme. Our study provides important insights into the underlying physicochemical properties at E-AB sensors' surface and their fundamentals.

ACKNOWLEDGEMENTS

I would like to express my sincere gratitude to those who have supported and encouraged me throughout my research journey. First and foremost, I am deeply grateful to my supervisor, Prof. Philippe Dauphin Ducharme, for his unwavering support, guidance, and mentorship. His expertise, enthusiasm, and dedication have been instrumental in shaping my research ideas and providing me with the necessary direction to achieve my research goals. I am also grateful for the invaluable contributions of my colleagues at the PDD lab for their insights, and ideas that enriched my research experience. Additionally, I would like to extend my sincere appreciation to Prof. Pedro A. Segura for his critical evaluation and insightful feedback on my work. Furthermore, I would like to acknowledge the financial support of the Natural Sciences and Engineering Research Council of Canada (NSERC), which has enabled me to pursue my research goals and provided me with the necessary resources to carry out my experiments.

I am also grateful to my dear friends Elahe Tavassoli and Kiarash Farahmandrad, who always helped me with their expertise in graphical designs and have been my constant company and pillars of support throughout my studies. Elahe has always been there to listen to my endless rants and complaints about the challenges of research. She never hesitated to give me a hard time when I needed it most, but her tough love and big smile were the constant source of encouragement that always pushed me to work harder and smarter. As for Kiarash, his talent for making me laugh with his razor-sharp wit and sarcastic quips was a lifesaver. Whenever I was feeling down in the dumps, he had a knack for lifting my spirits and helping me bounce back from even the darkest depths of despair and start anew. I am lucky to have such wonderful friends who never give up on me.

I would like to express my heartfelt appreciation to my family, whose love and support have been an unfaltering source of strength throughout my life. Their constant encouragement and sacrifices have helped me pursue my dreams with confidence. Without their support, I could not have achieved this milestone, and for that, I will always be grateful.

Finally, I humbly dedicate this work to the memory of those lost in the tragic Ukrainian PS752 flight, their families, and the valiant Iranian women who have fearlessly fought for their rights and the cause of women's liberation. To those who have given their lives in the name of the #woman_life_freedom revolution, your bravery and sacrifice will forever inspire me to use my voice for the greater good. May your legacies live on, and may we continue to strive toward a more just and equitable world in your honor.

TABLE OF CONTENT

LIST OF ABBREVIATIONS

AC	Alternating current
BSA	Bovine serum albumin
CPE	Constant phase element
DC	Direct current
EIS	Electrochemical impedance spectroscopy
E-AB	Electrochemical aptamer-based biosensor
E-DNA	Electrochemical DNA-based
GCE	Glassy-carbon electrode
GOx	Glucose oxidase
HAAA	Human anti-animal antibody
ITC	Isothermal titration calorimetry
LAR	Ligation amplification reaction
LOD	Limit of detection
NMR	Nuclear magnetic resonance
Ox	Oxidative species
PBS	Phosphate-buffered saline
PCR	Polymerase chain reaction
Red	Reductive species
SELEX	Systematic evolution of ligands by exponential enrichment
SWV	Square-wave voltammetry
TCEP	Tris(2-carboxyethyl)phosphine hydrochloride
TiP	Titanium Phosphate
TMA	Transcription-mediated amplification
uPA.	Urokinase plasminogen activator
WHO	World health organization

LIST OF TABLES

LIST OF FIGURES

LIST OF EQUATIONS

CHAPTER 1: INTRODUCTION

1.1. Problem

Medication errors are a common and serious problem in the healthcare industry.[1] These errors can occur at any stage, from medication prescription to its dispensing, administration and monitoring.[2,3] They can have serious consequences, including harm to patients, increased healthcare costs, and decreased trust in the healthcare system. Research has shown that yearly around 22000 people lose their lives in the U.S. because of medication errors and causes, according to the World Health Organization (WHO), an estimated 1,300,000 individual annual injuries.[4,5] A study in 2016 estimated that medication errors cost 21 billion USD to the U.S. economy in additional treatments yearly.[6]

Medication errors can occur due to various factors, including inadequate communication between healthcare providers, incomplete or inaccurate documentation of medication orders, failure to identify drug interactions, and inaccurate dosage administration.[7] In the latter case, for example, a healthcare provider may not be familiar with the correct dosage of a medication and may prescribe or administer the wrong dose. Providing the wrong dosage or miscalculating dosage can have serious consequences on a patient's health. If a patient receives too little medicine, it may not be effective in treating their condition, leading to ongoing or worsening symptoms. On the other hand, if a patient receives too much medicine, it can lead to harmful side effects or even an overdose, which can be potentially life-threatening. Miscalculating the dosage of a medicine can also interfere with the overall treatment plan and potentially cause additional health problems and a waste of both financial and clinical resources.

For instance, one of the highly prescribed medicines to treat severe or life-threatening infections caused by certain types of bacteria, particularly those that are resistant to other antibiotics, is vancomycin. It is often used to treat infections in the skin, bones, and urinary tract, as well as infections in the bloodstream. Vancomycin is generally considered to be a highly effective antibiotic, and it is often prescribed in cases where other antibiotics have not been effective or when a patient is allergic to other antibiotics. According to statistics, 1 out of 5 patients admitted to U.S. hospitals is dosed with vancomycin.[8,9] It is often given intravenously in a hospital setting, and it is usually prescribed for a specific length of time based on the severity of the infection and the patient's response to treatment. Like all medications, vancomycin can cause side effects, which may increase if a patient receives the wrong

dosage (i.e., nausea, diarrhea, low blood pressure, allergic reactions, hearing loss, kidney problems, and inflammation of the pancreas). Studies indicate that out of every 5 adults dosed with vancomycin in U.S. hospitals, 2 develop an acute kidney injury and some of those can eventually die.[10,11] Vancomycin is just one example out of thousands of medicines being prescribed during clinical procedures each of which having its own risk.[12–16]

1.2. Challenges

Personalized medicine approaches are emerging to solve challenges associated with medication errors. Those offer tailored medical treatments that meet an individual specific needs and characteristics. Personalized medicine approaches are based on the idea that each person is unique and that their medical treatment should be customized. Approaches can involve offering tailored treatment according to: 1) disease severity and prevention; 2) individual preferences; 3) metabolism differences influenced by individual lifestyle (e.g., physical activities, diet, etc.), body composition, age, gender, and genetics, which alter medication pharmacokinetics (i.e., the study of how a drug is absorbed, distributed, metabolized, and eliminated from the body).[17–19]

Understanding and monitoring the pharmacokinetics of a drug is essential for optimizing its therapeutic effects and minimizing the risk of adverse reactions. Currently, typical clinical diagnosis methods (above 70% of all clinical decisions are made using those), however, rely on laboratory-bound cumbersome and slow analytical methods ran by trained personnel (i.e., high-performance liquid chromatography coupled to mass spectrometry) that only provide a single snapshot of one's health.[20] As a result, clinicians do not own real-time and continuous data associated with the metabolization of the drug and its possible interactions with other medications the patient is taking. Being able to track the molecules in real-time directly in complex matrices would provide improved decision-making and transform medicine to help prevent medication errors.[21] Having access to such tools can also improve our understanding of drug action mechanisms and identify new potential therapeutics.[22] Overall, the ability to monitor molecules in real-time in complex matrices can provide important insights into a wide range of biological processes and can have many practical applications in areas such as medicine, drug development, and biotechnology.

1.3. Existing technologies

The integration of biosensors in analytical protocols facilitates the real-time and continuous monitoring of biomolecules in complex matrices, thereby providing a powerful tool for biomolecular analysis. Biosensors are comprised of three main components: a recognition element (also known as a bioreceptor), a transducer, and a signal processor. The recognition element is a specialized molecule that selectively binds to the target molecule or analyte to be detected. The transducer converts the biological response of the recognition element into a measurable physical signal while the signal processor converts the physical signal from the transducer into a usable output, such as a digital readout. These three components work together seamlessly to detect and quantify the presence and concentration of the target molecule or compound in the sample (Figure 1).

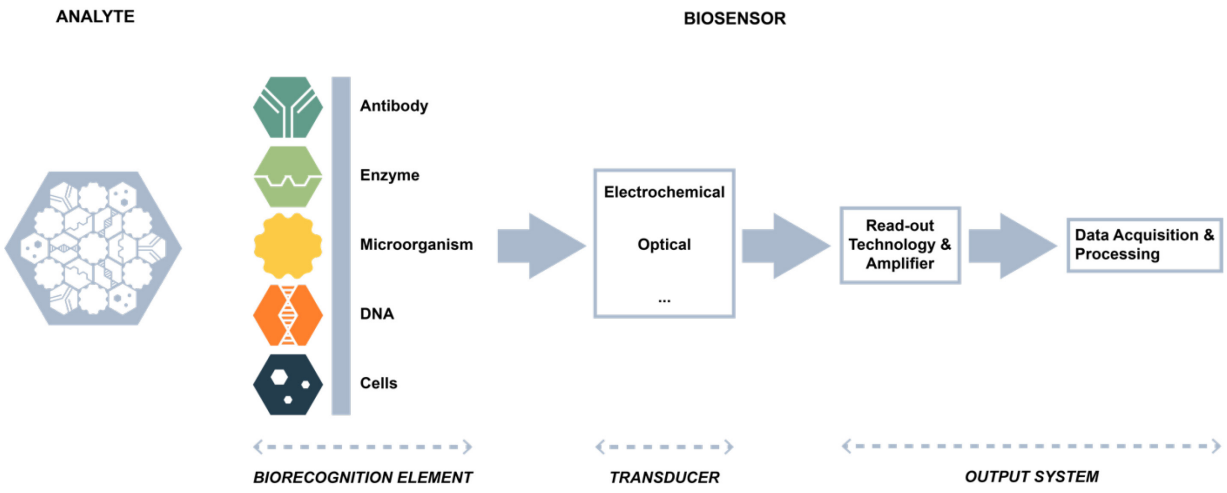

Figure 1. A biosensing procedure consists of three stages: detection of the analyte using a recognition element (i.e., enzymes, antibodies, DNAs, etc.), translation of the binding event via a transducer (i.e., optical, electrochemical, piezoelectric, etc.), and a signal processing step for read-out.[23]

1.3.1 Transducer

Several types of transducers can be utilized in biosensors, including piezoelectric, thermometric, optical, and electrochemical, converting the binding event to a measurable signal. Of these, optical and electrochemical transducers are the most commonly used in clinical applications due to their high sensitivity and ease of utilization.[24–26]

1.3.1.1 *Optical transducer*

Optical transducers utilize changes in light absorption, reflection, or fluorescence to detect the presence of a target substance. These transducers employ various optical techniques, such as spectrophotometry, fluorescence, and luminescence, to measure the physical signal produced by the biological recognition event. One of the major advantages of optical transducers is their high sensitivity, as they can detect small changes in light intensity. Moreover, optical transducers can detect multiple target substances simultaneously, using, for example, different wavelengths of light for each target. Optical transducers, however, are limited by the need for a clear path for light to reach the detection system, interference from other sources of light and changes in environmental conditions (i.e., temperature or humidity). Another significant limitation of this type of transducer is its limited use in in-vivo measurements in clinical applications due to the scattering and absorption of light by tissues which makes accurate molecular quantification challenging.[27]

1.3.1.2 *Electrochemical transducer*

An electrochemical transducer in a biosensor detects and quantifies the target biomolecule in a biological sample by measuring the change in current flow generated by a redox reaction taking place at a working electrode. Electrochemical transducers can be miniaturized due to their simple design, allowing for the development of low-cost and compact biosensors that can be easily integrated into portable devices. This is, in contrast to optical transducers, which tend to be bulkier and larger in size, as they require optical components such as lenses and filters, as well as light sources and detectors. Another advantage of electrochemical transducers is that they afford real-time, continuous measurements and can readily deploy in undiluted complex matrices to afford in-vivo measurements. Moreover, electrochemical transducers in biosensors are highly sensitive, enabling them to detect and measure even trace amounts of analytes in complex biological samples. Overall, the combination of sensitivity, real-time capabilities, miniaturizability and ability to readily deploy directly in the body makes the electrochemical transducer a prime candidate to develop biosensors for point-of-care applications.[28–30]

1.3.2 Recognition element

Biological recognition elements include enzymes, antibodies, and nucleic acids, which interact selectively with different classes of target analytes to produce a measurable output signal. Enzymes, for example, can catalyze specific chemical reactions, while antibodies can bind to their corresponding antigens with high specificity. Nucleic acids can also be employed as bioreceptors, particularly in the detection of specific DNA sequences. Each type of bioreceptor has its own unique advantages and limitations, and the choice of bioreceptor for a particular biosensor application depends on the nature of the target analyte and the desired sensitivity and selectivity of the biosensor.[31–34]

1.3.2.1 *Enzymes*

Enzymes are biomolecules that catalyze specific chemical reactions in living organisms. They are typically composed of amino acids and are responsible for a wide range of biological processes, including metabolism, DNA replication, and cellular signaling. Enzymes are highly specific in their actions, only catalyzing particular reactions with specific substrates. Their selectivity arises from the unique three-dimensional structure of the enzyme, which creates an active site that is complementary to the shape and chemical properties of the substrate.[35–37]

Enzymatic electrochemical biosensors

Electrochemical enzymatic biosensors rely on the immobilization of an enzyme on an electrode surface, which upon reaction with its analyte undergoes a change in electrical current due to the production of a side-product by the enzyme that can be electrolyzed or due to the consumption of the analyte by the enzyme.[38–42] A well-known electrochemical enzymatic biosensor is the continuous glucose monitor. It typically consists of a microneedle-bound enzyme (i.e., glucose oxidase (GOx)) that is inserted transdermally in interstitial fluid and capable of monitoring glucose concentrations continuously and in real-time (Figure 2). This device utilizes the enzymatic reaction of glucose to produce hydrogen peroxide and gluconic acid. While applying a voltage to the microneedle electrode, it is possible to oxidize H_2O_2 so that it generates O_2 and electrons (reaction II). The generated current from the released electrons is

then measured as the electrochemical signal of the sensor allowing to quantify the glucose concentration in the sample using a calibration curve.[43–45]

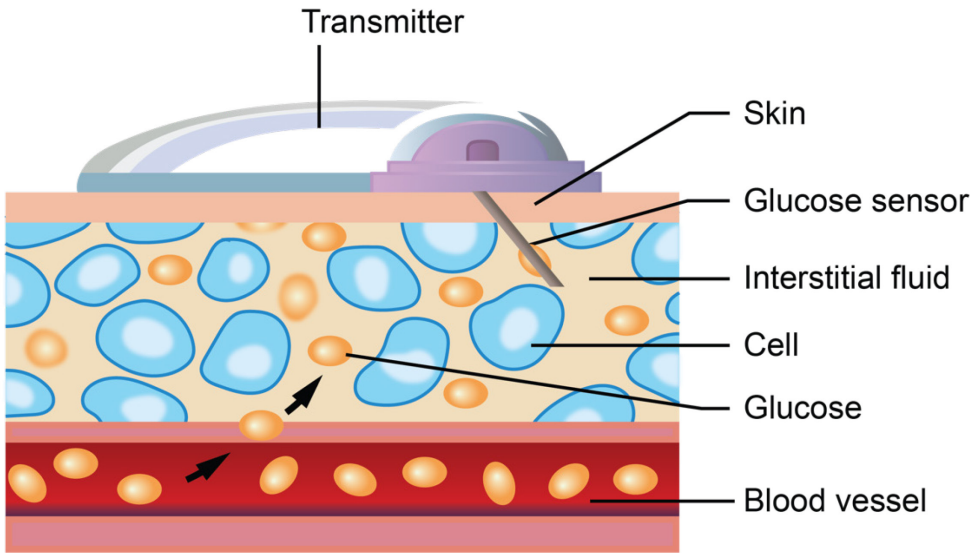

Figure 2. The illustration shows the use of a transdermal glucose monitor to measure glucose levels that have diffused from the bloodstream into the interstitial fluid through the skin.[46]

$$\text{Glucose} + O_2 \rightarrow \text{Gluconic acid} + H_2O_2 \qquad \text{(reaction I)}$$

$$H_2O_2 \xrightarrow{\text{Voltage}} O_2 + 2H^+ + 2e^- \qquad \text{(reaction II)}$$

Due to the electrochemical signal transduction mechanism, continuous glucose monitors are designed to provide real-time (i.e., one measurement every ~20 min) glucose readings, an unprecedented feat that has allowed millions of people suffering from Type-I and Type-II diabetes to self-diagnose and make frequent adjustments to their insulin doses. Despite their affordability (< 150$), wearability and ease of use, the continuous glucose monitors still suffer from a few limitations including: 1) the need for frequent inconvenient calibrations; and 2) cannot be easily adaptable for the measurement of other molecules.[47,48] The latter is because there is only a limited number of enzymes able to undergo a given reaction that we can measure electrochemically (i.e., glutamate, acetylcholine, etc.) as developing enzymes that possess those attributes proves challenging (proteins with the right stability in different experimental conditions, selectivity, and activity).[49–51]

1.3.2.2 *Antibodies*

Antibodies are common recognition elements used in biosensors. They are proteins that are produced by the immune system in response to the presence of a foreign substance (i.e., antigen), such as a virus or bacteria. They are highly specific, meaning that each antibody is designed to recognize and bind to a particular antigen.[52–54] There are various approaches to produce antibodies. The first involves animals' immunization with the antigen, which elicits an immune response and leads to the production of antibodies against it. These antibodies can then be purified and recovered from the animal's blood or tissues.[55–57] A second relies on genetically modified animals, such as mice, to produce humanized antibodies. The main advantage of using transgenic mice to produce antibodies is that they can produce human-like antibodies, which are less likely to be recognized as foreign by the human immune system. This reduces the likelihood of an immune response to the antibodies, which can occur with traditional antibody production methods that use animals such as rabbits.[58–62] Moreover, the use of transgenic mice also allows for the production of fully humanized antibodies, which eliminates the risk of human anti-animal antibody (HAAA) formation.[63] A third is in vitro methods, referred to as phage display or yeast surface display, which involve the use of libraries of genetic material encoding the variable regions of antibody molecules, from which generated antibodies can be selected and purified thus preventing the use of animals.[64] These methods also allow for the genetic engineering of the antibodies to optimize their properties, such as stability, specificity, or affinity.[65] Overall, the choice of method for generating antibodies depends on the specific requirements and desired properties of the antibodies.

Antibody-based electrochemical biosensors (Immunosensors)

Electrochemical biosensors utilizing antibodies as recognition elements (i.e., immunosensors) rely on their electrode immobilization to detect analytes like proteins, toxins, and pathogens.[66–68] A common approach to developing electrochemical immunosensors is known as the "sandwich immunoassay." The basic principle of the sandwich assay is to capture the analyte of interest between two antibodies, one of which is immobilized on the sensor surface, while the other is labelled with an electroactive marker, such as an enzyme or a nanoparticle (Figure 3A). An example of a sandwich assay in an electrochemical biosensor is the detection of a disease biomarker in a sample using two antibodies, one of which is

immobilized on a gold electrode surface, while the other is labelled with Titanium Phosphate (TiP) nanoparticles.[69] In this assay, the disease biomarker in the sample binds to the immobilized antibody, forming a sandwich complex. The TiP-labeled antibody is then added to the sample and binds to the disease biomarker, forming a second layer in the sandwich complex. The TiPs are then functionalized with a redox probe (here Cd^{2+}), that can be oxidized and reduced at the glassy-carbon electrode (GCE) surface. The change in the redox state of the probe can be detected by running an electrochemical measurement, such as cyclic voltammetry or square-wave voltammetry, on the sensor's surface (Figure 3B). The current generated by the oxidation and reduction of the probe is then used to calculate the concentration of the disease biomarker in the sample (Figure 3C).

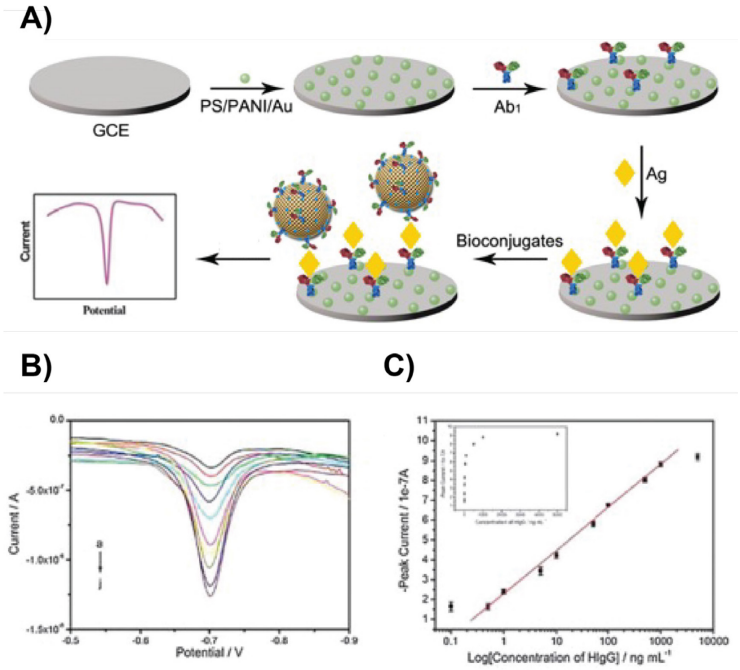

Figure 3. (A) The electrochemical sandwich immunoassay involves the use of an electrode coated with an antibody to capture the target analyte, and the subsequent adsorption of secondary labelled antibodies onto the captured antigens by the first antibodies. (B) As the target analyte concentration increases, the peak current generated by the redox probe's oxidation process also increases proportionally. (C) The calibration curve represents the relationship between the concentration of the target analyte and the signal generated by the immunoassay established in order to determine the unknown concentration of the target analyte. Reprinted with permission from *Chemical Communications*, **2012**, *48*, 4474–4476. Copyright 2023 Royal Society of Chemistry.

While antibodies offer several benefits as recognition elements in biosensors, including their high sensitivity, as well as their versatility, there are also several limitations to consider. To start, antibodies

may undergo denaturation or degradation due to several factors such as exposure to high temperatures, pH changes outside of their optimal range, exposure to detergents or organic solvents, prolonged storage, enzymes or proteases, and high shear forces (e.g., using homogenizer or centrifuge). These can compromise their recognition capabilities and impact the performance and accuracy of the assay or biosensor.[70–72] Second, the production of high-quality antibodies is labour-intensive, costly, and may not be feasible for all analytes.[73] Finally, the use of multiple antibodies in a sandwich assay architecture increases the number of steps to complete the analysis thus increasing the risk of errors.

1.3.2.3 *DNAs*

DNAs are another commonly employed recognition element in the design and production of biosensors due to their ability to selectively bind to and recognize specific DNA or RNA sequences through base pairing.[74,75] The use of DNA as a recognition element in biosensors has enabled the development of a wide range of applications, including diagnosing diseases and monitoring food safety.[76,77]

Electrochemical DNA-based biosensors (E-DNA biosensors)

Electrochemical DNA-based (E-DNA) biosensors are comprised of an electrode (typically gold)-bound DNA modified with a thiol anchor at one extremity and labelled at the other extremity with a redox reporter (i.e., methylene blue, ferrocene, anthraquinone) (Figure 4A). Following electrode modification with DNA, the surface is further functionalized using an excess of an alkanethiol (e.g., 2-mercaptoethanol). Doing so has been found to improve the structure of relatively disordered self-assembled monolayers by gradually removing oligonucleotides that were adsorbed non-specifically on the electrode, favoring the upright orientation of the DNA and impeding other undesired electrochemical processes such as oxygen reduction. Due to the relative proximity of the redox reporter (here ferrocene) to the electrode surface given that the DNA is in a stem loop form, upon oxidation of ferrocene at the electrode surface, the electron transfer is facilitated resulting in high measured currents (Figure 4B). Recognition of the complementary DNA sequence (i.e., cDNA) opens the stem structure, causing the ferrocene label to move further from the electrode surface, and as a result, diminish electron transfer resulting in lowered measured currents. The measured current is then used for calibrating the sensor and thus enables for direct quantification of DNA present in the matrix with limits of detection (LOD) as low

as femtomolar.[78] While E-DNA biosensors offer many benefits, including high sensitivity, selectivity, robustness, versatility, and minimal sample preparation, one significant limitation is that they are typically designed to detect only complementary DNAs, rather than a broad range of molecules further limiting their generalizability for point-of-care measurements.

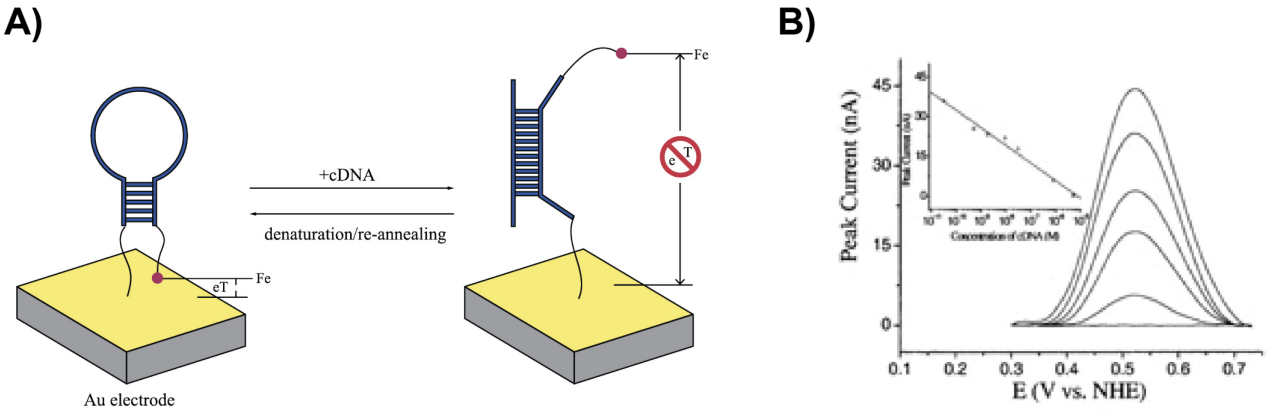

Figure 4. E-DNA biosensors are comprised of an electrode-bound, redox-reporter-modified DNA attached to a gold electrode functionalized with an alkanethiol. (A) Here, the DNA employed is in its stem-loop conformation which maintains the redox reporter (ferrocene) in the proximity of the electrode surface, allowing for rapid electron transfer. Once the stem-loop structure hybridizes with the complementary DNA sequence, the stem-loop structure is disrupted and the kinetic of electron transfer is hindered, presumably because of the increased distance separating the ferrocene label from the electrode surface. (B) Anodic scans of an electrochemical DNA-based biosensor using alternating current voltammetry show a gradual decrease over increasing concentrations of the complementary DNA. Reporting the peak current over the concentration of the complementary DNA produces a calibration curve of the sensor which demonstrates the high sensitivity and ability of this class of sensor for detecting DNA/RNA strands. Reprinted from *Proceeding of the National Academy of Sciences of the United States of America (PNAS)*, **2003**, *100 (16)*, 9134-9137. Copyright 2023 National Academy of Sciences.

1.3.2.4 *Aptamers*

Aptamers are recognition elements with promises to address the different challenges discussed previously and enable the development of a generalizable sensing platform for the measurements of several classes of molecules. Aptamers are short (i.e., around 20 – 100 nucleotides), single-stranded oligonucleotides that are engineered to selectively bind to a wide range of target molecules including proteins, small molecules, and even cells and viruses.[79–81] Aptamers are synthesized via a process called "Systematic evolution of ligands by exponential enrichment" or SELEX, through which sequences are artificially selected and amplified to possess a high affinity toward different classes of molecules (Figure 5).

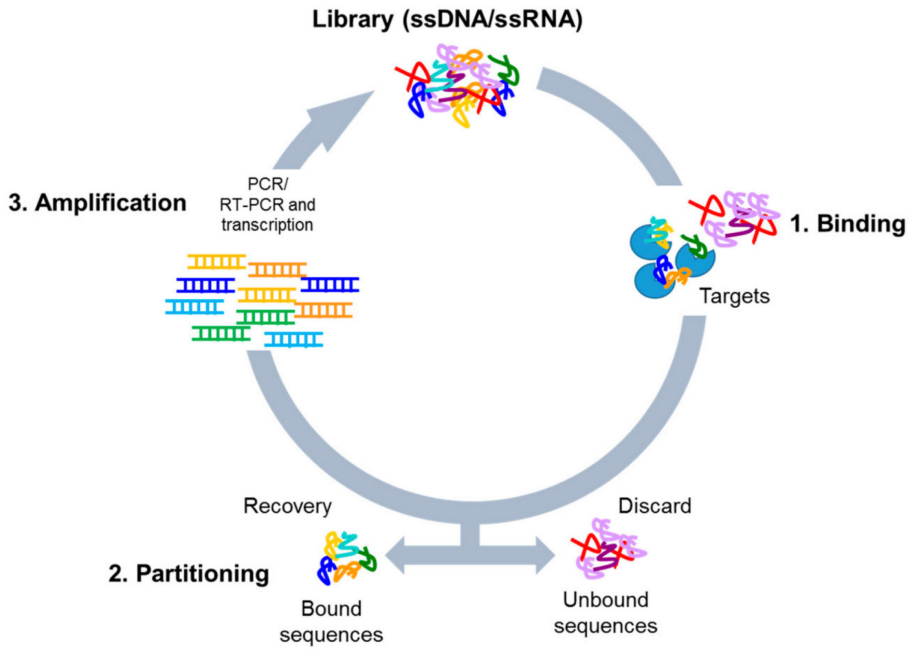

Figure 5. Illustration of aptamers synthesis via systematic evolution of ligands by exponential enrichment (SELEX) process for the in vitro selection and amplification of high-affinity sequences. Reprinted from *Biomedicines*, **2017**, *5*, 49. Open access.

SELEX involves several steps to produce DNA sequences specific for certain analytes. The first step is the synthesis of a large number of random oligonucleotide sequences, which will serve as the starting "library". The library is typically designed to have a high degree of diversity, where each member has a different sequence or structure. The library is then incubated with the target molecule and competent binder sequences are retained while others are discarded. This step can be performed using various methods, such as affinity chromatography, magnetic bead separation, or immobilization on a solid surface. The retained strands are then amplified using polymerase chain reaction (PCR) or other amplification methods (e.g., ligation amplification reaction (LAR), transcription-mediated amplification (TMA)), to produce a large number of copies of each sequence. The amplified strands are then subjected to other rounds of selection and amplification (typically 8-12 times), with the process being repeated until a population of high-affinity sequences is obtained. The final population is sequenced using high-throughput sequencing methods and prevalent sequences are then characterized to determine their affinity for the target, selectivity, and other properties. The sequence bearing the highest affinity and selectivity for the target molecule is then selected for further development.[82,83] Advantageously, SELEX allows to

the production of highly selective aptamers toward a broad range of target molecules thus enabling the development of generalizable sensing approaches.

Aptamers have several advantages over other recognition elements, such as antibodies. To start, aptamers are generally more stable than antibodies and can withstand a wider range of environmental conditions, such as pH, temperature, and humidity. This makes them suitable for long-term storage and in challenging environments.[84] Compared to antibodies, aptamers are generally smaller in size, which could potentially confer benefits in certain scenarios, such as facilitating better penetration into tissues when designing miniaturized biosensors.[85] Aptamers can be synthesized chemically, which is simpler than the production of antibodies. This makes them more accessible, easier and cheaper to produce on a larger scale.[86] Aptamers can be easily modified with a variety of labels, such as fluorescent tags, allowing for detection by various methods. Aptamers are generally non-toxic and do not elicit an immune response, making them suitable for use in in-vivo applications.[87] This versatility makes them suitable for use in a wide range of applications.[88–90]

Characterization of aptamers using isothermal titration calorimetry (ITC) technique

Understanding the binding behavior of aptamers is crucial for their development as diagnostic and therapeutic agents. Various characterization methods have been developed to study the binding of aptamers, including surface plasmon resonance, fluorescence-based assays, and isothermal titration calorimetry (ITC).[91–93] Amongst these, the latter is a technique of choice as it measures the heat produced or absorbed during a binding event. Unlike other techniques, ITC does not require labelling of the aptamer or its target, and can therefore provide label-free data, reducing the likelihood of artifacts which leaves it as a gold standard approach for studying molecular interactions.

ITC provides information about the thermodynamics of the interaction, including binding affinity, enthalpy, and entropy. For this, ITC experiments typically rely on two chambers: a sample cell and a reference cell, both containing an identical solvent (Figure 6A). The sample cell is where the binding reaction takes place, while the reference cell is used to correct for the background heat changes that may occur in the absence of a binding reaction. The sample cell is surrounded by a temperature-controlled jacket that maintains the temperature of the sample at a constant value throughout the experiment. A thermistor or thermocouple is positioned inside the sample cell to monitor the temperature. When the

binding reaction occurs, heat is either released or absorbed by the system, and the temperature of the sample cell changes. This change in temperature is measured by the thermistor or thermocouple, which sends a signal to the calorimeter electronics. The calorimeter electronics use the temperature data from the thermistor or thermocouple to calculate the heat that is released or absorbed by the system during the binding reaction. This information is used to generate a titration curve, which is a plot of the heat released or absorbed as a function of the amount of ligand added to the sample cell. To perform an ITC experiment, the ligand is added to the sample cell in small, incremental steps, and the heat released or absorbed is measured after each step.[94] By analyzing the resulting titration curve, it is possible to determine the binding affinity, stoichiometry, and thermodynamics of the interaction (Figure 6B).

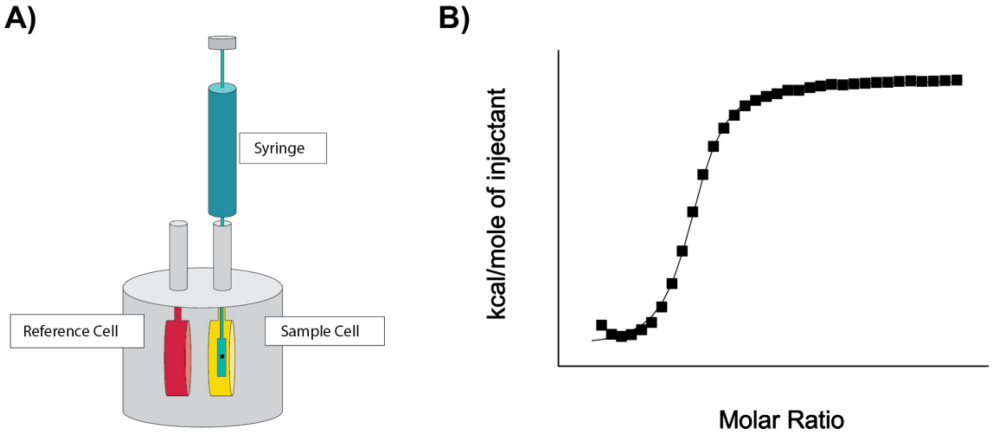

Figure 6. (A) Isothermal titration calorimeters consist of a sample and reference cell, both with identical solvents. The sample cell holds the binding reaction while the reference cell accounts for background heat changes. The sample cell temperature remains constant while a thermistor or thermocouple monitors the temperature.[94] (B) The heat released or absorbed by the reaction is measured by the thermistor or thermocouple, and this data is used to generate a titration curve to determine the binding affinity, stoichiometry, and thermodynamics of the interaction.

Label-free electrochemical biosensors (non-reagentless)

Building on the advantages of aptamers as recognition elements in biosensors, label-free electrochemical biosensors utilizing aptamers provide a highly sensitive and selective method for target detection, with the added benefits of cost-effectiveness and ease of modification. These sensors are typically comprised of gold-electrode-bound aptamer deposited on an alkanethiol self-assembled monolayer immersed in a

solution of an indirect redox mediator (e.g., $[Fe(CN)_6]^{3-/4-}$).[95] In absence of the target, while fixing the electrode potential to electrolyze the redox mediator, a relatively small resistance to the charge transferred is measured. Upon addition of the target (here urokinase plasminogen activator protein labelled as uPA), the resistance of charge transfer increases due to the aptamer structural rearrangement and binding to the target that impedes the diffusion of the redox mediator to the electrode (Figure 7).

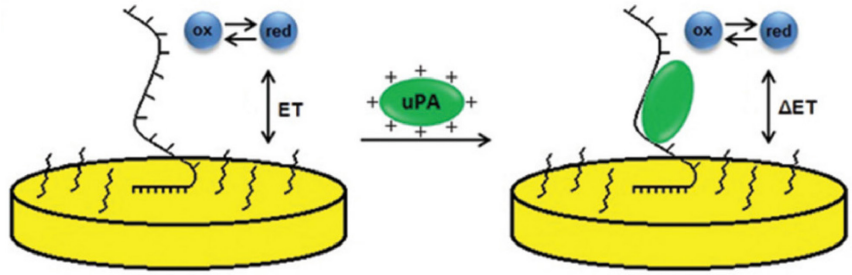

Figure 7. Label-free electrochemical aptamer-based biosensors are typically comprised of an electrode-bound aptamer that is immersed in a solution of a redox mediator (here $[Fe(CN)_6]^{3-/4-}$). Upon addition of the target (here urokinase plasminogen activator labelled as uPA), the aptamer undergoes a binding-induced structural rearrangement that alters the diffusion of the redox mediator to the electrode surface, which results in a decrease in the charge transferred. Reprinted with permission from *Analyst*, **2015**, *140*, 3794. Copyright 2023 Royal Society of Chemistry.

Electrochemical impedance spectroscopy (EIS)

Label-free electrochemical biosensors are commonly interrogated using electrochemical impedance spectroscopy (EIS). EIS is an electroanalytical technique that is performed under steady-state conditions while applying a small perturbation (i.e., a sinusoidally oscillating potential or current (AC) wave, see Eq.1) to an electrochemical cell and measuring the resulting voltage or current response that will be linearly correlated while having a shift in phase (φ) (see Eq. 2). Doing so as a function of the frequency of the perturbation allows to derive the impedance of the system. The resulting complex impedance spectrum obtained from this measurement provides information about the resistance, capacitance and inductance of the system, which can be related to the electrochemical phenomenon (e.g., diffusion of the target molecules, formation of the double layer, etc.) at the electrode interface.[96] Since the impedance is measured over a broad range of interrogating frequencies and these different phenomena occur at different time scales, EIS is capable of discerning and deconvoluting the contributions of various electrochemical

processes. As a result, EIS enables sensitive measurements and can help inform on the physicochemical processes taking place at biosensors' interfaces.[97,98]

$$E(t) = E_0 \text{ Sin } (\omega t) \quad \text{(Eq. 1.1)}$$

$$I(t) = I_0 \text{ Sin } (\omega t + \varphi) \quad \text{(Eq. 1.2)}$$

Where the correlation between angular frequency (ω), and frequency (f) is defined by the following equation:

$$\omega = 2\pi f \quad \text{(Eq. 1.3)}$$

The impedance (Z) of the system is determined in a similar manner as resistance is calculated using Ohm's law in a typical direct current (DC) circuit:

$$Z = E(t) / I(t) \quad \text{(Eq. 1.4)}$$

To quantify the contribution to the impedance originating from the different electrochemical processes, the system is modelled using simple well-known impedances of electrical circuits elements, such as resistors, capacitors, and inductors (see Eqs. 6 and 7 for the impedance of a resistor and a capacitor). For instance, the solution resistance of an electrochemical system (resistance of the solution separating the working and counter electrode) is represented by a resistor, while the electrical double-layer formation at the electrode interface is modelled by a capacitor.[99] Utilizing the mathematical framework of complex numbers enables the effective representation of the impedance of a system interrogated via electrochemical impedance spectroscopy. This mathematical framework provides a convenient means of handling and manipulating impedance data and facilitates the determination of equivalent circuit models that describe the system's behaviour (Eq. 5).

$$Z = Z_{Re} + j\, Z_{Im} \quad \text{(Eq. 1.5)}$$

where the ($j^2 = -1$)

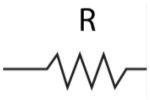

$$I(t) = E(t) / R$$

$$I(t) = E_0 \, \mathrm{Sin}\,(\omega t) / R$$

$$Z_{sol} = R_{sol} \qquad \text{(Eq. 1.6)}$$

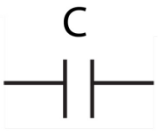

$$C_{int} = Q / E(t)$$

$$I = dQ / dt = C_{int} (dE / dt) = C_{int} (dE_0 \mathrm{Sin}\,(\omega t) / dt)$$

$$I = C_{int} E_0 \omega \mathrm{Cos}\,(\omega t) = \omega C_{int} E_0 \mathrm{Sin}\,(\omega t + \pi/2)$$

$$Z_{int} = -j / (\omega C_{int}) \qquad \text{(Eq. 1.7)}$$

Another element used to model the impedance of electrochemical systems is known as the constant phase element (CPE). A constant phase element is a mathematical approximation used to represent the impedance behaviour of an electrochemical system in the frequency domain. A CPE has a frequency-dependent impedance that is described by a power law relationship and a phase angle that is constant with frequency. CPEs are considered a more general and flexible type of impedance element compared to resistors and capacitors as they can model both capacitive and inductive behaviour, with the ability to account for deviations from ideal behaviour. A widely employed constant phase element used in label-free electrochemical biosensors is known as the Warburg element (W). It represents the diffusion process of ions in an electrode-electrolyte system and is characterized by a constant phase angle, typically at 45 degrees. The Warburg element is commonly used to describe the behaviour of slow kinetics in electrochemical systems and provides insights into the rate-limiting step in the reaction mechanism.

To obtain the overall impedance of the circuit, the impedance of the elements in series and parallel must be calculated using equations 8 and 9, respectively.

$$Z_{total} = Z_1 + Z_2 \qquad \text{(Eq. 1.8)}$$

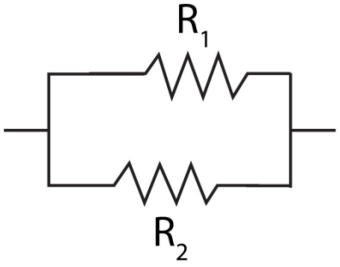

$$1 / Z_{total} = 1 / Z_1 + 1 / Z_2 \qquad \text{(Eq. 1.9)}$$

For a system that includes a faradic process such as the electron transfer from the redox species (reagent) in label-free electrochemical biosensors, the equivalent electrical circuit will be similar to the one depicted in Figure 8. In the non-faradaic branch of the circuit, R_{sol} and C_{int} are representing the solution resistance and the capacitive behaviour of the double layer formation, while in the faradaic branch, the resistance electrons face to transfer and the diffusion of the redox molecule to the electrode are modeled using R_{ct}, and W, respectively.[95]

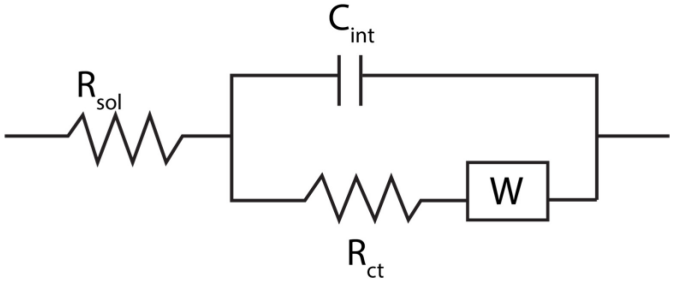

Figure 8. The equivalent electrical circuit of an electrochemical system undergoing a faradic (charge transfer) reaction. The solution resistance, double layer formation, diffusion of ion transport and charge transfer resistance of the redox species are represented by R_{sol}, C_{int}, W, and R_{ct}, respectively.[95]

The charge transfer in small perturbation conditions without mass transport in the system follows the Butler-Volmer equation:

$$I = I_0 \left(e^{\left(\frac{-\alpha n F \eta}{RT}\right)} - e^{\left(\frac{(1-\alpha) n F \eta}{RT}\right)}\right) \qquad \text{(Eq. 1.10)}$$

Where I_0, α (between 0 – 1), n, F, η, R, and T are the exchange current, transfer coefficient, the number of possible exchanged electrons in the reaction, Faraday constant, overpotential (relative to the

equilibrium potential of the reaction), gas constant, and temperature, respectively. In a small enough η regime (i.e., mV), the correlation between E and I is considered to be linear and the approximation of

$$e^x \approx 1 + x \qquad \text{(Eq. 1.11)}$$

could be assumed for simplification. As a result, the Butler-Volmer equation can be rewritten as:

$$I = I_0 (- nF\eta / RT) \qquad \text{(Eq. 1.12)}$$

In order to determine the impedance of the charge transfer resistor element, the correlation between the η and I in the Butler-Volmer equation can be written as follows:

$$\eta / I = (- RT / nF) / I_0$$
$$Z_{ct} = R_{ct} = - RT / nFI_0 \qquad \text{(Eq. 1.13)}$$

To calculate the overall impedance of the system including the diffusion phenomenon, the first step is to determine the impedance of the parallel section:

$$\frac{1}{Z} = \frac{1}{R_{ct} + Z_W} - \frac{1}{\frac{j}{\omega C_{int}}}$$

$$\frac{1}{Z} = \frac{1}{R_{ct} + Z_W} + j\omega C_{int}$$

$$Z_{total} = \frac{R_{ct} + Z_W}{1 + j\omega C_{int}(R_{ct} + Z_W)} \qquad \text{(Eq. 1.14)}$$

Where the Z_W is the Warburg impedance:

$$Z_W = (\sigma / \sqrt{\omega}) - (j\sigma / \sqrt{\omega}) \qquad \text{(Eq. 1.15)}$$

While

$$\sigma = \frac{\left(\frac{RT}{nFC_O^*\sqrt{D_O}}\right) + \left(\frac{RT}{nFC_R^*\sqrt{D_R}}\right)}{\sqrt{2}nFA} \qquad \text{(Eq. 1.16)}$$

The electrode surface area is shown by A, while the concentration of the oxidative and reductive species in the bulk of the solution, and their corresponding diffusion coefficients, are represented via C_O^*, C_R^*, D_O, and D_R, respectively.

The overall impedance is then obtained by adding the impedance of the solution resistance in series with the parallel section:

$$Z_{total} = R_{sol} + \frac{R_{ct} + Z_W}{1 + j\omega C_{int}(R_{ct} + Z_W)} \qquad \text{(Eq. 1.17)}$$

Plotting the impedance magnitude (|Z|) versus the frequency of the applied perturbation produces a diagram known as a Bode plot. This plot consists of two logarithmic graphs, one for the magnitude of the impedance and one for the phase shift between the applied voltage and the resulting current (Figure 9).

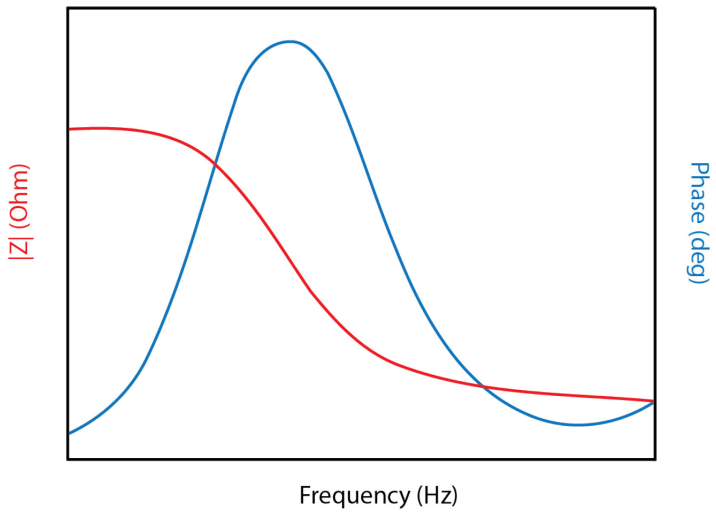

Figure 9. Bode plot presenting the alteration of impedance magnitude (red line) and phase (blue line) of the system described in Figure 8 versus the interrogation frequency.

The shape and characteristics of the Bode plot can be used to infer information about the electrical properties and behavior of the system being tested, such as the presence of capacitive or resistive elements and the overall resistance and reactance of the system. Peaks or dips in the magnitude plot can indicate if the impedance is governed by certain physicochemical phenomena. For instance, when looking at the Bode representation of the label-free electrochemical biosensor for the uPA example (Figure 10A), we see that the low-frequency range (1 – 5 Hz) is the most responsive to signal changes when uPA is added. The authors observe this via a monotonic decrease in phase and an increase in the total impedance in those lower interrogation frequencies. Figure 10B depicts a concentration-dependent modulation in the charge transfer resistance attributed to the specific binding of uPA to the aptamer sequence. At pH 7.4, the uPA protein is positively charged, and upon binding to the aptamer, the structure undergoes a rearrangement resulting in an increase in negative surface charge density. This structural alteration also introduces a diffusion barrier, impeding the charge transfer reaction of ferricyanide on the protein/aptamer layer.

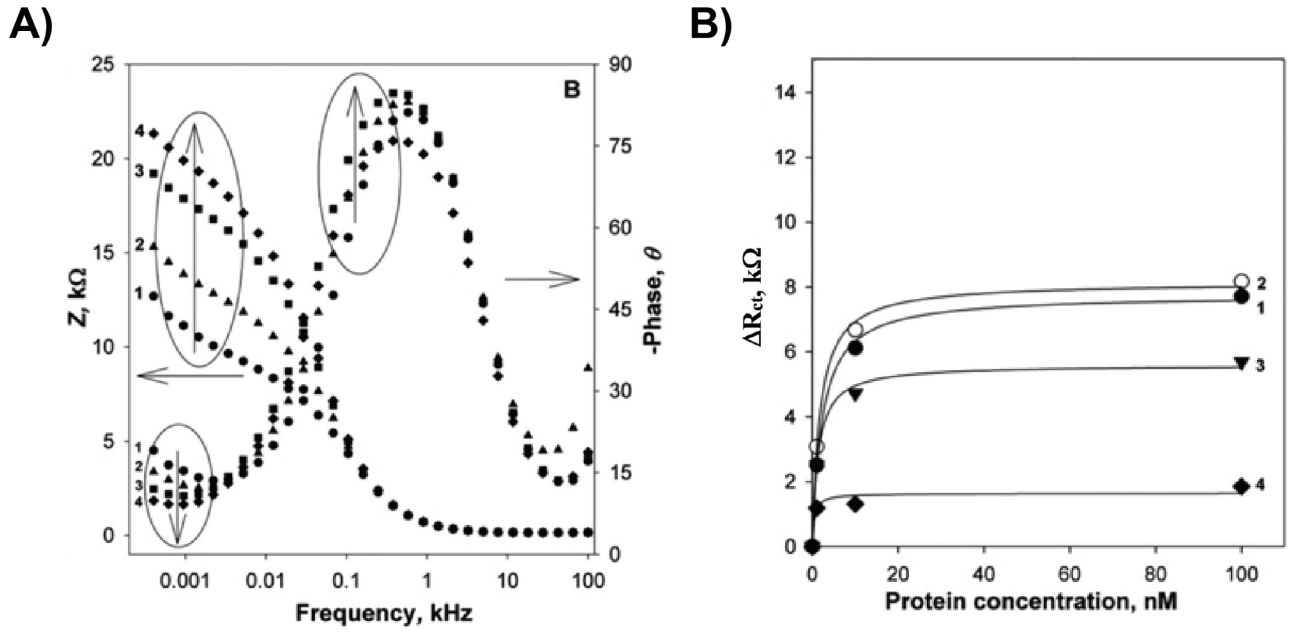

Figure 10. (A) Measured Bode plots when sensors are in presence of (1) 0 nM (2) 1 nM (3) 10 nM (4) 100 nM uPA and $[Fe(CN)_6]^{3-/4-}$. Both impedance and phase diagrams show that when interrogating using lower frequencies (1 – 5 Hz), a change is measured, presumably originating from aptamer-target binding. (B) The calibration curve of the sensor using the change in the charge transfer resistance, ΔR_{ct}, against protein concentrations obtained from an aptamer-modified electrode after 30 min incubation in various solutions, including (1) uPA, (2) uPA and 100 nM bovine serum albumin (BSA), (3) BSA alone, and (4) uPA and serum. The data were analyzed by fitting to the Langmuir adsorption isotherm and Scatchard's model. The Randles

circuit in Fig. 8 is utilized to fit the EIS data. Reprinted with permission from *Analyst*, **2015**, *140*, 3794. Copyright 2023 Royal Society of Chemistry.

While label-free electrochemical biosensors offer a highly sensitive means of measuring target concentrations, they suffer from several limitations. To start, there is still to be a demonstration of this class of sensor to deploy directly in the body. This is in part because, the electrochemical signal is dependent on the overall mediator accessibility to the electrode surface, which like aptamer binding can be altered by the accumulation of biomolecules on the sensor surface induced by a body's immune response. As a result, the build-up of these substances on the sensor can interfere with its ability to discern target molecule binding leading to decreased sensitivity and reproducibility over time. Moreover, the label-free electrochemical biosensors' application for in-vivo measurements is limited due to the high concentration of the reagent (e.g., $[Fe(CN)_6]^{3-/4-}$ with a typical concentration of 5 – 10 mM) needed to obtain a measurable signal, which could potentially be toxic.[100]

1.4. Electrochemical aptamer-based biosensors

Electrochemical aptamer-based biosensors (E-AB) address the limitations of other classes of biosensors (i.e., generalizability, stability and production of recognition elements, sensor's signal dependence on electrode fouling). E-AB biosensors are comprised of a redox-reporter-modified aptamer that is immobilized on a gold electrode surface functionalized with an alkanethiol monolayer (typically of 6-mercapto-1-hexanol) (Figure 11). The latter is used to prevent fouling, orient the aptamer on the electrode surface and mitigate other undesired electrochemical processes to take place on the electrode surface (i.e., oxygen reduction reaction). Given that aptamers can be made to bind several target molecules, there have been over 15 E-AB biosensors developed to date and this number is likely to grow.[101–112] These sensors can be miniaturized into a handheld device, manufactured for limited costs and can enable the simultaneous detection of multiple biological compounds (i.e., multiplexing) further lowering the costs of analyses. E-AB biosensors have achieved a feat in bioanalytical chemistry of being able to afford sub-second real-time and continuous measurements of the concentrations of molecules directly in complex matrices or in the body. The real-time monitoring ability of E-AB biosensors is made possible thanks to the electrochemical signal transduction they rely on and due to the fast (< seconds) aptamer binding kinetics. The real-time monitoring capability of these sensors is particularly useful in applications where

rapid and accurate results are critical, such as in the monitoring of the pharmacokinetics of drugs or in the early detection of diseases.[113,114] E-AB biosensors are thus foreseen as promising candidates for developing innovative tools for personalized medicine at the point-of-care to improve our understanding of pharmacokinetics, address drug delivery challenges, and medication errors.[115]

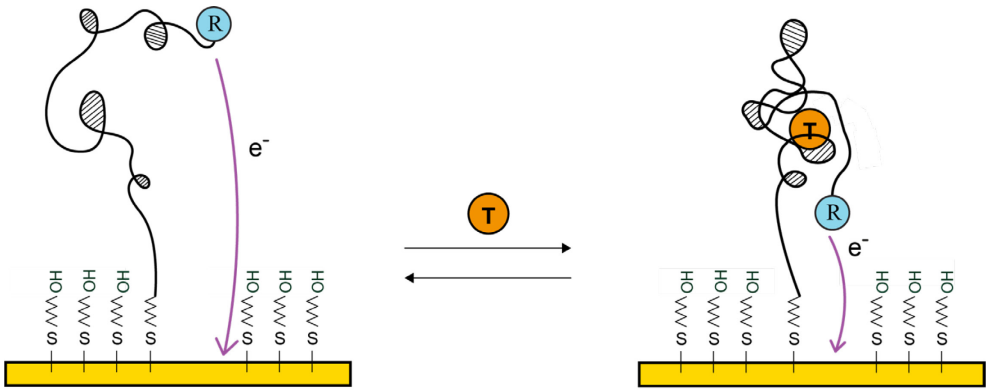

Figure 11. E-AB sensors are composed of a redox-reporter-modified aptamer as their recognition element. The aptamer is immobilized on an alkanethiol-coated gold electrode via a thiol-modified terminal. Upon addition of the target, a change in the transfer of electrons from the redox reporter occurs, which can be measured using various electrochemical techniques. This allows for the determination of the concentration of the target.[110]

1.4.1 Square-wave voltammetry

E-AB biosensors have been postulated to undergo, upon target binding, a conformational change causing a change in the electron transfer kinetics of the redox reporter. This can be monitored using a diverse set of electrochemical techniques, including cyclic voltammetry, electrochemical phase interrogation, chronoamperometry, and pulse voltammetric approaches such as square-wave voltammetry. Square-wave voltammetry represents the most commonly used method to this end due to its high sensitivity, which is attributed to its distinctive sampling method.[116]

Square-wave voltammetry relies on an incrementing staircase ramping potential wave superimpose on square-wave pulses (Figure 12A). The main parameters of the square-wave potential modulation are the scan increment (ΔE) of the staircase ramp, the square-wave pulse amplitude (E_{sw}), and the duration of the potential pulse (t_p). During each potential step, two small, oppositely oriented

pulses of equal duration (t_p) are applied. The duration of the pulse is often expressed in terms of the square-wave frequency ($f = 1/2t_p$). The pulse duration (t_p) is designated as $t_p = \tau/2$, where τ is the duration of the potential pulse (Figure 12B). The scan rate of the square-wave potential waveform can be defined as:

$$v = f \Delta E$$

Positive and negative pulses are referred to as the forward (I_f) and backward (I_b) pulses, respectively, which produce pulsing current variations (Figure 12C). The current in square-wave voltammetry is sampled at the end of each potential pulse only (Figure 12D) and to further improve the sensitivity of the approach, the two current values can be subtracted to obtain the net current (I_{net}):

$$I_{net} = I_f - I_b$$

The subtraction procedure used to calculate the net current allows to reduce the non-faradaic contribution to the measured current and in turn maximizes the faradaic contribution, making square-wave voltammetry one of the most sensitive voltammetric techniques.[117]

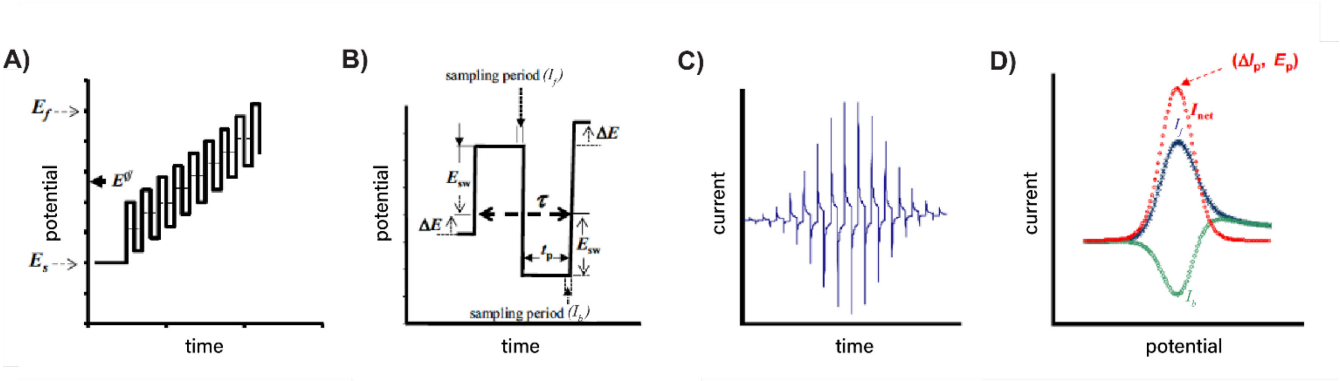

Figure 12. (A) A small staircase ramping potential pulse superimposed on a square-wave pulse function is applied in square-wave voltammetry. (B) A single pulse cycle in the square-wave voltammetry approach relies on setting ΔE, E_{sw}, and t_p, which represent the potential scan increment, pulse amplitude, and duration of each oppositely oriented pulse, while the overall pulse duration and the current generated from the forward and backward pulses are shown via τ, I_f, and I_b, respectively. (C) Pulsing the potential and sampling the current in such fashion produces forward and backward currents. (D) A common square-wave voltammogram includes forward (blue) and backward (green) pulses voltammogram which are then subtracted from one another to return the net current (red) improving the sensitivity of the measurement by reducing the non-faradaic contribution to the measured current. Reprinted with permission from *ChemTexts* **2018**, *4*, 17. Copyright 2023 Springer.

Faradaic and non-faradaic processes always occur during an electrochemical experiment. For instance, a simple redox reaction at the electrode/electrolyte interface, as shown in reaction 3, where the Red and Ox are the dissolved reductive and oxidative species in the solution, and *n* is the number of electrons exchanged, when at and above the couple's formal potential, generates a faradaic current.

$$Red \rightarrow Ox + ne^- \qquad \text{(reaction 3)}$$

Simultaneously to the faradaic reaction, upon application of a voltage, an electrical double layer forms at the interface of the electrode. This is caused by the migration of excess countercharge at the electrode interface (Figure 13A), which behaves as a capacitor and generates a non-faradaic current. In cases where the concentration of the electroactive reactant is low (i.e., μM regime), the charging current can be significantly higher than the faradaic current and thus limit our ability to analytically resolve the concentrations of analytes. Hence, the non-faradaic current limits the sensitivity in electroanalytical measurements.[116] Square-wave voltammetry overcomes this and maximizes the contribution of the measured current from the faradaic reaction by applying small potential steps or increments (a few mV). In doing so, the charging current (I_{dl}) typically drops to negligible levels after a few milliseconds (or less) due to the faster time scale required to form the electrical double layer (exponentially decreasing as a function of time), while the faradaic current (I_{ct}) remains higher for a longer period of time (decreases as the inverse of the square-root of time) (Figure 13B). This strategy is commonly employed in what is referred to as pulse voltammetric techniques, which notably include square-wave voltammetry.

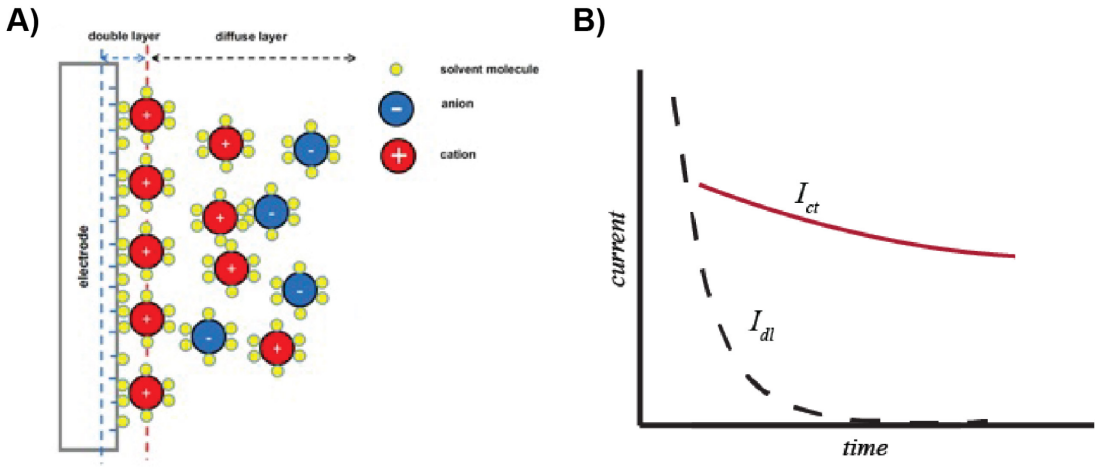

Figure 13. (A) A sketch of the double layer formation at the electrode's interface. (B) The faradaic (I_{ct}) and charging (I_{dl}) current variation versus time is shown. Reprinted with permission from *ChemTexts* **2018**, *4*, 17. Copyright 2023 Springer.

The amount of charge transferred in square-wave voltammetry that is measured at a specific interrogating frequency can be determined by extracting the voltammogram's peak current and dividing it by the frequency. Doing so allows monitoring of the population of redox species that are capable of transferring electrons at a given rate (Figure 14). This strategy is particularly useful to characterize E-AB sensors to identify aptamer states (i.e., unbound and bound) and square-wave interrogating frequencies for calibration which is chosen to maximize the differences in charge transferred while minimizing the charge transferred in the absence of the target.[118,119]

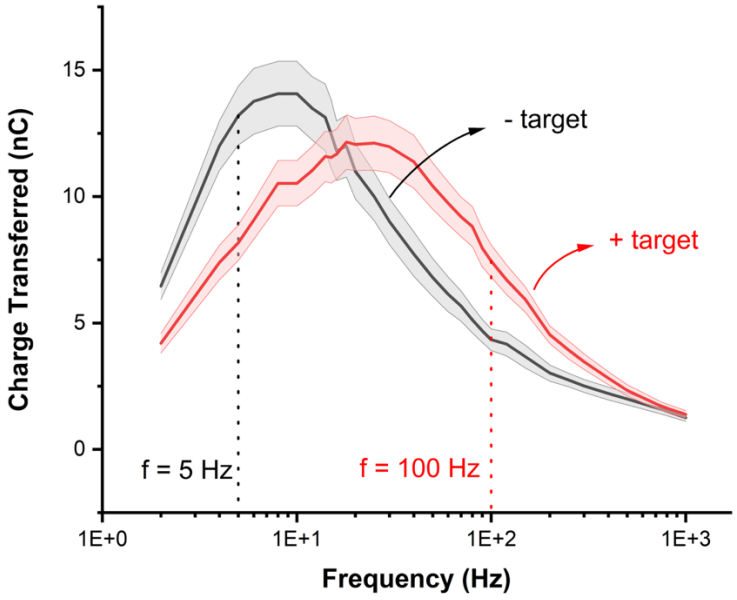

Figure 14. Acquiring charge transferred versus square-wave frequency when sensors are in the absence or presence of the target helps select the interrogation frequency for calibrating the sensors. The shaded area around the curves represents the standard deviation of the average measurements.

If the amount of charge transferred in the unbound state is higher than in the bound state at a particular frequency, the signal (γ) is referred to as "signal-off". On the other hand, if the amount of charge transferred in the bound state is higher than in the unbound state at a particular frequency, the signal is referred to as "signal-on".[120] Performing calibration of sensors at these respective square-wave frequencies produces responses of varying intensities, which we refer to as gain (i.e., the measured signal at a given concentration divided by the signal measured in the absence of the target) (Figure 15).

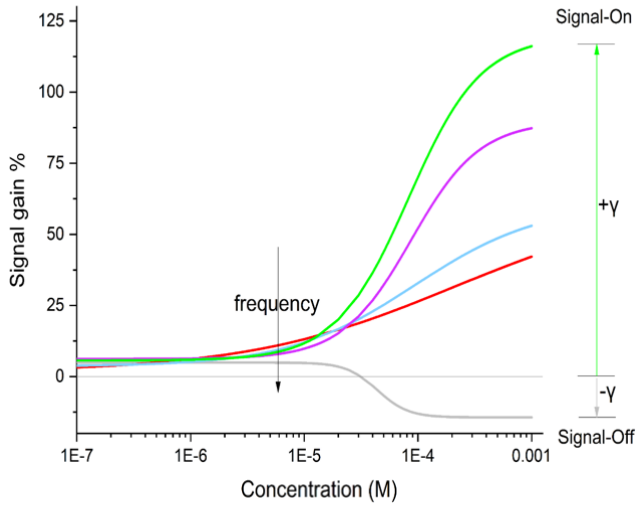

Figure 15. Square-wave signal gain (i.e., the response of the sensor measured with respect to the one measured in absence of the target) of an E-AB sensor varying from signal-on to signal-off by changing the electrochemical interrogation frequency.[120]

1.5. Objectives of thesis

Despite the multitude of advantages electrochemical aptamer-based sensors possess over other analytical approaches, such as affordability, generalizability, miniaturization, and the ability to afford real-time molecular monitoring in complex matrices, they are limited by low affinity relative to the clinically relevant range of target molecules, impeding their widespread implementation in point-of-care applications.[121–126]

In response, we plan to investigate the relatively low affinity of E-AB sensors by pursuing the following objectives:

1) Examination of the sensitivity of electrochemical interrogation methods in evaluating aptamer's affinity in E-AB sensors via comparing the performance of square-wave voltammetry and electrochemical impedance spectroscopy techniques.
2) Delving into the underlying conformational change signaling mechanism of E-AB sensors to gain a comprehensive understanding of the parameters impacting aptamer affinity.

In summary, this thesis seeks to improve the analytical performance of E-AB sensors with the hopes that will improve their translation for “real-world” applications at the point-of-care and develop improved personalized medicine alternatives.

References:

(1) Andel, C.; Davidow, S. L.; Hollander, M.; Moreno, D. A. The Economics of Health Care Quality and Medical Errors. *J. Health CARE FINANCE* **2012**.

(2) Kuitunen, S.; Niittynen, I.; Airaksinen, M.; Holmström, A.-R. Systemic Causes of In-Hospital Intravenous Medication Errors: A Systematic Review. *J. Patient Saf.* **2021**, *17* (8), e1660–e1668. https://doi.org/10.1097/PTS.0000000000000632.

(3) Agyemang, R. E. O.; While, A. Medication Errors: Types, Causes and Impact on Nursing Practice. *Br. J. Nurs.* **2010**, *19* (6), 380–385. https://doi.org/10.12968/bjon.2010.19.6.47237.

(4) Rodwin, B. A.; Bilan, V. P.; Merchant, N. B.; Steffens, C. G.; Grimshaw, A. A.; Bastian, L. A.; Gunderson, C. G. Rate of Preventable Mortality in Hospitalized Patients: A Systematic Review and Meta-Analysis. *J. Gen. Intern. Med.* **2020**, *35* (7), 2099–2106. https://doi.org/10.1007/s11606-019-05592-5.

(5) WHO (2017) WHO launches global effort to halve medication-related error in 5 years. Available on: https://www.who.int/news/item/29-03-2017-who-launches-global-effort-to-halve-medication-related-errors-in-5-years, last access: 2023-06-05

(6) da Silva, B. A.; Krishnamurthy, M. The Alarming Reality of Medication Error: A Patient Case and Review of Pennsylvania and National Data. *J. Community Hosp. Intern. Med. Perspect.* **2016**, *6* (4), 31758. https://doi.org/10.3402/jchimp.v6.31758.

(7) Aronson, J. K. Medication Errors: Definitions and Classification. *Br. J. Clin. Pharmacol.* **2009**, *67* (6), 599–604. https://doi.org/10.1111/j.1365-2125.2009.03415.x.

(8) Goodman, K. E.; Cosgrove, S. E.; Pineles, L.; Magder, L. S.; Anderson, D. J.; Dodds Ashley, E.; Polk, R. E.; Quan, H.; Trick, W. E.; Woeltje, K. F.; Leekha, S.; Harris, A. D. Significant Regional Differences in Antibiotic Use Across 576 US Hospitals and 11 701 326 Adult Admissions, 2016–2017. *Clin. Infect. Dis.* **2021**, *73* (2), 213–222. https://doi.org/10.1093/cid/ciaa570.

(9) Gaggl, M.; Pate, V.; Stürmer, T.; Kshirsagar, A. V.; Layton, J. B. The Comparative Risk of Acute Kidney Injury of Vancomycin Relative to Other Common Antibiotics. *Sci. Rep.* **2020**, *10* (1), 17282. https://doi.org/10.1038/s41598-020-73687-9.

(10) van Hal, S. J.; Paterson, D. L.; Lodise, T. P. Systematic Review and Meta-Analysis of Vancomycin-Induced Nephrotoxicity Associated with Dosing Schedules That Maintain Troughs between 15 and

20 Milligrams per Liter. *Antimicrob. Agents Chemother.* **2013**, *57* (2), 734–744. https://doi.org/10.1128/AAC.01568-12.

(11) Jeffres, M. N. The Whole Price of Vancomycin: Toxicities, Troughs, and Time. *Drugs* **2017**, *77* (11), 1143–1154. https://doi.org/10.1007/s40265-017-0764-7.

(12) Greene, S. B.; Williams, C. E.; Pierson, S.; Hansen, R. A.; Carey, T. S. Medication Error Reporting in Nursing Homes: Identifying Targets for Patient Safety Improvement. *Qual. Saf. Health Care* **2010**, *19* (3), 218–222. https://doi.org/10.1136/qshc.2008.031260.

(13) Fusco, J. A.; Paulus, E. J.; Shubat, A. R.; Miah, S. Warfarin and Rivaroxaban Duplication: A Case Report and Medication Error Analysis. *Drug Saf. - Case Rep.* **2015**, *2* (1), 5. https://doi.org/10.1007/s40800-015-0007-3.

(14) Donihi, A. C. Use of a Standardized Protocol to Decrease Medication Errors and Adverse Events Related to Sliding Scale Insulin. *Qual. Saf. Health Care* **2006**, *15* (2), 89–91. https://doi.org/10.1136/qshc.2005.014381.

(15) Wittich, C. M.; Burkle, C. M.; Lanier, W. L. Medication Errors: An Overview for Clinicians. *Mayo Clin. Proc.* **2014**, *89* (8), 1116–1125. https://doi.org/10.1016/j.mayocp.2014.05.007.

(16) Hellman, R. A Systems Approach to Reducing Errors in Insulin Therapy in the Inpatient Setting. *Endocr. Pract.* **2004**, *10*, 100–108. https://doi.org/10.4158/EP.10.S2.100.

(17) Yamamoto, Y.; Kanayama, N.; Nakayama, Y.; Matsushima, N. Current Status, Issues and Future Prospects of Personalized Medicine for Each Disease. *J. Pers. Med.* **2022**, *12* (3), 444. https://doi.org/10.3390/jpm12030444.

(18) Goetz, L. H.; Schork, N. J. Personalized Medicine: Motivation, Challenges, and Progress. *Fertil. Steril.* **2018**, *109* (6), 952–963. https://doi.org/10.1016/j.fertnstert.2018.05.006.

(19) Mathur, S.; Sutton, J. Personalized Medicine Could Transform Healthcare. *Biomed. Rep.* **2017**, *7* (1), 3–5. https://doi.org/10.3892/br.2017.922.

(20) Division of Laboratory Systems (DLS) (2018) Strengthening clinical laboratories. Available on: https://www.cdc.gov/csels/dls/strengthening-clinical-labs.html, last access: 2023-06-05

(21) Wu, H.-Y.; Cunningham, B. T. Point-of-Care Detection and Real-Time Monitoring of Intravenously Delivered Drugs via Tubing with an Integrated SERS Sensor. *Nanoscale* **2014**, *6* (10), 5162–5171. https://doi.org/10.1039/C4NR00027G.

(22) Flatebo, C.; Conkright, W. R.; Beckner, M. E.; Batchelor, R. H.; Kippin, T. E.; Heikenfeld, J.; Plaxco, K. W. Efforts toward the Continuous Monitoring of Molecular Markers of Performance. *J. Sci. Med. Sport* **2023**, S1440244023000282. https://doi.org/10.1016/j.jsams.2023.01.010.

(23) Said, N. A. M.; Ogurtsov, V. I.; Herzog, G. ELECTROCHEMICAL BIOSENSOR BASED ON MICROFABRICATED ELECTRODE ARRAYS FOR LIFE SCIENCES APPLICATIONS. **2014**. https://doi.org/10.13140/RG.2.2.11066.49603.

(24) Sethi, R. S. Transducer Aspects of Biosensors. *Biosens. Bioelectron.* **1994**, *9* (3), 243–264. https://doi.org/10.1016/0956-5663(94)80127-4.

(25) Brecht, A.; Gauglitz, G. Optical Probes and Transducers. *Biosens. Bioelectron.* **1995**, *10* (9–10), 923–936. https://doi.org/10.1016/0956-5663(95)99230-I.

(26) Thévenot, D. R.; Toth, K.; Durst, R. A.; Wilson, G. S. ELECTROCHEMICAL BIOSENSORS: RECOMMENDED DEFINITIONS AND CLASSIFICATION *. *Anal. Lett.* **2001**, *34* (5), 635–659. https://doi.org/10.1081/AL-100103209.

(27) Koschinsky, T.; Heinemann, L. Sensors for Glucose Monitoring: Technical and Clinical Aspects. *Diabetes Metab. Res. Rev.* **2001**, *17* (2), 113–123. https://doi.org/10.1002/dmrr.188.

(28) Idili, A.; Parolo, C.; Ortega, G.; Plaxco, K. W. Calibration-Free Measurement of Phenylalanine Levels in the Blood Using an Electrochemical Aptamer-Based Sensor Suitable for Point-of-Care Applications. *ACS Sens.* **2019**, *4* (12), 3227–3233. https://doi.org/10.1021/acssensors.9b01703.

(29) Campuzano, S.; Pedrero, M.; Yáñez-Sedeño, P.; Pingarrón, J. M. New Challenges in Point of Care Electrochemical Detection of Clinical Biomarkers. *Sens. Actuators B Chem.* **2021**, *345*, 130349. https://doi.org/10.1016/j.snb.2021.130349.

(30) Wang, J. Electrochemical Biosensors: Towards Point-of-Care Cancer Diagnostics. *Biosens. Bioelectron.* **2006**, *21* (10), 1887–1892. https://doi.org/10.1016/j.bios.2005.10.027.

(31) Van Dorst, B.; Mehta, J.; Bekaert, K.; Rouah-Martin, E.; De Coen, W.; Dubruel, P.; Blust, R.; Robbens, J. Recent Advances in Recognition Elements of Food and Environmental Biosensors: A Review. *Biosens. Bioelectron.* **2010**, *26* (4), 1178–1194. https://doi.org/10.1016/j.bios.2010.07.033.

(32) Kleinjung, F.; Klussmann, S.; Erdmann, V. A.; Scheller, F. W.; Fürste, J. P.; Bier, F. F. High-Affinity RNA as a Recognition Element in a Biosensor. *Anal. Chem.* **1998**, *70* (2), 328–331. https://doi.org/10.1021/ac9706483.

(33) Justino, C. I. L.; Freitas, A. C.; Pereira, R.; Duarte, A. C.; Rocha Santos, T. A. P. Recent Developments in Recognition Elements for Chemical Sensors and Biosensors. *TrAC Trends Anal. Chem.* **2015**, *68*, 2–17. https://doi.org/10.1016/j.trac.2015.03.006.

(34) Yao, C.; Zhu, T.; Qi, Y.; Zhao, Y.; Xia, H.; Fu, W. Development of a Quartz Crystal Microbalance Biosensor with Aptamers as Bio-Recognition Element. *Sensors* **2010**, *10* (6), 5859–5871. https://doi.org/10.3390/s100605859.

(35) Walsh, C. Enabling the Chemistry of Life. *Nature* **2001**, *409* (6817), 226–231. https://doi.org/10.1038/35051697.

(36) Dong, Z.; Luo, Q.; Liu, J. Artificial Enzymes Based on Supramolecular Scaffolds. *Chem. Soc. Rev.* **2012**, *41* (23), 7890. https://doi.org/10.1039/c2cs35207a.

(37) Vargas-Bernal, R.; Rodrguez-Miranda, E.; Herrera-Prez, G. Evolution and Expectations of Enzymatic Biosensors for Pesticides. In *Pesticides - Advances in Chemical and Botanical Pesticides*; Soundararajan, R. P., Ed.; InTech, 2012. https://doi.org/10.5772/46227.

(38) Ronkainen, N. J.; Halsall, H. B.; Heineman, W. R. Electrochemical Biosensors. *Chem. Soc. Rev.* **2010**, *39* (5), 1747. https://doi.org/10.1039/b714449k.

(39) Xie, Y.; Liu, T.; Chu, Z.; Jin, W. Recent Advances in Electrochemical Enzymatic Biosensors Based on Regular Nanostructured Materials. *J. Electroanal. Chem.* **2021**, *893*, 115328. https://doi.org/10.1016/j.jelechem.2021.115328.

(40) Trojanowicz, M. Determination of Pesticides Using Electrochemical Enzymatic Biosensors. *Electroanalysis* **2002**, *14* (19–20), 1311–1328. https://doi.org/10.1002/1521-4109(200211)14:19/20<1311::AID-ELAN1311>3.0.CO;2-7.

(41) Pan, C.; Wei, H.; Han, Z.; Wu, F.; Mao, L. Enzymatic Electrochemical Biosensors for in Situ Neurochemical Measurement. *Curr. Opin. Electrochem.* **2020**, *19*, 162–167. https://doi.org/10.1016/j.coelec.2019.12.008.

(42) Soares, I. P.; da Silva, A. G.; da Fonseca Alves, R.; de Souza Corrêa, R. A. M.; Ferreira, L. F.; Franco, D. L. Electrochemical Enzymatic Biosensor for Tyramine Based on Polymeric Matrix Derived from 4-Mercaptophenylacetic Acid. *J. Solid State Electrochem.* **2019**, *23* (3), 985–995. https://doi.org/10.1007/s10008-019-04204-w.

(43) Facchinetti, A.; Sparacino, G.; Guerra, S.; Luijf, Y. M.; DeVries, J. H.; Mader, J. K.; Ellmerer, M.; Benesch, C.; Heinemann, L.; Bruttomesso, D.; Avogaro, A.; Cobelli, C.; on behalf of the AP@home

Consortium. Real-Time Improvement of Continuous Glucose Monitoring Accuracy. *Diabetes Care* **2013**, *36* (4), 793–800. https://doi.org/10.2337/dc12-0736.

(44) Kumar Das, S.; Nayak, K. K.; Krishnaswamy, P. R.; Kumar, V.; Bhat, N. Review—Electrochemistry and Other Emerging Technologies for Continuous Glucose Monitoring Devices. *ECS Sens. Plus* **2022**, *1* (3), 031601. https://doi.org/10.1149/2754-2726/ac7abb.

(45) Zou, Y.; Chu, Z.; Guo, J.; Liu, S.; Ma, X.; Guo, J. Minimally Invasive Electrochemical Continuous Glucose Monitoring Sensors: Recent Progress and Perspective. *Biosens. Bioelectron.* **2023**, *225*, 115103. https://doi.org/10.1016/j.bios.2023.115103.

(46) Paldus, B.; Lee, M. H.; O'Neal, D. N. Insulin Pumps in General Practice. *Aust. Prescr.* **2018**, *41* (6), 186–190. https://doi.org/10.18773/austprescr.2018.056.

(47) Vaddiraju, S.; Burgess, D. J.; Tomazos, I.; Jain, F. C.; Papadimitrakopoulos, F. Technologies for Continuous Glucose Monitoring: Current Problems and Future Promises. *J. Diabetes Sci. Technol.* **2010**, *4* (6), 1540–1562. https://doi.org/10.1177/193229681000400632.

(48) Ginsberg, B. H. Factors Affecting Blood Glucose Monitoring: Sources of Errors in Measurement. *J. Diabetes Sci. Technol.* **2009**, *3* (4), 903–913. https://doi.org/10.1177/193229680900300438.

(49) Schultz, J.; Uddin, Z.; Singh, G.; Howlader, M. M. R. Glutamate Sensing in Biofluids: Recent Advances and Research Challenges of Electrochemical Sensors. *The Analyst* **2020**, *145* (2), 321–347. https://doi.org/10.1039/C9AN01609K.

(50) Fenoy, G. E.; Marmisollé, W. A.; Azzaroni, O.; Knoll, W. Acetylcholine Biosensor Based on the Electrochemical Functionalization of Graphene Field-Effect Transistors. *Biosens. Bioelectron.* **2020**, *148*, 111796. https://doi.org/10.1016/j.bios.2019.111796.

(51) Rathee, K.; Dhull, V.; Dhull, R.; Singh, S. Biosensors Based on Electrochemical Lactate Detection: A Comprehensive Review. *Biochem. Biophys. Rep.* **2016**, *5*, 35–54. https://doi.org/10.1016/j.bbrep.2015.11.010.

(52) Zeng, X.; Shen, Z.; Mernaugh, R. Recombinant Antibodies and Their Use in Biosensors. *Anal. Bioanal. Chem.* **2012**, *402* (10), 3027–3038. https://doi.org/10.1007/s00216-011-5569-z.

(53) Sharma, S.; Byrne, H.; O'Kennedy, R. J. Antibodies and Antibody-Derived Analytical Biosensors. *Essays Biochem.* **2016**, *60* (1), 9–18. https://doi.org/10.1042/EBC20150002.

(54) Parlak, O.; Richter-Dahlfors, A. Bacterial Sensing and Biofilm Monitoring for Infection Diagnostics. *Macromol. Biosci.* **2020**, *20* (11), 2000129. https://doi.org/10.1002/mabi.202000129.

(55) Hau, J.; Hendriksen, C. F. M. Refinement of Polyclonal Antibody Production by Combining Oral Immunization of Chickens with Harvest of Antibodies from the Egg Yolk. *ILAR J.* **2005**, *46* (3), 294–299. https://doi.org/10.1093/ilar.46.3.294.

(56) Andersson, B. Studies on the Regulation of Avidity at the Level of the Single Antibody-Forming Cell. *J. Exp. Med.* **1970**, *132* (1), 77–88. https://doi.org/10.1084/jem.132.1.77.

(57) Hanan, R.; Oyama, J. Inhibition of Antibody Formation in Mature Rabbits by Contact with the Antigen at an Early Age. *J. Immunol.* **1954**, *73* (1), 49–53. https://doi.org/10.4049/jimmunol.73.1.49.

(58) Jakobovits, A.; Amado, R. G.; Yang, X.; Roskos, L.; Schwab, G. From XenoMouse Technology to Panitumumab, the First Fully Human Antibody Product from Transgenic Mice. *Nat. Biotechnol.* **2007**, *25* (10), 1134–1143. https://doi.org/10.1038/nbt1337.

(59) Green, L. L. Antibody Engineering via Genetic Engineering of the Mouse: XenoMouse Strains Are a Vehicle for the Facile Generation of Therapeutic Human Monoclonal Antibodies. *J. Immunol. Methods* **1999**, *231* (1–2), 11–23. https://doi.org/10.1016/S0022-1759(99)00137-4.

(60) Lee, E.-C.; Liang, Q.; Ali, H.; Bayliss, L.; Beasley, A.; Bloomfield-Gerdes, T.; Bonoli, L.; Brown, R.; Campbell, J.; Carpenter, A.; Chalk, S.; Davis, A.; England, N.; Fane-Dremucheva, A.; Franz, B.; Germaschewski, V.; Holmes, H.; Holmes, S.; Kirby, I.; Kosmac, M.; Legent, A.; Lui, H.; Manin, A.; O'Leary, S.; Paterson, J.; Sciarrillo, R.; Speak, A.; Spensberger, D.; Tuffery, L.; Waddell, N.; Wang, W.; Wells, S.; Wong, V.; Wood, A.; Owen, M. J.; Friedrich, G. A.; Bradley, A. Complete Humanization of the Mouse Immunoglobulin Loci Enables Efficient Therapeutic Antibody Discovery. *Nat. Biotechnol.* **2014**, *32* (4), 356–363. https://doi.org/10.1038/nbt.2825.

(61) Lonberg, N. Human Antibodies from Transgenic Animals. *Nat. Biotechnol.* **2005**, *23* (9), 1117–1125. https://doi.org/10.1038/nbt1135.

(62) Roque, A. C. A.; Lowe, C. R.; Taipa, M. A. Antibodies and Genetically Engineered Related Molecules: Production and Purification. *Biotechnol. Prog.* **2004**, *20* (3), 639–654. https://doi.org/10.1021/bp030070k.

(63) Gorovits, B.; McNally, J.; Fiorotti, C.; Leung, S. Protein-Based Matrix Interferences in Ligand-Binding Assays. *Bioanalysis* **2014**, *6* (8), 1131–1140. https://doi.org/10.4155/bio.14.56.

(64) Hoogenboom, H. R.; de Bruïne, A. P.; Hufton, S. E.; Hoet, R. M.; Arends, J.-W.; Roovers, R. C. Antibody Phage Display Technology and Its Applications. *Immunotechnology* **1998**, *4* (1), 1–20. https://doi.org/10.1016/S1380-2933(98)00007-4.

(65) Conroy, P. J.; Hearty, S.; Leonard, P.; O'Kennedy, R. J. Antibody Production, Design and Use for Biosensor-Based Applications. *Semin. Cell Dev. Biol.* **2009**, *20* (1), 10–26. https://doi.org/10.1016/j.semcdb.2009.01.010.

(66) Holford, T. R. J.; Davis, F.; Higson, S. P. J. Recent Trends in Antibody Based Sensors. *Biosens. Bioelectron.* **2012**, *34* (1), 12–24. https://doi.org/10.1016/j.bios.2011.10.023.

(67) Ivnitski, D.; Abdel-Hamid, I.; Atanasov, P.; Wilkins, E.; Stricker, S. Application of Electrochemical Biosensors for Detection of Food Pathogenic Bacteria. *Electroanalysis* **2000**, *12* (5), 317–325. https://doi.org/10.1002/(SICI)1521-4109(20000301)12:5<317::AID-ELAN317>3.0.CO;2-A.

(68) Singh, A.; Pasha, S. K.; Manickam, P.; Bhansali, S. Single-Domain Antibody Based Thermally Stable Electrochemical Immunosensor. *Biosens. Bioelectron.* **2016**, *83*, 162–168. https://doi.org/10.1016/j.bios.2016.04.054.

(69) Feng, L.-N.; Peng, J.; Zhu, Y.-D.; Jiang, L.-P.; Zhu, J.-J. Synthesis of Cd2+-Functionalized Titanium Phosphate Nanoparticles and Application as Labels for Electrochemical Immunoassays. *Chem. Commun.* **2012**, *48* (37), 4474. https://doi.org/10.1039/c2cc31552a.

(70) Ma, H.; Ó'Fágáin, C.; O'Kennedy, R. Antibody Stability: A Key to Performance - Analysis, Influences and Improvement. *Biochimie* **2020**, *177*, 213–225. https://doi.org/10.1016/j.biochi.2020.08.019.

(71) Tomita, S.; Matsuda, A.; Nishinami, S.; Kurita, R.; Shiraki, K. One-Step Identification of Antibody Degradation Pathways Using Fluorescence Signatures Generated by Cross-Reactive DNA-Based Arrays. *Anal. Chem.* **2017**, *89* (15), 7818–7822. https://doi.org/10.1021/acs.analchem.7b01264.

(72) Akazawa-Ogawa, Y.; Nagai, H.; Hagihara, Y. Heat Denaturation of the Antibody, a Multi-Domain Protein. *Biophys. Rev.* **2018**, *10* (2), 255–258. https://doi.org/10.1007/s12551-017-0361-8.

(73) Yang, O.; Qadan, M.; Ierapetritou, M. Economic Analysis of Batch and Continuous Biopharmaceutical Antibody Production: A Review. *J. Pharm. Innov.* **2020**, *15* (1), 182–200. https://doi.org/10.1007/s12247-018-09370-4.

(74) Santhanam, M.; Algov, I.; Alfonta, L. DNA/RNA Electrochemical Biosensing Devices a Future Replacement of PCR Methods for a Fast Epidemic Containment. *Sensors* **2020**, *20* (16), 4648. https://doi.org/10.3390/s20164648.

(75) Campuzano, S.; Pedrero, M.; Barderas, R.; Pingarrón, J. M. Empowering Electrochemical Biosensing through Nanostructured or Multifunctional Nucleic Acid or Peptide Biomaterials. *Adv. Mater. Technol.* **2022**, *7* (10), 2200310. https://doi.org/10.1002/admt.202200310.

(76) Zhang, Z.; Sen, P.; Adhikari, B. R.; Li, Y.; Soleymani, L. Development of Nucleic-Acid-Based Electrochemical Biosensors for Clinical Applications. *Angew. Chem. Int. Ed.* **2022**, *61* (50). https://doi.org/10.1002/anie.202212496.

(77) Curulli, A. Electrochemical Biosensors in Food Safety: Challenges and Perspectives. *Molecules* **2021**, *26* (10), 2940. https://doi.org/10.3390/molecules26102940.

(78) Fan, C.; Plaxco, K. W.; Heeger, A. J. Electrochemical Interrogation of Conformational Changes as a Reagentless Method for the Sequence-Specific Detection of DNA. *Proc. Natl. Acad. Sci.* **2003**, *100* (16), 9134–9137. https://doi.org/10.1073/pnas.1633515100.

(79) Lakhin, A. V.; Tarantul, V. Z.; Gening, L. V. Aptamers: Problems, Solutions and Prospects. *Acta Naturae* **2013**, *5* (4), 34–43. https://doi.org/10.32607/20758251-2013-5-4-34-43.

(80) Li, F.; Zhang, H.; Wang, Z.; Newbigging, A. M.; Reid, M. S.; Li, X.-F.; Le, X. C. Aptamers Facilitating Amplified Detection of Biomolecules. *Anal. Chem.* **2015**, *87* (1), 274–292. https://doi.org/10.1021/ac5037236.

(81) Byun, J. Recent Progress and Opportunities for Nucleic Acid Aptamers. *Life* **2021**, *11* (3), 193. https://doi.org/10.3390/life11030193.

(82) Ruscito, A.; DeRosa, M. C. Small-Molecule Binding Aptamers: Selection Strategies, Characterization, and Applications. *Front. Chem.* **2016**, *4*. https://doi.org/10.3389/fchem.2016.00014.

(83) Catuogno, S.; Esposito, C. L. Aptamer Cell-Based Selection: Overview and Advances. *Biomedicines* **2017**, *5* (4), 49. https://doi.org/10.3390/biomedicines5030049.

(84) Song, K.-M.; Lee, S.; Ban, C. Aptamers and Their Biological Applications. *Sensors* **2012**, *12* (1), 612–631. https://doi.org/10.3390/s120100612.

(85) Ospina-Villa, J. D.; Cisneros-Sarabia, A.; Sánchez-Jiménez, M. M.; Marchat, L. A. Current Advances in the Development of Diagnostic Tests Based on Aptamers in Parasitology: A Systematic Review. *Pharmaceutics* **2020**, *12* (11), 1046. https://doi.org/10.3390/pharmaceutics12111046.

(86) Thiviyanathan, V.; Gorenstein, D. G. Aptamers and the next Generation of Diagnostic Reagents. *PROTEOMICS - Clin. Appl.* **2012**, *6* (11–12), 563–573. https://doi.org/10.1002/prca.201200042.

(87) Fu, Z.; Xiang, J. Aptamers, the Nucleic Acid Antibodies, in Cancer Therapy. *Int. J. Mol. Sci.* **2020**, *21* (8), 2793. https://doi.org/10.3390/ijms21082793.

(88) Niederlender, S.; Fontaine, J.-J.; Karadjian, G. Potential Applications of Aptamers in Veterinary Science. *Vet. Res.* **2021**, *52* (1), 79. https://doi.org/10.1186/s13567-021-00948-4.

(89) Schmitz, F. R. W.; Valério, A.; de Oliveira, D.; Hotza, D. An Overview and Future Prospects on Aptamers for Food Safety. *Appl. Microbiol. Biotechnol.* **2020**, *104* (16), 6929–6939. https://doi.org/10.1007/s00253-020-10747-0.

(90) Zhang, Y.; Lai, B.; Juhas, M. Recent Advances in Aptamer Discovery and Applications. *Molecules* **2019**, *24* (5), 941. https://doi.org/10.3390/molecules24050941.

(91) Amirjani, A.; Rahbarimehr, E. Recent Advances in Functionalization of Plasmonic Nanostructures for Optical Sensing. *Microchim. Acta* **2021**, *188* (2), 57. https://doi.org/10.1007/s00604-021-04714-3.

(92) E. Wang, R.; Zhang, Y.; Cai, J.; Cai, W.; Gao, T. Aptamer-Based Fluorescent Biosensors. *Curr. Med. Chem.* **2011**, *18* (27), 4175–4184. https://doi.org/10.2174/092986711797189637.

(93) Slavkovic, S.; Johnson, P. E. Isothermal Titration Calorimetry Studies of Aptamer-Small Molecule Inter- Actions: Practicalities and Pitfalls. *OPEN ACCESS* **2018**, *2*.

(94) Minetti, C. A.; Remeta, D. P. Forces Driving a Magic Bullet to Its Target: Revisiting the Role of Thermodynamics in Drug Design, Development, and Optimization. *Life* **2022**, *12* (9), 1438. https://doi.org/10.3390/life12091438.

(95) Jarczewska, M.; Kékedy-Nagy, L.; Nielsen, J. S.; Campos, R.; Kjems, J.; Malinowska, E.; Ferapontova, E. E. Electroanalysis of PM-Levels of Urokinase Plasminogen Activator in Serum by Phosphorothioated RNA Aptamer. *The Analyst* **2015**, *140* (11), 3794–3802. https://doi.org/10.1039/C4AN02354D.

(96) Lazanas, A. Ch.; Prodromidis, M. I. Electrochemical Impedance Spectroscopy─A Tutorial. *ACS Meas. Sci. Au* **2023**, acsmeasuresciau.2c00070. https://doi.org/10.1021/acsmeasuresciau.2c00070.

(97) Vivier, V.; Orazem, M. E. Impedance Analysis of Electrochemical Systems. *Chem. Rev.* **2022**, *122* (12), 11131–11168. https://doi.org/10.1021/acs.chemrev.1c00876.

(98) Rahbarimehr, E.; Chao, H. P.; Churcher, Z. R.; Slavkovic, S.; Kaiyum, Y. A.; Johnson, P. E.; Dauphin-Ducharme, P. Finding the Lost Dissociation Constant of Electrochemical Aptamer-Based Biosensors. *Anal. Chem.* **2023**, *95* (4), 2229–2237. https://doi.org/10.1021/acs.analchem.2c03566.

(99) Magar, H. S.; Hassan, R. Y. A.; Mulchandani, A. Electrochemical Impedance Spectroscopy (EIS): Principles, Construction, and Biosensing Applications. *Sensors* **2021**, *21* (19), 6578. https://doi.org/10.3390/s21196578.

(100) Liu, Z.; Sun, M.; Zhao, H.; Zhao, M. Acute Self-Induced Poisoning With Sodium Ferrocyanide and Methanol Treated With Plasmapheresis and Continuous Renal Replacement Therapy

Successfully: A Case Report. *Medicine (Baltimore)* **2015**, *94* (21), e890. https://doi.org/10.1097/MD.0000000000000890.

(101) Yu, Z.; Lai, R. Y. A Reagentless and Reusable Electrochemical Aptamer-Based Sensor for Rapid Detection of Ampicillin in Complex Samples. *Talanta* **2018**, *176*, 619–624. https://doi.org/10.1016/j.talanta.2017.08.057.

(102) Dauphin-Ducharme, P.; Yang, K.; Arroyo-Currás, N.; Ploense, K. L.; Zhang, Y.; Gerson, J.; Kurnik, M.; Kippin, T. E.; Stojanovic, M. N.; Plaxco, K. W. Electrochemical Aptamer-Based Sensors for Improved Therapeutic Drug Monitoring and High-Precision, Feedback-Controlled Drug Delivery. *ACS Sens.* **2019**, *4* (10), 2832–2837. https://doi.org/10.1021/acssensors.9b01616.

(103) Arroyo-Currás, N.; Somerson, J.; Vieira, P. A.; Ploense, K. L.; Kippin, T. E.; Plaxco, K. W. Real-Time Measurement of Small Molecules Directly in Awake, Ambulatory Animals. *Proc. Natl. Acad. Sci.* **2017**, *114* (4), 645–650. https://doi.org/10.1073/pnas.1613458114.

(104) Idili, A.; Gerson, J.; Kippin, T.; Plaxco, K. W. Seconds-Resolved, In Situ Measurements of Plasma Phenylalanine Disposition Kinetics in Living Rats. *Anal. Chem.* **2021**, *93* (8), 4023–4032. https://doi.org/10.1021/acs.analchem.0c05024.

(105) Wu, Y.; Ranallo, S.; Del Grosso, E.; Chamoro-Garcia, A.; Ennis, H. L.; Milosavić, N.; Yang, K.; Kippin, T.; Ricci, F.; Stojanovic, M.; Plaxco, K. W. Using Spectroscopy to Guide the Adaptation of Aptamers into Electrochemical Aptamer-Based Sensors. *Bioconjug. Chem.* **2023**, *34* (1), 124–132. https://doi.org/10.1021/acs.bioconjchem.2c00275.

(106) Ferguson, B. S.; Hoggarth, D. A.; Maliniak, D.; Ploense, K.; White, R. J.; Woodward, N.; Hsieh, K.; Bonham, A. J.; Eisenstein, M.; Kippin, T. E.; Plaxco, K. W.; Soh, H. T. Real-Time, Aptamer-Based Tracking of Circulating Therapeutic Agents in Living Animals. *Sci. Transl. Med.* **2013**, *5* (213). https://doi.org/10.1126/scitranslmed.3007095.

(107) Idili, A.; Arroyo-Currás, N.; Ploense, K. L.; Csordas, A. T.; Kuwahara, M.; Kippin, T. E.; Plaxco, K. W. Seconds-Resolved Pharmacokinetic Measurements of the Chemotherapeutic Irinotecan *in Situ* in the Living Body. *Chem. Sci.* **2019**, *10* (35), 8164–8170. https://doi.org/10.1039/C9SC01495K.

(108) Somerson, J.; Plaxco, K. Electrochemical Aptamer-Based Sensors for Rapid Point-of-Use Monitoring of the Mycotoxin Ochratoxin A Directly in a Food Stream. *Molecules* **2018**, *23* (4), 912. https://doi.org/10.3390/molecules23040912.

(109) Shaver, A.; Kundu, N.; Young, B. E.; Vieira, P. A.; Sczepanski, J. T.; Arroyo-Currás, N. Nuclease Hydrolysis Does Not Drive the Rapid Signaling Decay of DNA Aptamer-Based Electrochemical Sensors in Biological Fluids. *Langmuir* **2021**, *37* (17), 5213–5221. https://doi.org/10.1021/acs.langmuir.1c00166.

(110) Xiao, Y.; Uzawa, T.; White, R. J.; DeMartini, D.; Plaxco, K. W. On the Signaling of Electrochemical Aptamer-Based Sensors: Collision- and Folding-Based Mechanisms. *Electroanalysis* **2009**, *21* (11), 1267–1271. https://doi.org/10.1002/elan.200804564.

(111) White, R. J.; Rowe, A. A.; Plaxco, K. W. Re-Engineering Aptamers to Support Reagentless, Self-Reporting Electrochemical Sensors. *The Analyst* **2010**, *135* (3), 589. https://doi.org/10.1039/b921253a.

(112) Parolo, C.; Idili, A.; Ortega, G.; Csordas, A.; Hsu, A.; Arroyo-Currás, N.; Yang, Q.; Ferguson, B. S.; Wang, J.; Plaxco, K. W. Real-Time Monitoring of a Protein Biomarker. *ACS Sens.* **2020**, *5* (7), 1877–1881. https://doi.org/10.1021/acssensors.0c01085.

(113) Arroyo-Currás, N.; Dauphin-Ducharme, P.; Ortega, G.; Ploense, K. L.; Kippin, T. E.; Plaxco, K. W. Subsecond-Resolved Molecular Measurements in the Living Body Using Chronoamperometrically Interrogated Aptamer-Based Sensors. *ACS Sens.* **2018**, *3* (2), 360–366. https://doi.org/10.1021/acssensors.7b00787.

(114) Downs, A. M.; Gerson, J.; Ploense, K. L.; Plaxco, K. W.; Dauphin-Ducharme, P. Subsecond-Resolved Molecular Measurements Using Electrochemical Phase Interrogation of Aptamer-Based Sensors. *Anal. Chem.* **2020**, *92* (20), 14063–14068. https://doi.org/10.1021/acs.analchem.0c03109.

(115) Arroyo-Currás, N.; Dauphin-Ducharme, P.; Scida, K.; Chávez, J. L. From the Beaker to the Body: Translational Challenges for Electrochemical, Aptamer-Based Sensors. *Anal. Methods* **2020**, *12* (10), 1288–1310. https://doi.org/10.1039/D0AY00026D.

(116) Li, H.; Dauphin-Ducharme, P.; Ortega, G.; Plaxco, K. W. Calibration-Free Electrochemical Biosensors Supporting Accurate Molecular Measurements Directly in Undiluted Whole Blood. *J. Am. Chem. Soc.* **2017**, *139* (32), 11207–11213. https://doi.org/10.1021/jacs.7b05412.

(117) Mirceski, V.; Skrzypek, S.; Stojanov, L. Square-Wave Voltammetry. *ChemTexts* **2018**, *4* (4), 17. https://doi.org/10.1007/s40828-018-0073-0.

(118) Komorsky-Lovrić, Š.; Lovrić, M. Measurements of Redox Kinetics of Adsorbed Azobenzene by "a Quasireversible Maximum" in Square-Wave Voltammetry. *Electrochimica Acta* **1995**, *40* (11), 1781–1784. https://doi.org/10.1016/0013-4686(95)00097-X.

(119) Lovrić, M.; Komorsky-Lovric, Š. Square-Wave Voltammetry of an Adsorbed Reactant. *J. Electroanal. Chem. Interfacial Electrochem.* **1988**, *248* (2), 239–253. https://doi.org/10.1016/0022-0728(88)85089-7.

(120) Dauphin-Ducharme, P.; Plaxco, K. W. Maximizing the Signal Gain of Electrochemical-DNA Sensors. *Anal. Chem.* **2016**, *88* (23), 11654–11662. https://doi.org/10.1021/acs.analchem.6b03227.

(121) Blum, R. A.; Kohli, R. K.; Harrison, N. J.; Schentag, J. J. Pharmacokinetics of Ampicillin (2.0 Grams) and Sulbactam (1.0 Gram) Coadministered to Subjects with Normal and Abnormal Renal Function and with End-Stage Renal Disease on Hemodialysis. *Antimicrob. Agents Chemother.* **1989**, *33* (9), 1470–1476. https://doi.org/10.1128/AAC.33.9.1470.

(122) Newton, P.; Simpson, A.; Wanwimolruk, S.; Maliakal, P.; Villegas, L.; Kuypers, D.; White, N. J. Oral Quinine Pharmacokinetics and Dietary Salt Intake. *Eur. J. Clin. Pharmacol.* **2001**, *57* (2), 111–113. https://doi.org/10.1007/s002280100283.

(123) Blaho, K.; Logan, B.; Winbery, S.; Park, L.; Schwilke, E. Blood Cocaine and Metabolite Concentrations, Clinical Findings, and Outcome of Patients Presenting to an ED. *Am. J. Emerg. Med.* **2000**, *18* (5), 593–598. https://doi.org/10.1053/ajem.2000.9282.

(124) Speth, P. A. J.; van Hoesel, Q. G. C. M.; Haanen, C. Clinical Pharmacokinetics of Doxorubicin: *Clin. Pharmacokinet.* **1988**, *15* (1), 15–31. https://doi.org/10.2165/00003088-198815010-00002.

(125) Forrester, T. An Estimate of Adenosine Triphosphate Release into the Venous Effluent from Exercising Human Forearm Muscle. *J. Physiol.* **1972**, *224* (3), 611–628. https://doi.org/10.1113/jphysiol.1972.sp009915.

(126) Li, S.; Marquardt, R. R.; Frohlich, A. A.; Vitti, T. G.; Crow, G. Pharmacokinetics of Ochratoxin A and Its Metabolites in Rats. *Toxicol. Appl. Pharmacol.* **1997**, *145* (1), 82–90. https://doi.org/10.1006/taap.1997.8155.

CHAPTER 2: FINDING THE LOST DISSOCIATION CONSTANT OF ELECTROCHEMICAL APTAMER-BASED BIOSENSORS

2.1. Author's note

This article was submitted on August 15, 2022, to *Analytical Chemistry*, accepted on December 26, 2022, and published on January 13, 2023. *Anal. Chem.* **2023**, *95*, 4, 2229–2237.

It should be noted that the references pertaining to this article are included in the bibliography at the end of this chapter.

2.2. Authors' contributions

Erfan Rahbarimehr designed and performed all electrochemical measurements and wrote the manuscript jointly with Prof. Philippe Dauphin Ducharme. Hoi Pui Chao, Zachary R. Churcher, Sladjana Slavkovic, and Yunus A. Kaiyum designed and performed all ITC measurements in Prof. Philip E. Johnson's laboratory at York University. Prof. Philip E. Johnson revised the manuscript.

2.3. ABSTRACT

Electrochemical aptamer-based (E-AB) biosensors afford real-time measurements of the concentrations of molecules directly in complex matrices and in the body, offering alternative strategies to develop innovative personalized medicine tools. While different electroanalytical techniques have been used to interrogate E-AB sensors (i.e., cyclic voltammetry, electrochemical impedance spectroscopy, and chronoamperometry) to resolve the change in electron transfer of the aptamer's covalently attached redox reporter, square-wave voltammetry remains a widely used technique due to its ability to maximize the redox reporter's faradic contribution to the measured current. Several E-AB sensors interrogated with this technique, however, show lower aptamer affinity (i.e., μM−mM) even in the face of employing aptamers that have high affinities (i.e., nM−μM) when characterized using solution techniques such as isothermal titration calorimetry (ITC) or fluorescence spectroscopy. Given past reports showing that E-AB sensor's response is dependent on square-wave interrogation parameters (i.e., frequency and amplitude), we hypothesized that the difference in dissociation constants measured with solution techniques stemmed from the electrochemical interrogation technique itself. In response, we decided to compare six dissociation constants of aptamers when characterized in solution with ITC and when interrogated on electrodes with electrochemical impedance spectroscopy, a technique able to, in contrast to square-wave voltammetry, deconvolute and quantify E-AB sensors' contributions to the measured current. In doing so, we found that we were able to measure dissociation constants that were either separated by 2−3-fold or within experimental errors. These results are in contrast with square-wave voltammetry-measured dissociation constants that are at the most separated by 2−3 orders of magnitude from ones measured by ITC. We thus envision that the versatility and time scales covered by electrochemical impedance spectroscopy offer the highest sensitivity to measure target binding in electrochemical biosensors relying on changes in electron transfer rates.

KEYWORDS. Aptamer, Electrochemical biosensor, Electrochemical aptamer-based biosensors, Square-wave voltammetry, Electrochemical impedance spectroscopy, Isothermal titration calorimetry

2.4. INTRODUCTION

Electrochemical aptamer-based (E-AB) biosensors are emerging analytical tools capable of expanding the number of molecules monitored at the point of care to solve the paradigm of personalized medicine. E-AB sensors are composed of a redox-reporter-modified short nucleic acid sequence (an aptamer) immobilized on a gold electrode surface that specifically binds to a target molecule (Figure 16).[1–4] Upon target recognition, the redox reporter undergoes a binding-induced change in electron transfer that is kinetically limited by its diffusion to the electrode[5–7] and/or an intrinsic change in its electron transfer (i.e., reorganizational energy),[8] allowing for fast (i.e., subsecond) quantitative determination of the target concentration directly in complex matrices and in the body.[9–13] Using aptamers for different ligands, E-AB sensors can measure a wide variety of targets (i.e., antibiotics, chemotherapeutics, drugs of abuse, proteins, etc.), highlighting their generalizability.[14–19] As E-AB sensors rely on an electrochemical signaling mechanism, they can be miniaturized and powered by a handheld portable device, leaving them ideally suited to transform our understanding of drug pharmacology and design precision medicine approaches for use at the patient's bedside.

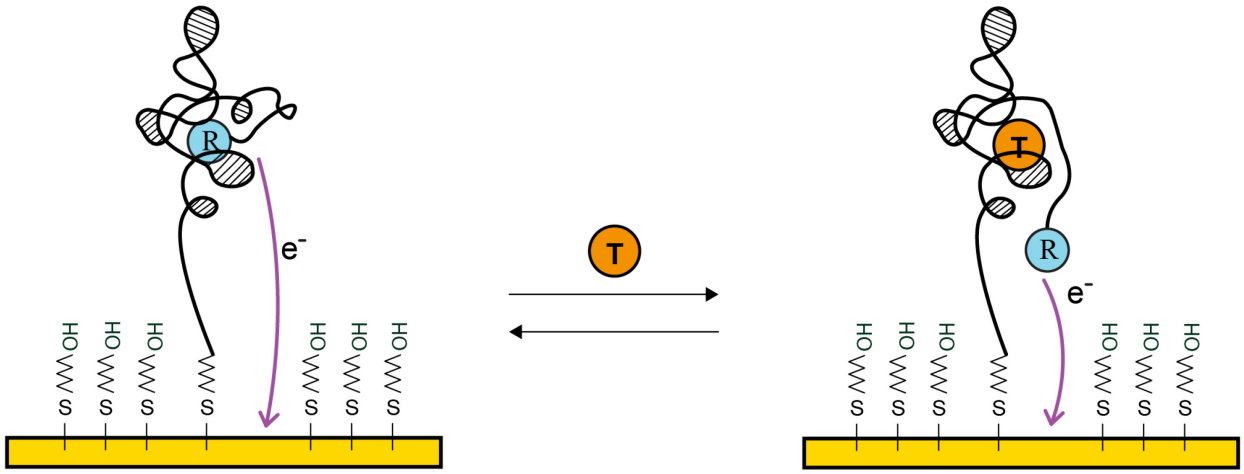

Figure 16. E-AB sensors are composed of a thiol-and-redox-reporter-modified aptamer sequence attached to an alkanethiol-coated gold electrode surface. Upon target recognition, aptamers undergo a binding-induced change in electron transfer that is kinetically limited by a diffusional change[5–7] and/or an intrinsic change in the electron transfer (i.e., reorganizational energy)[8] of the redox reporter, allowing for a quantitative means of measuring target concentration using a plethora of electrochemical techniques.

Despite their many advantages over gold-standard analytical approaches, E-AB sensors show relatively low aptamer affinity (i.e., μM−mM), which hampers their widespread use.[20,21] Aside from doxorubicin, the dissociation constants (K_D) of commonly reported E-AB sensors for adenosine triphosphate, quinine, cocaine, ochratoxin A, and ampicillin, for example, are several fold larger and do not cover the full clinically relevant range at which these molecules should be measured (see Table1). K_D values measured in solution with fluorescence methods and isothermal titration calorimetry (ITC) of the same aptamer sequences are, however, several orders of magnitude smaller and some cover the clinically relevant range (Table 1). We thus wondered why the results of E-AB sensors significantly differed from data acquired via solution-based approaches (i.e., ITC or fluorescence spectroscopy).

E-AB sensors have been examined using a plethora of electrochemical techniques. These include cyclic voltammetry,[45] electrochemical phase interrogation,[12] alternating-current cyclic voltammetry,[3] chronoamperometry,[11,46] and pulse voltammetry such as square-wave voltammetry.[47–49] The latter technique has been widely used as square-wave voltammetry relies on the measurement of two current values at each pulse prior to deriving a difference that leads to the minimization of nonfaradic background currents. Doing so allows for measurements of lower faradic currents essential to resolve electron-transfer reactions of low concentrations of surface-attached redox-reporter-modified aptamers typically used in E-AB sensors. Several reports, however, have found that E-AB sensors' "gain" (i.e., the response produced upon sensor target saturation), when interrogated using square-wave voltammetry, is dependent on the electrochemical interrogation parameters (i.e., square-wave frequency and amplitude).[50–52] We thus hypothesize that differences in E-AB sensors' K_D values with respect to the ones measured via solution measurements were caused by the interrogation parameters in square-wave voltammetry.

In response and to evaluate the impact of the measurement technique on the binding affinity measured by E-AB sensors, we investigated six aptamers using square-wave voltammetry, electrochemical impedance spectroscopy, and ITC methods. In doing so, we found that E-AB sensors' K_D values varied as a function of the electrochemical interrogation technique, while electrochemical impedance spectroscopy results revealed the closest K_D values to the ones measured in solution. We envision that our methodology could prove valuable in developing other sensitive electrochemical biosensors that rely on binding-induced change in electron transfer and determine the influence of attaching bioreceptors on electrodes.

Table 1. K_D values of the Same Aptamer Sequences Interrogated in E-AB Sensors and Using Solution-Based Approaches, Such as Isothermal Titration Calorimetry and Fluorescence Spectroscopy, Reveal Differences with Clinically Relevant Concentrations

target	DNA sequence (5' to 3')	clinical range (μM)	E-AB sensors (μM)	isothermal titration calorimetry (μM)	fluorescence spectroscopy (μM)
ampicillin	TTAGTTGGGGTTCAGTTGG	5.7 - 68.6 [refs[22–24]]	2500 [ref[25]]		0.0098 [ref[26]]
quinine	GGCGACAAGGAAAATCCTTCAACGAAGTGGGTCG-CC	7.4 - 24.4 [refs[27,28]]	~300 - 686 [ref[29]]	0.2 [ref[30]]	0.75 [ref[31]]
cocaine	GACAAGGAAAATCCTTCAATGAAGTGGGTC	0.2 - 3.2 [refs[32,33]]	90 [ref[4]]	45.3 [ref[34]]	
doxorubicin	GGGAATTCGAGCTCGGTACCATCTGTGTAAGGGG-TAAGGGGTGGGGGTGGGTACGTCTAGCTGCAGGC-ATGCAAGCTTGG	0.1 - 18.3 [ref[35]]	9 [ref[36]]		0.2 [ref[37]]
ATP	ACCTGGGGGAGTATTGCGGAGGAAGGT	0.02 - 10.9 [refs[38,39]]	~٢٠0000 [ref[21]]	133[1], 498[2] [ref[40]]	
ochratoxin A	GATCGGGTGTGGGTGGCGTAAAGGGAGC-ATCGGACA	0.025 - 2.5 [refs[41,42]]	6.5 [ref[43]]		0.2 [ref[44]]

[1,2] K_D values for the high and low affinity binding sites

2.5. MATERIALS & METHODS

Sulfuric acid, sodium hydroxide, quinine monohydrochloride dihydrate, vancomycin hydrochloride, and Tris−HCl were obtained from Fisher Scientific (Quebec, Canada). We obtained ochratoxin A from Toronto Research Chemicals (Ontario, Canada). 6-Mercapto-1-hexanol, tris(2- carboxyethyl)phosphine hydrochloride (TCEP), and phosphate-buffered saline (PBS) tablets were obtained from Sigma- Aldrich (Ontario, Canada). All reagents were used as received. PBS (1×) containing 137 mM sodium chloride, 2.7 mM potassium chloride, and 10 mM phosphate buffer was prepared by dissolving five tablets in 1 L of deionized water.

All methylene blue- and thiol-modified aptamer sequences (Figure S1) were purchased from and HPLC-purified by Bio Basic Inc. (Ontario, Canada) and used as received (Table 2). DNA was resolubilized in

deionized water to obtain a 100 μM stock solution. Concentration was assessed using an Implen NanoDrop spectrophotometer (Germany) using the DNA molar absorption coefficient at 260 nm. We then aliquoted the DNA in 2 μL vials and kept them at −20 °C.

2.5.1 Gold Electrode Fabrication and Electrochemical Cleaning

For all electrochemical measurements, we used a three-electrode setup consisting of an Ag|AgCl reference electrode, a platinum counter electrode, and a 2 mm diameter gold working electrode acquired from CH Instruments (Texas). All square-wave voltammetry experiments and electrode fabrication procedures were conducted using a CHI1040C potentiostat.

To fabricate E-AB biosensors, we first performed an electrochemical cleaning step[53] in which gold electrodes were cycled 300 times between −1 and −1.6 V in a 0.5 M NaOH solution at 1 V s^{-1} to remove any thiol residues. We then transferred the electrodes to 0.5 M H_2SO_4 where we applied a potential step from 0 to 2 V for a duration of 5 s followed by a cathodic pulse from 0 to −0.35 V for 10 s. This is followed by 40 cycles between −0.35 and 1.5 V in the same H_2SO_4 solution at 4 V s^{-1} and 8 cycles between the same potential boundaries at a scan rate of 0.1 V s^{-1}. Finally, we switched the electrodes in a 0.05 M H_2SO_4 solution and performed 4 cycles between −0.35 and 1.5 V at 0.1 V s^{-1}. We do so to determine the gold electrode electroactive area via integrating the gold oxide reduction peak and dividing it by the charge required to reduce a monolayer of oxide atoms.[54]

Table 2. Quinine, Vancomycin and Ochratoxin A-Binding Aptamers Sequences.

target	sequence name	5' modification	sequence (5' to 3')	3' modification
quinine	OR2	OH-$(CH_2)_6$-S-S-$(CH_2)_6$-O-	GACAG GGGGA ACCCC TCAAC GAAGT GGGTC	-O-$(CH_2)_6$-NH-CO-CH_2-Methylene blue
	OR3	OH-$(CH_2)_6$-S-S-$(CH_2)_6$-O-	GACAG CGCGA AGCGC TCAAC GAAGT GGGTC	-O-$(CH_2)_6$-NH-CO-CH_2-Methylene blue
	MN19	OH-$(CH_2)_6$-S-S-$(CH_2)_6$-O-	GACAA GGAAA ATCCT TCAAC GAAGT GGGTC	-O-$(CH_2)_6$-NH-CO-CH_2-Methylene blue
	MN20	OH-$(CH_2)_6$-S-S-$(CH_2)_6$-O-	GACAG GGGAA ACCCC TCAAC GAAGT GGGTC	-O-$(CH_2)_6$-NH-CO-CH_2-Methylene blue
vancomycin	vanco4trunc	OH-$(CH_2)_6$-S-S-$(CH_2)_6$-O-	CGAGG GTACC GCAAT AGTAC TTATT GTTCG CCTAT TGTGG GTCGG	-O-$(CH_2)_6$-NH-CO-CH_2-Methylene blue
ochratoxin A		OH-$(CH_2)_6$-S-S-$(CH_2)_6$-O-	GATCG GGTGT GGGTG GCGTA AAGGG AGCAT C	-O-$(CH_2)_6$-NH-CO-CH_2-Methylene blue

2.5.2. Functionalization of Gold Electrodes

We functionalized the freshly cleaned gold electrodes using a 200 nM stock solution of the reduced aptamer. To prepare this solution, we incubated for 1 h at room temperature 2 μL of 10 mM aqueous solution of TCEP to reduce the thiol−thiol bond of the desired aptamer aliquot. We then adjusted the concentration of the reduced aptamer to 200 nM using 1× PBS prior to immersing the cleaned electrodes in 100 μL of the aptamer solution for 1 h at room temperature. We rinsed the electrodes with excess 1× PBS prior to their immersion in a 5 mM 6-mercapto-1- hexanol 1× PBS solution for overnight incubation. Electrodes are then cleaned with excess 1× PBS prior to their use.

2.5.3. E-AB Sensor Characterization

Unless stated differently, we performed all E-AB sensor characterizations at 20 °C and in 1× PBS. We characterized the functionalized electrodes by first acquiring 3 cyclic voltammograms between 0 and −0.5 V at a scan rate of 0.1 V s^{-1} to measure the density of the aptamer. Following the integration of the voltammogram's methylene blue reduction peak, we obtained, on average, an aptamer density of 1.1 × 10^{12} molecules cm^{-2}. We then performed square-wave voltammetry interrogation with frequencies varying from 2 to 1000 Hz while maintaining the potential increments fixed to 1 mV and an amplitude of 25 mV. Using Lovric's formalism[55,56] and extracting the peak current using the open-source data processing tool SACMES,[57] we determined the redox reporter's electron-transfer rate when sensors were in the absence of target. We repeated this step when exposing sensors to saturating amounts of the desired target to determine the optimal square-wave interrogation frequencies (Figure S2). Specifically, given the lower solubility of quinine and ochratoxin A in aqueous environments, we prepared the highest stock solution (i.e., 20 mM) of quinine using 25:75 ethanol to 1× PBS ratio, which we then diluted using 1× PBS, and the highest stock solution (i.e., 800 μM) of ochratoxin A using dimethylsulfoxide, which we then diluted using Tris 1× buffer (containing 20 mM $CaCl_2$, 120 mM NaCl, and 5 mM KCl) adjusted at a pH of 8.

2.5.4. E-AB Sensor Characterization Using Square-Wave Voltammetry

We interrogated the sensors at square-wave frequencies to produce signal-on or signal-off responses while challenging the sensors with increasing amounts of the target (see the representative square-wave

voltammograms in Figure S3). Extracting the peak currents of voltammograms measured at varying target concentrations returns sigmoidal binding traces that we fit to the Langmuir−Hill equation to determine the aptamer's dissociation constant.

2.5.5. E-AB Sensor Characterization Using Electrochemical Impedance Spectroscopy

We performed all of the electrochemical impedance spectroscopy analyses using a BioLogic VMP-300 potentiostat. For MN19, MN20, OR2, and OR3 quinine-binding variants, we degassed using a constant flow of Ar given their lower charge-transfer rates when in the absence of quinine (see Figure S4). For all measurements, we first acquired a cyclic voltammogram between 0 and −0.5 V vs Ag|AgCl to determine the methylene blue redox potential through an average of the oxidation and reduction peak potentials. We then used this potential for potentiostatic electrochemical impedance measurements as a fixed value and applied a sinusoidal perturbation of 10 mV in amplitude. We varied the frequencies of the oscillations from 10 kHz to 0.1 Hz and performed 10 measurements per decade of frequencies (a total of 50 points per measurement, see Figure S5 for a representative Bode representation of one measurement). Each measurement requires less than 5 min, and we typically acquire 25 points to resolve an entire binding trace, thus amounting to 1250 sensor interrogations over a 2 h period. Through this period, we did not observe experimentally significant changes in the sensor's phase response (Figure S6). We repeated these measurements when sensors were exposed to an increasing amount of the aptamer's corresponding target. As commonly done and per past literature,[58–62] we performed a nonlinear fit of the resulting impedimetric traces using BioLogic's algorithms to the equivalent circuit diagram (Figure 3B). From this, we determined the interfacial charge-transfer resistance (i.e., R_{ct}) associated with the electron-transfer reaction of the redox reporter. We then plotted these values as a function of target concentration that we fitted to a Langmuir−Hill equation or a two distinct binding site equation to determine K_D values (eq 1).

$$\text{norm\_}R_{ct} = V_{max\_1}\frac{(1-b)\cdot[S]^{n\_1}}{K_{D\_1}^{n\_1} + [S]^{n\_1}} + V_{max\_2}\frac{b\cdot[S]^{n\_2}}{K_{D\_2}^{n\_2} + [S]^{n\_2}} \qquad \text{(Eq. 2.1)}$$

where $\text{norm\_}R_{ct}$ represents the measured normalized charge transfer resistance, [S] is the target concentration, V_{max}_1 and V_{max}_2 are the maximal responses generated by each binding site, n_1 and n_2 are the Hill coefficients associated with each binding site, and b is the dependence of the signal on the target concentration.

2.5.6. Aptamer Characterization Using Isothermal Titration Calorimetry

We performed ITC experiments using a MicroCal VP-ITC instrument following procedures outlined previously.[63] We degassed samples prior to use with a MicroCal ThermoVac unit. In accordance with our electrochemical measurements, we performed all experiments at 20 °C and corrected for the heat of dilution of the titrant. We performed experiments with the aptamer in the cell and the ligand in the syringe. To allow the aptamer to anneal in an intramolecular fashion, we heated all aptamer samples in a boiling water bath for 3 min and then cooled those in an ice bath prior to ITC measurements. Binding experiments consisted of an initial delay of 60 s during which we performed the first injection of 2 µL followed by a 300 s delay, which we removed from data fitting. We then successively added 8 µL of ligand for 34 independent injections spaced at every 300 s. We performed quinine-binding experiments with MN19, MN20, OR2, and OR3 variants that we prepared either at 20 or 40 µM and titrated using a ligand concentration of 0.312 or 0.624 mM prepared in 1× PBS buffer.

We performed titrations of the vancomycin-binding aptamer with vancomycin by diluting a stock aptamer solution to 80 µM and using a ligand concentration of 1.248 mM, also prepared in 1× PBS buffer. We performed titrations of the ochratoxin-binding aptamer with ochratoxin A using an aptamer concentration of 20 µM and a ligand concentration of 0.312 mM in a buffer of 10 mM Tris (pH 8.0), 20 mM $CaCl_2$, 5 mM KCl, and 120 mM NaCl containing 3% (v/v) DMSO. We fitted all data to a one- set-of sites binding model using the manufacturer-provided data-fitting package within Origin 7.

2.6. RESULTS AND DISCUSSION

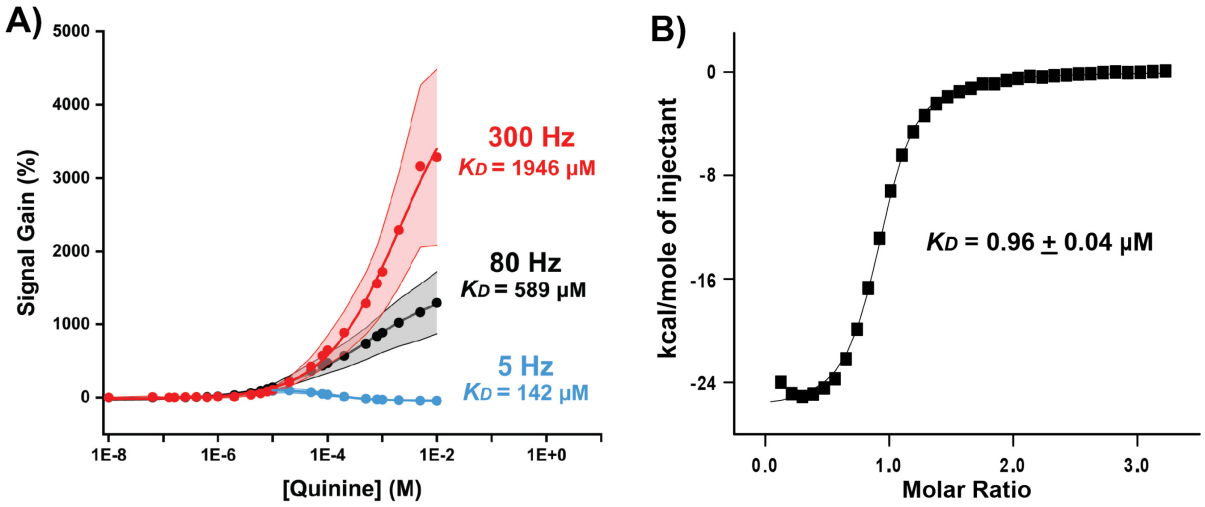

Figure 17. As expected, when interrogating E-AB sensors with the widely used technique, square-wave voltammetry, we observe signal-off to signal-on responses with variable sensor gains. (A) When looking at the quinine-binding MN19 aptamer variant, for example, we measured gains varying from −44 to 3284% depending on the square-wave frequency. In doing so, we observed that when fitting the binding curve to the Langmuir−Hill equation, the determined K_D values varied as a function of square-wave frequency. Specifically, the MN19 aptamer variant produced K_D values of 142 and 1946 μM, values separated by more than an order of magnitude, when interrogating at 5 and 300 Hz, respectively. We thus foresee that this could in part explain differences with solution measurements. (B) When challenging aptamers with increasing amounts of their respective targets in the solution and monitoring the heat released from binding using ITC, we measured lower K_D values for all of the aptamers we tested. The MN19 quinine-binding aptamer, for example, produced a K_D value of 0.96 ± 0.04 μM. This value is more than 2 orders of magnitude smaller than values measured using the lowest square-wave voltammetry frequency. We likewise observed this difference between the solution and surface measurements for other aptamers we tested (Figures S7 and S8 and Table 3).

E-AB sensors interrogated using square-wave voltammetry displayed frequency-dependent K_D values. We observed this when electrochemically interrogating six different E-AB sensors with increasing amounts of their respective targets using previously reported aptamers binding quinine,[64] vancomycin,[14] and ochratoxin A.[44] In doing so, we found that, for example, the quinine-binding MN19 aptamer variant produced signal-off to signal-on responses that depend on the square-wave interrogation frequency with gains varying from −44 to +3284% (Figure 17A). We likewise observed this biosensor gain dependence on the square-wave frequency when looking at the other aptamers (Figure S7). We also found that the binding curves for a single aptamer measured at each of the square-wave frequencies yielded different K_D values. Measuring frequency-dependent K_D values is counterintuitive since an aptamer, as a recognition element, should interact with target molecules with one affinity, at a particular set of experimental conditions, and thus yield a single K_D value. When fitting the binding traces to the Langmuir−Hill equation, the quinone binding MN19 aptamer variant produced K_D values of around 142 μM at 5 Hz and 1946 μM at 300 Hz, values separated by more than an order of magnitude (Figure 17A). We observed similar trends for the other aptamers we investigated and found that the quinine-binding MN20 aptamer produced the largest K_D value difference depending on the square-wave interrogation parameters. Such differences are significant and could lead to incompatible E-AB sensors for a given application due to high aptamer affinity with respect to the target's clinically relevant range.

ITC-derived binding results revealed K_D values that significantly differ from the ones measured with square-wave voltammetry. We investigated this by titrating quinine, vancomycin, and ochratoxin A with the corresponding aptamers at the same temperature and buffer conditions as for our square-wave

voltammetry experiments and monitored the heat released from binding (Figures 17B and S8). In doing so, we found that, for example, the MN19 quinine-binding aptamer variant produced a K_D value of 0.96 ± 0.04 μM (Figure 17B). Considering the close structural similarities to MN20, OR2, and OR3, notably within the reported ligand-binding site,[30] all K_D values we measured using ITC fell within a ∼2-fold difference from one another (Table 3). We measured the largest and lowest K_D values for vancomycin- and ochratoxin A-binding aptamers, respectively (Table 3). When comparing the K_D value measured for the MN19 quinine-binding aptamer with our square-wave voltammetry results at the lowest frequency (5 Hz in Figure 17A), for example, we observed differences of more than two orders of magnitude (Table 3). When compared with K_D values measured at higher square-wave frequencies (i.e., >100 Hz), this gap further increased to more than three orders of magnitude. This trend also holds for the MN20, OR2, and OR3 variants, which also produced K_D values more than two orders of magnitude apart from ones measured using ITC. From all aptamers we tested, only the vancomycin-binding aptamer produced experimentally equivalent K_D values when measured in the solution or when electrode-attached. We envision that this is because of two reasons. To start, the weaker binding of vancomycin makes solution K_D value determination via ITC more challenging due to the higher target and aptamer concentrations required. Second, we presume that because the vancomycin-binding aptamer has a faster redox reporter electron-transfer rate when the E-AB sensor is in the absence of the target (i.e., 48 s^{-1} vs <2 s^{-1} for the quinine-binding aptamers, for example), square-wave voltammetry is sensitive enough over the entire square-wave frequency spectra to monitor the binding-induced change in electron transfer incurred by the sensor. Our ITC results thus confirmed the large reported differences in affinities between the solution and surface measurements for five out of six aptamers we tested (Table 1).

We hypothesize that differences in K_D values measured in solution via ITC and on the surface via square-wave voltammetry could be explained by either (1) a difference in how binding is transduced or (2) differences in measurement sensitivities. Our first hypothesis is because, in isothermal titration calorimetry, target binding is measured due to the heat released or taken up,[64,65] while in square-wave voltammetry, target binding is secondary to the measured change in the redox reporter electron transfer that is kinetically limited by its diffusion to the electrode[5–7] or its intrinsic electron transfer (i.e., reorganizational energy).[8] As a result of this, one may argue that because of the difference in signal transduction mechanisms and that in one case aptamers are unlabeled while in the other aptamers are surface-attached and labeled with a thiol and a redox reporter, K_D values cannot be directly compared. We, nevertheless, expected trends and were interested to observe whether K_D values of the different

aptamers remained unchanged. For instance, with the highest K_D value of 60 μM measured by ITC (Table 3), the vancomycin-binding showed the second-lowest K_D value measured in square-wave voltammetry of all aptamers tested. We thus proposed, as our second hypothesis, that square-wave voltammetry lacks sensitivity to measure binding. This is because, when changing the interrogation frequency in square-wave voltammetry, in addition to measuring competing nonfaradic and faradic current contributions (i.e., oxygen reduction current contribution is more important at frequencies <10 Hz (see Figure S4)), we tuned the time scale at which we measured the redox reporter's electron-transfer event that ultimately yielded in what we referred as an "apparent" K_D value. An apparent K_D value implicates that at certain square-wave interrogation frequencies, methylene blue's electron transfer occurs on a different time scale than the one at which the measurement is performed, generating a different faradic response. Thus, to report an E-AB sensors' "true" K_D value, it is essential to deconvolute the faradic contribution to the current originating from the covalently attached redox reporter and measure electron transfer over several time scales.

Measuring the faradic contribution to the current at E-AB sensors can be achieved via various means. DC interrogation techniques such as cyclic voltammetry[45] and chronoamperometry,[11,46] for example, have been used to this end. Like square-wave voltammetry, the former has shown to return a scan-rate-dependent K_D value, which is again counterintuitive in the context of a target molecule interacting with an aptamer. The latter, in contrast, does return a single K_D value. Deconvoluting the faradic contribution to the current of the redox reporter using chronoamperometry, however, remains challenging due to multiple exponential decays (i.e., electrical double layer formation, faradic electron transfer from other processes) of similar time scales. Electrochemical impedance spectroscopy, an AC interrogation technique, in contrast, allows for the deconvolution and quantification of the contributions to the current due to its ability to scan over a wide range of time scales. While electrochemical impedance spectroscopy has largely been used to interrogate electrochemical biosensors that undergo "faradic" or "nonfaradic" changes due to diffusional changes in a free-solution redox reporter (typically $Fe(CN)_6^{3-/4-}$)[66] or changes in the electrode's double layer,[67] we instead decided to directly interrogate the covalently attached redox reporter, a strategy that advantageously allows for subsecond and direct measurement in undiluted complex matrices.[68] We thus explored the applicability of this technique to resolve the E-AB sensor's true K_D value as we envisioned the multifrequency it used will increase our resolution of the electron transfer of the redox reporter.

Interrogation of E-AB sensors using electrochemical impedance spectroscopy returns the lowest K_D values measured electrochemically. We observed this when we titrated quinine, vancomycin, and ochratoxin A to their corresponding E-AB sensors on which we applied a sinusoidally oscillating potential pulse of varying frequencies centered around the formal potential of the redox reporter. Doing so produced a frequency-dependent alternating-current response that is offset from the potential pulse due to interfacial resistive and capacitive contributions that we measured as a shift in the phase. Upon exposure to increasing amounts of quinine, as is the case for the other sensors we tested, the MN19 E-AB sensor produced a shift in phase toward higher frequencies (Figure 18A). To deconvolute and quantify the different resistive and capacitive contributions to the measured current response, we modeled the impedimetric response using the equivalent circuit diagram fitting approach. We decided to rely on a previously reported equivalent circuit diagram[58] (Figure 18B), in which a solution resistance (R_{sol}) is placed in series to a nonfaradic branch (represented by a constant-phase element, C_{int}) used to model the formation of the electrical double layer and a faradic branch (represented by a resistor, R_{ct}, in series with a constant-phase element, C_{DNA}) to model the electron-transfer reaction occurring between the electrode and the redox reporter. As previously reported,[58] aside from R_{ct}, all circuit elements remained constant as a function of the target concentration (Figure S10). Considering that R_{ct} is inversely proportional to the electron-transfer rate of the redox reporter,[58] this parameter changed as a function of increasing amounts of the target because of the binding-induced change in electron transfer incurred by the redox reporter covalently attached to the aptamer.[4] When looking at the quinine-binding MN19 E-AB sensor, R_{ct} values initially increased at lower target concentrations and then decreased when sensors were exposed to higher target concentrations (Figure 18C). Fitting the charge-transfer resistance using a two-site binding model equation (see the experimental section) returned a K_D value of 0.54 μM, while the second charge-transfer transition returned a K_D value of 4.3 μM. With structural similarities closely matching the MN19 variant (Figure S1), MN20, OR2, and OR3 quinine-binding aptamers also produced two binding events with K_D values of 2.2, 1.4, and 0.72 μM and 4.3, 18.2, and 3.4 μM, respectively. E-AB sensors binding vancomycin and ochratoxin A, in contrast, exhibited a single binding event with K_D values of 9.7 and 0.11 μM, respectively (Figure S9). Together, all K_D values measured using electrochemical impedance spectroscopy were the lowest values ever reported for any of the corresponding aptamers when attached to electrodes and interrogated electrochemically.

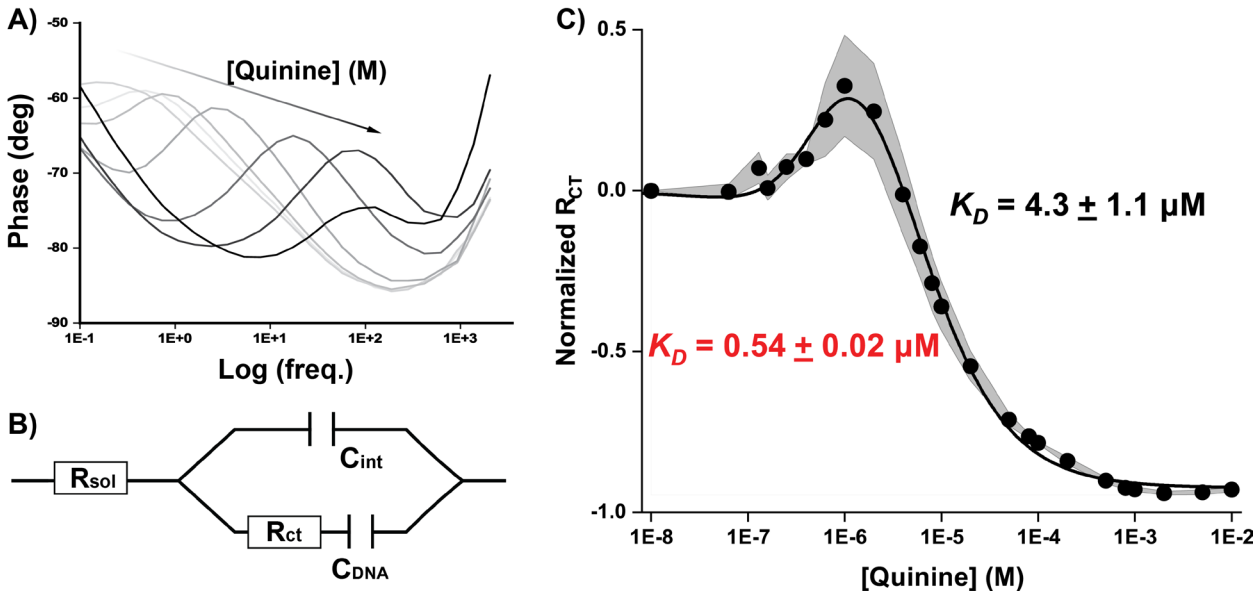

Figure 18. In interrogating E-AB sensors over a broad range of frequencies (10kHz – 0.1Hz) using electrochemical impedance spectroscopy while challenging with increasing amounts of the target, we observe a shift in the phase response that quantitatively reports on target concentration. (**A**) When looking at the quinine-binding MN19 aptamer, for example, we measured 2 orders of magnitude shift of the phase peak over a 10^5-fold change in quinine concentration (each phase trace correspond to 0, 0.2, 2, 20, 100, 500, 1000, and 10000 µM of quinine). We interpreted this shift as a change in the electron transfer rate of the covalently attached redox reporter induced by target binding. (**B**) To quantify this change in electron transfer rate, we used the equivalent electrical circuit modeling method with a diagram previously reported[47] in which a solution resistance (R_{sol}) is placed in series to faradaic (R_{ct} in series with a constant phase element pseudocapacitance C_{DNA}) and non-faradaic (C_{int}) branches. (**C**) In doing so, we found that the charge transfer resistance initially increased at low target concentrations and then sigmoidally decreased at higher target concentrations. In fitting this trace to a two-binding site model (see equation in experimental section), we measured K_D values of 0.54 ± 0.02 µM and 4.3 ± 1.1 µM, which approach values measured by ITC.

Our electrochemical impedance spectroscopy results show two discrete binding events for all quinine-binding aptamers. The ability of the MN19 aptamer variant to allow for two quinine molecule binding has previously been reported in low-ionic-strength buffers (<140 mM).[69] In this report, Neves and co-workers proposed that this family of aptamers had low- and high-affinity binding sites for quinine and cocaine, where accessibility to the low-affinity site is hindered at higher NaCl concentrations. We thus presumed that our electrochemical impedance spectroscopy results were indicative of these two binding sites since both low-affinity and high-affinity sites had closely matching K_D values with ITC (i.e., 0.54 vs 0.96 µM for the high-affinity site measured in the same experimental conditions and 4.3 vs 4.9 µM[69]

for the low-affinity site measured in different buffer and temperature conditions (20 vs 15 °C and 1× PBS vs 2× Tris buffer)). To further support past results, we challenged the OR3 aptamer with increasing amounts of quinine while in buffers of higher ionic strengths (i.e., 1× PBS with 0.3, 1, or 2 M NaCl). In doing so, we measured larger changes in charge-transfer resistance for both transitions (Figure S11). These results confirmed the impact of ionic strength on the binding mechanism of the aptamer but differed from ones previously reported via ITC (ionic strengths we used far exceeded the ones used by Neves and co-workers to hinder ligand binding). We thus presume that the reason we can still observe the low-affinity binding site even in the face of using high-ionic-strength buffers is associated with the application of a voltage to our electrode. This is because as an electrical double layer forms in the vicinity of an electrode, sodium ions migrate, ultimately altering the neighboring salt concentration, which changes the ionic strength that surface-attached aptamers experience.

Interrogating E-AB sensors via electrochemical impedance spectroscopy returned K_D values within experimental error equivalent to ones measured by ITC, an observation that contrasts with square-wave voltammetry results, where we measured differences as high as three orders of magnitude (Table 3). We hypothesize that this originates because of three reasons. To start, square-wave voltammetry, in performing a measurement at a single interrogation frequency, is unable to provide sufficient information to resolve the E-AB's electron-transfer rate. Electrochemical impedance spectroscopy, in contrast, allows for a more efficient multifrequency scan, thus increasing our resolution to quantify the binding-induced change in electron transfer of E-AB sensors. Second, due to instrument limitations (we could only acquire square-wave voltammograms at frequencies above 2 Hz), we could only access lower interrogation frequencies (<2 Hz) using electrochemical impedance spectroscopy. Interrogating E-AB sensors in this lower-frequency window allowed us to increase our resolution for measuring the binding-induced change in electron-transfer rate and especially the one for the slower target-free aptamer condition. Finally, square-wave voltammetry and electrochemical impedance spectroscopy differ in potential waveforms, where the potential is scanned across a large window (in our case from −0.05 to −0.5 V vs Ag|AgCl) in the former while the potential is fixed throughout an experiment (in our case ∼ −0.25 V vs Ag|AgCl) in the latter. One could envision that the differences in K_D values we observe between the two techniques originate from DNA− surface electrostatic interactions.[70,71] While we cannot discard that such a phenomenon takes place here, our results suggest that aptamers in E-AB sensors maintain their competent binding conformations when interrogated either in square-wave voltammetry or electrochemical impedance spectroscopy. We envision that acquiring square-wave voltammograms at frequencies

spanning large enough time scales (mHz to kHz) could provide sufficient resolution of the binding-induced change in electron transfer of the redox reporter using Lovric's formalism[55,56] and thus report the aptamer's true K_D value. Doing so, however, is time-consuming (several hours to acquire sufficient square-wave voltammograms to span these time scales for a single target concentration). A potentiostatic electrochemical impedance spectroscopy experiment, in contrast, takes less than 5 min to cover these time scales and offers highly resolved impedimetric results that can then be fitted using linearized current−potential equations from well-known circuit elements. Thus, electrochemical impedance spectroscopy efficiently provides well-resolved true K_D value measurements of surface-attached aptamers. We envisioned that this approach should be more widely adopted to enhance the limits of detection from this class of sensors and other electrochemical sensors to access concentration measurements in clinically relevant ranges.

Table 3. K_D Values of Quinine-, Vancomycin-, and Ochratoxin A-Binding Aptamers Measured in the Solution via ITC and on the Surface Using Square-Wave Voltammetry or Electrochemical Impedance Spectroscopy Revealing That the Latter Technique Closely Approaches Values Measured by ITC[a]

		K_D value measured by technique (μM)		
target	aptamer	square-wave voltammetry	isothermal titration calorimetry	electrochemical impedance spectroscopy
quinine[b]	MN19	142 ± 19 − 1946 ± 188	0.96 ± 0.04	0.54 ± 0.02
	MN20	114 ± 17 − 3523 ± 261	1.0 ± 0.1	2.2 ± 1.2
	OR2	318 ± 36 − 3119 ± 297	1.96 ± 0.30	1.4 ± 0.3
	OR3	87 ± 6 − 1333 ± 152	0.9 ± 0.1	0.72 ± 0.27
vancomycin[b]	Vanco4trunc	32 ± 2 − 51 ± 4	47.6 ± 23.4	9.7 ± 0.8
ochratoxin A[c]	OTA	0.23 ± 0.02 − 0.44 ± 0.05	0.055 ± 0.009	0.11 ± 0.02

[a]Errors represent the standard deviation of the mean measured for at least three independent sensors or ITC runs. [b]Data acquired at 20 °C in 1× PBS buffer (137 mM NaCl, 2.7 mM KCl, pH = 7.4). [c]Data acquired at 20 °C in 10 mM Tris (pH 8.0), 20 mM $CaCl_2$, 5 mM KCl, and 120 mM NaCl.

2.7. CONCLUSIONS

In this study, we investigated the effect of the interrogation technique on the dissociation constant of E-AB sensors. We started our investigation with one of the most used E-AB sensor interrogation technique, square-wave voltammetry. Given the signal gain dependence of E-AB sensors on the interrogating square-wave frequency, we found that aptamers' dissociation constants are likewise dependent on this parameter. While tuning square-wave frequency can be useful to tune E-AB sensors' gain and dynamic

range for sensing purposes, measuring multiple dissociation constants, which can vary over an order of magnitude for the same aptamer, is counterintuitive, and we thus decided to explore an alternative interrogation technique, electrochemical impedance spectroscopy. This technique can deconvolute interfacial resistive and capacitive contributions to the measured current by measuring the phase shift of the sinusoidally oscillating current response over a broad range of frequencies, thus offering an enhanced resolution of the change in electron transfer of the sensor's redox reporter. Our electrochemical impedance spectroscopy results revealed the lowest electrochemically measured K_D values reported for the different aptamers studied. We then compared our K_D values with the gold-standard technique, ITC, and found that values obtained using electrochemical impedance spectroscopy were within experimental errors or only 2−3-fold apart from one another. In light of our results, due to its enhanced capabilities to deconvolute and quantify various processes, we thus envision that interrogating E-AB sensors using electrochemical impedance spectroscopy will enable more accurate measurements using this class of sensors and increase their adoption for measurements of target concentrations directly in undiluted complex matrices and in the body. More broadly, we envision that our methodology could likewise prove of value in other electrochemical biosensor relying on changes in electron transfer rates.

References

(1) Ferapontova, E. E.; Olsen, E. M.; Gothelf, K. V. An RNA Aptamer-Based Electrochemical Biosensor for Detection of Theophylline in Serum. *J. Am. Chem. Soc.* **2008**, *130* (13), 4256–4258. https://doi.org/10.1021/ja711326b.

(2) Zuo, X.; Song, S.; Zhang, J.; Pan, D.; Wang, L.; Fan, C. A Target-Responsive Electrochemical Aptamer Switch (TREAS) for Reagentless Detection of Nanomolar ATP. *J. Am. Chem. Soc.* **2007**, *129* (5), 1042–1043. https://doi.org/10.1021/ja067024b.

(3) White, R. J.; Phares, N.; Lubin, A. A.; Xiao, Y.; Plaxco, K. W. Optimization of Electrochemical Aptamer-Based Sensors via Optimization of Probe Packing Density and Surface Chemistry. *Langmuir* **2008**, *24* (18), 10513–10518. https://doi.org/10.1021/la800801v.

(4) Baker, B. R.; Lai, R. Y.; Wood, M. S.; Doctor, E. H.; Heeger, A. J.; Plaxco, K. W. An Electronic, Aptamer-Based Small-Molecule Sensor for the Rapid, Label-Free Detection of Cocaine in Adulterated Samples and Biological Fluids. *J. Am. Chem. Soc.* **2006**, *128* (10), 3138–3139. https://doi.org/10.1021/ja056957p.

(5) Huang, K.-C.; White, R. J. Random Walk on a Leash: A Simple Single-Molecule Diffusion Model for Surface-Tethered Redox Molecules with Flexible Linkers. *J. Am. Chem. Soc.* **2013**, *135* (34), 12808–12817. https://doi.org/10.1021/ja4060788.

(6) Dauphin-Ducharme, P.; Arroyo-Currás, N.; Adhikari, R.; Somerson, J.; Ortega, G.; Makarov, D. E.; Plaxco, K. W. Chain Dynamics Limit Electron Transfer from Electrode-Bound, Single-Stranded Oligonucleotides. *J. Phys. Chem. C* **2018**, *122* (37), 21441–21448. https://doi.org/10.1021/acs.jpcc.8b06111.

(7) Uzawa, T.; Cheng, R. R.; White, R. J.; Makarov, D. E.; Plaxco, K. W. A Mechanistic Study of Electron Transfer from the Distal Termini of Electrode-Bound, Single-Stranded DNAs. *J. Am. Chem. Soc.* **2010**, *132* (45), 16120–16126. https://doi.org/10.1021/ja106345d.

(8) Demaille, C.; Clément, N.; Chovin, A.; Kim, S. H.; Zheng, Z. *The Electrochemical Response of Electrode-Attached Redox Oligo-Nucleotides Is Governed by Low Activation Energy Electron Transfer Kinetics*; preprint; Chemistry, 2022. https://doi.org/10.26434/chemrxiv-2022-212hs.

(9) Dauphin-Ducharme, P.; Yang, K.; Arroyo-Currás, N.; Ploense, K. L.; Zhang, Y.; Gerson, J.; Kurnik, M.; Kippin, T. E.; Stojanovic, M. N.; Plaxco, K. W. Electrochemical Aptamer-Based

Sensors for Improved Therapeutic Drug Monitoring and High-Precision, Feedback-Controlled Drug Delivery. *ACS Sens.* **2019**, *4* (10), 2832–2837. https://doi.org/10.1021/acssensors.9b01616.

(10) Dauphin-Ducharme, P.; Ploense, K. L.; Arroyo-Currás, N.; Kippin, T. E.; Plaxco, K. W. Electrochemical Aptamer-Based Sensors: A Platform Approach to High-Frequency Molecular Monitoring In Situ in the Living Body. In *Biomedical Engineering Technologies: Volume 1*; Ossandon, M. R., Baker, H., Rasooly, A., Eds.; Springer US: New York, NY, 2022; pp 479–492. https://doi.org/10.1007/978-1-0716-1803-5_25.

(11) Arroyo-Currás, N.; Dauphin-Ducharme, P.; Ortega, G.; Ploense, K. L.; Kippin, T. E.; Plaxco, K. W. Subsecond-Resolved Molecular Measurements in the Living Body Using Chronoamperometrically Interrogated Aptamer-Based Sensors. *ACS Sens.* **2018**, *3* (2), 360–366. https://doi.org/10.1021/acssensors.7b00787.

(12) Downs, A. M.; Gerson, J.; Ploense, K. L.; Plaxco, K. W.; Dauphin-Ducharme, P. Subsecond-Resolved Molecular Measurements Using Electrochemical Phase Interrogation of Aptamer-Based Sensors. *Anal. Chem.* **2020**, *92* (20), 14063–14068. https://doi.org/10.1021/acs.analchem.0c03109.

(13) Li, H.; Dauphin-Ducharme, P.; Ortega, G.; Plaxco, K. W. Calibration-Free Electrochemical Biosensors Supporting Accurate Molecular Measurements Directly in Undiluted Whole Blood. *J. Am. Chem. Soc.* **2017**, *139* (32), 11207–11213. https://doi.org/10.1021/jacs.7b05412.

(14) Downs, A. M.; Gerson, J.; Leung, K. K.; Honeywell, K. M.; Kippin, T.; Plaxco, K. W. Improved Calibration of Electrochemical Aptamer-Based Sensors. *Sci. Rep.* **2022**, *12* (1), 5535. https://doi.org/10.1038/s41598-022-09070-7.

(15) Asai, K.; Yamamoto, T.; Nagashima, S.; Ogata, G.; Hibino, H.; Einaga, Y. An Electrochemical Aptamer-Based Sensor Prepared by Utilizing the Strong Interaction between a DNA Aptamer and Diamond. *The Analyst* **2020**, *145* (2), 544–549. https://doi.org/10.1039/C9AN01976F.

(16) White, R. J.; Plaxco, K. W. Engineering New Aptamer Geometries for Electrochemical Aptamer-Based Sensors; Fell, Jr., N. F., Swaminathan, V. S., Eds.; Orlando, Florida, USA, 2009; p 732105. https://doi.org/10.1117/12.820419.

(17) Xiao, Y.; Lubin, A. A.; Heeger, A. J.; Plaxco, K. W. Label-Free Electronic Detection of Thrombin in Blood Serum by Using an Aptamer-Based Sensor. *Angew. Chem.* **2005**, *117* (34), 5592–5595. https://doi.org/10.1002/ange.200500989.

(18) Lai, R. Y.; Plaxco, K. W.; Heeger, A. J. Aptamer-Based Electrochemical Detection of Picomolar Platelet-Derived Growth Factor Directly in Blood Serum. *Anal. Chem.* **2007**, *79* (1), 229–233. https://doi.org/10.1021/ac061592s.

(19) Cash, K. J.; Ricci, F.; Plaxco, K. W. An Electrochemical Sensor for the Detection of Protein−Small Molecule Interactions Directly in Serum and Other Complex Matrices. *J. Am. Chem. Soc.* **2009**, *131* (20), 6955–6957. https://doi.org/10.1021/ja9011595.

(20) Swensen, J. S.; Xiao, Y.; Ferguson, B. S.; Lubin, A. A.; Lai, R. Y.; Heeger, A. J.; Plaxco, K. W.; Soh, H. Tom. Continuous, Real-Time Monitoring of Cocaine in Undiluted Blood Serum via a Microfluidic, Electrochemical Aptamer-Based Sensor. *J. Am. Chem. Soc.* **2009**, *131* (12), 4262–4266. https://doi.org/10.1021/ja806531z.

(21) White, R. J.; Rowe, A. A.; Plaxco, K. W. Re-Engineering Aptamers to Support Reagentless, Self-Reporting Electrochemical Sensors. *The Analyst* **2010**, *135* (3), 589. https://doi.org/10.1039/b921253a.

(22) Lorenzen, J. M.; Broll, M.; Kaever, V.; Burhenne, H.; Hafer, C.; Clajus, C.; Knitsch, W.; Burkhardt, O.; Kielstein, J. T. Pharmacokinetics of Ampicillin/Sulbactam in Critically Ill Patients with Acute Kidney Injury Undergoing Extended Dialysis. *Clin. J. Am. Soc. Nephrol.* **2012**, *7* (3), 385–390. https://doi.org/10.2215/CJN.05690611.

(23) Yokoyama, Y.; Matsumoto, K.; Ikawa, K.; Watanabe, E.; Yamamoto, H.; Imoto, Y.; Morikawa, N.; Takeda, Y. The Pharmacokinetics of Ampicillin–Sulbactam in Anuric Patients: Dosing Optimization for Prophylaxis during Cardiovascular Surgery. *Int. J. Clin. Pharm.* **2016**, *38* (4), 771–775. https://doi.org/10.1007/s11096-016-0286-5.

(24) Takesue, Y.; Watanabe, A.; Kusachi, S.; Matsumoto, T.; Iwamoto, A.; Totsuka, K.; Sunakawa, K.; Yagisawa, M.; Sato, J.; Oguri, T.; Nakanishi, K.; Takesue, Y.; Takesue, Y.; Hanaki, H.; Kusachi, S.; Sumiyama, Y.; Kitagawa, Y.; Sumiyama, Y.; Kitagawa, Y.; Wakabayashi, G.; Koyama, I.; Yanaga, K.; Konishi, T.; Fukushima, R.; Seki, S.; Imai, S.; Shintani, T.; Tsukada, H.; Tsukada, K.; Omura, K.; Mikamo, H.; Takeyama, H.; Kusunoki, M.; Kubo, S.; Shimizu, J.; Hirai, T.; Ohge, H.; Kadowaki, A.; Okamoto, K.; Yanagihara, K. Nationwide Surveillance of Antimicrobial Susceptibility Patterns of Pathogens Isolated from Surgical Site Infections (SSI) in Japan. *J. Infect. Chemother.* **2012**, *18* (6), 816–826. https://doi.org/10.1007/s10156-012-0509-1.

(25) Yu, Z.; Lai, R. Y. A Reagentless and Reusable Electrochemical Aptamer-Based Sensor for Rapid Detection of Ampicillin in Complex Samples. *Talanta* **2018**, *176*, 619–624. https://doi.org/10.1016/j.talanta.2017.08.057.

(26) Song, K.-M.; Jeong, E.; Jeon, W.; Cho, M.; Ban, C. Aptasensor for Ampicillin Using Gold Nanoparticle Based Dual Fluorescence–Colorimetric Methods. *Anal. Bioanal. Chem.* **2012**, *402* (6), 2153–2161. https://doi.org/10.1007/s00216-011-5662-3.

(27) Newton, P.; Simpson, A.; Wanwimolruk, S.; Maliakal, P.; Villegas, L.; Kuypers, D.; White, N. J. Oral Quinine Pharmacokinetics and Dietary Salt Intake. *Eur. J. Clin. Pharmacol.* **2001**, *57* (2), 111–113. https://doi.org/10.1007/s002280100283.

(28) Kloprogge, F.; Jullien, V.; Piola, P.; Dhorda, M.; Muwanga, S.; Nosten, F.; Day, N. P. J.; White, N. J.; Guerin, P. J.; Tarning, J. Population Pharmacokinetics of Quinine in Pregnant Women with Uncomplicated Plasmodium Falciparum Malaria in Uganda. *J. Antimicrob. Chemother.* **2014**, *69* (11), 3033–3040. https://doi.org/10.1093/jac/dku228.

(29) Shaver, A.; Kundu, N.; Young, B. E.; Vieira, P. A.; Sczepanski, J. T.; Arroyo-Currás, N. Nuclease Hydrolysis Does Not Drive the Rapid Signaling Decay of DNA Aptamer-Based Electrochemical Sensors in Biological Fluids. *Langmuir* **2021**, *37* (17), 5213–5221. https://doi.org/10.1021/acs.langmuir.1c00166.

(30) Slavkovic, S.; Churcher, Z. R.; Johnson, P. E. Nanomolar Binding Affinity of Quinine-Based Antimalarial Compounds by the Cocaine-Binding Aptamer. *Bioorg. Med. Chem.* **2018**, *26* (20), 5427–5434. https://doi.org/10.1016/j.bmc.2018.09.017.

(31) Shoara, A. A.; Slavkovic, S.; Donaldson, L. W.; Johnson, P. E. Analysis of the Interaction between the Cocaine-Binding Aptamer and Its Ligands Using Fluorescence Spectroscopy. *Can. J. Chem.* **2017**, *95* (12), 1253–1260. https://doi.org/10.1139/cjc-2017-0380.

(32) Blaho, K.; Logan, B.; Winbery, S.; Park, L.; Schwilke, E. Blood Cocaine and Metabolite Concentrations, Clinical Findings, and Outcome of Patients Presenting to an ED. *Am. J. Emerg. Med.* **2000**, *18* (5), 593–598. https://doi.org/10.1053/ajem.2000.9282.

(33) Jones, A. W.; Holmgren, A. Concentrations of Cocaine and Benzoylecgonine in Femoral Blood from Cocaine-Related Deaths Compared with Venous Blood from Impaired Drivers. *J. Anal. Toxicol.* **2014**, *38* (1), 46–51. https://doi.org/10.1093/jat/bkt094.

(34) Neves, M. A. D.; Reinstein, O.; Saad, M.; Johnson, P. E. Defining the Secondary Structural Requirements of a Cocaine-Binding Aptamer by a Thermodynamic and Mutation Study. *Biophys. Chem.* **2010**, *153* (1), 9–16. https://doi.org/10.1016/j.bpc.2010.09.009.

(35) Speth, P. A. J.; van Hoesel, Q. G. C. M.; Haanen, C. Clinical Pharmacokinetics of Doxorubicin: *Clin. Pharmacokinet.* **1988**, *15* (1), 15–31. https://doi.org/10.2165/00003088-198815010-00002.

(36) Chamorro-Garcia, A.; Ortega, G.; Mariottini, D.; Green, J.; Ricci, F.; Plaxco, K. W. Switching the Aptamer Attachment Geometry Can Dramatically Alter the Signalling and Performance of Electrochemical Aptamer-Based Sensors. *Chem. Commun.* **2021**, *57* (88), 11693–11696. https://doi.org/10.1039/D1CC04557A.

(37) Simon, A. J.; Vallée-Bélisle, A.; Ricci, F.; Plaxco, K. W. Intrinsic Disorder as a Generalizable Strategy for the Rational Design of Highly Responsive, Allosterically Cooperative Receptors. *Proc. Natl. Acad. Sci.* **2014**, *111* (42), 15048–15053. https://doi.org/10.1073/pnas.1410796111.

(38) Forrester, T. An Estimate of Adenosine Triphosphate Release into the Venous Effluent from Exercising Human Forearm Muscle. *J. Physiol.* **1972**, *224* (3), 611–628. https://doi.org/10.1113/jphysiol.1972.sp009915.

(39) Harkness, R. A.; Simmonds, R. J.; Coade, S. B. Purine Transport and Metabolism in Man: The Effect of Exercise on Concentrations of Purine Bases, Nucleosides and Nucleotides in Plasma, Urine, Leucocytes and Erythrocytes. *Clin. Sci.* **1983**, *64* (3), 333–340. https://doi.org/10.1042/cs0640333.

(40) Slavkovic, S.; Zhu, Y.; Churcher, Z. R.; Shoara, A. A.; Johnson, A. E.; Johnson, P. E. Thermodynamic Analysis of Cooperative Ligand Binding by the ATP-Binding DNA Aptamer Indicates a Population-Shift Binding Mechanism. *Sci. Rep.* **2020**, *10* (1), 18944. https://doi.org/10.1038/s41598-020-76002-8.

(41) Li, S.; Marquardt, R. R.; Frohlich, A. A.; Vitti, T. G.; Crow, G. Pharmacokinetics of Ochratoxin A and Its Metabolites in Rats. *Toxicol. Appl. Pharmacol.* **1997**, *145* (1), 82–90. https://doi.org/10.1006/taap.1997.8155.

(42) Fuchs, R.; Hult, K. Ochratoxin A in Blood and Its Pharmacokinetic Properties. *Food Chem. Toxicol.* **1992**, *30* (3), 201–204. https://doi.org/10.1016/0278-6915(92)90034-I.

(43) Somerson, J.; Plaxco, K. Electrochemical Aptamer-Based Sensors for Rapid Point-of-Use Monitoring of the Mycotoxin Ochratoxin A Directly in a Food Stream. *Molecules* **2018**, *23* (4), 912. https://doi.org/10.3390/molecules23040912.

(44) Cruz-Aguado, J. A.; Penner, G. Determination of Ochratoxin A with a DNA Aptamer. *J. Agric. Food Chem.* **2008**, *56* (22), 10456–10461. https://doi.org/10.1021/jf801957h.

(45) Pellitero, M. A.; Curtis, S. D.; Arroyo-Currás, N. Interrogation of Electrochemical Aptamer-Based Sensors via Peak-to-Peak Separation in Cyclic Voltammetry Improves the Temporal Stability and Batch-to-Batch Variability in Biological Fluids. *ACS Sens.* **2021**, *6* (3), 1199–1207. https://doi.org/10.1021/acssensors.0c02455.

(46) Dauphin-Ducharme, P.; Arroyo-Currás, N.; Plaxco, K. W. High-Precision Electrochemical Measurements of the Guanine-, Mismatch-, and Length-Dependence of Electron Transfer from Electrode-Bound DNA Are Consistent with a Contact-Mediated Mechanism. *J. Am. Chem. Soc.* **2019**, *141* (3), 1304–1311. https://doi.org/10.1021/jacs.8b11341.

(47) Idili, A.; Gerson, J.; Parolo, C.; Kippin, T.; Plaxco, K. W. An Electrochemical Aptamer-Based Sensor for the Rapid and Convenient Measurement of l-Tryptophan. *Anal. Bioanal. Chem.* **2019**, *411* (19), 4629–4635. https://doi.org/10.1007/s00216-019-01645-0.

(48) Dauphin-Ducharme, P.; Arroyo-Currás, N.; Kurnik, M.; Ortega, G.; Li, H.; Plaxco, K. W. Simulation-Based Approach to Determining Electron Transfer Rates Using Square-Wave Voltammetry. *Langmuir* **2017**, *33* (18), 4407–4413. https://doi.org/10.1021/acs.langmuir.7b00359.

(49) Li, H.; Dauphin-Ducharme, P.; Arroyo-Currás, N.; Tran, C. H.; Vieira, P. A.; Li, S.; Shin, C.; Somerson, J.; Kippin, T. E.; Plaxco, K. W. A Biomimetic Phosphatidylcholine-Terminated Monolayer Greatly Improves the In Vivo Performance of Electrochemical Aptamer-Based Sensors. *Angew. Chem. Int. Ed.* **2017**, *56* (26), 7492–7495. https://doi.org/10.1002/anie.201700748.

(50) Schoukroun-Barnes, L. R.; Wagan, S.; White, R. J. Enhancing the Analytical Performance of Electrochemical RNA Aptamer-Based Sensors for Sensitive Detection of Aminoglycoside Antibiotics. *Anal. Chem.* **2014**, *86* (2), 1131–1137. https://doi.org/10.1021/ac4029054.

(51) White, R. J.; Plaxco, K. W. Exploiting Binding-Induced Changes in Probe Flexibility for the Optimization of Electrochemical Biosensors. *Anal. Chem.* **2010**, *82* (1), 73–76. https://doi.org/10.1021/ac902595f.

(52) Schoukroun-Barnes, L. R.; Macazo, F. C.; Gutierrez, B.; Lottermoser, J.; Liu, J.; White, R. J. Reagentless, Structure-Switching, Electrochemical Aptamer-Based Sensors. *Annu. Rev. Anal. Chem.* **2016**, *9* (1), 163–181. https://doi.org/10.1146/annurev-anchem-071015-041446.

(53) Dauphin-Ducharme, P.; Plaxco, K. W. Maximizing the Signal Gain of Electrochemical-DNA Sensors. *Anal. Chem.* **2016**, *88* (23), 11654–11662. https://doi.org/10.1021/acs.analchem.6b03227.

(54) Zhang, S.; Hu, R.; Hu, P.; Wu, Z.-S.; Shen, G.-L.; Yu, R.-Q. Blank Peak Current-Suppressed Electrochemical Aptameric Sensing Platform for Highly Sensitive Signal-on Detection of Small Molecule. *Nucleic Acids Res.* **2010**, *38* (20), e185–e185. https://doi.org/10.1093/nar/gkq728.

(55) Lovrić, M.; Komorsky-Lovric, Š. Square-Wave Voltammetry of an Adsorbed Reactant. *J. Electroanal. Chem. Interfacial Electrochem.* **1988**, *248* (2), 239–253. https://doi.org/10.1016/0022-0728(88)85089-7.

(56) Komorsky-Lovrić, Š.; Lovrić, M. Measurements of Redox Kinetics of Adsorbed Azobenzene by "a Quasireversible Maximum" in Square-Wave Voltammetry. *Electrochimica Acta* **1995**, *40* (11), 1781–1784. https://doi.org/10.1016/0013-4686(95)00097-X.

(57) Curtis, S. D.; Ploense, K. L.; Kurnik, M.; Ortega, G.; Parolo, C.; Kippin, T. E.; Plaxco, K. W.; Arroyo-Currás, N. Open Source Software for the Real-Time Control, Processing, and Visualization of High-Volume Electrochemical Data. *Anal. Chem.* **2019**, *91* (19), 12321–12328. https://doi.org/10.1021/acs.analchem.9b02553.

(58) Creager, S. E.; Wooster, T. T. A New Way of Using Ac Voltammetry To Study Redox Kinetics in Electroactive Monolayers. *Anal. Chem.* **1998**, *70* (20), 4257–4263. https://doi.org/10.1021/ac9804821.

(59) Lasia, A. *Electrochemical Impedance Spectroscopy and Its Applications*; Springer New York: New York, NY, 2014. https://doi.org/10.1007/978-1-4614-8933-7.

(60) *Electrochemical Methods: Fundamentals and Applications, 3rd Edition | Wiley*. Wiley.com. https://www.wiley.com/en-ca/Electrochemical+Methods%3A+Fundamentals+and+Applications%2C+3rd+Edition-p-9781119334064 (accessed 2023-02-23).

(61) Lin, Z.; Li, X.; Kraatz, H.-B. Impedimetric Immobilized DNA-Based Sensor for Simultaneous Detection of Pb^{2+}, Ag^{+}, and Hg^{2+}. *Anal. Chem.* **2011**, *83* (17), 6896–6901. https://doi.org/10.1021/ac2014096.

(62) Jarczewska, M.; Kékedy-Nagy, L.; Nielsen, J. S.; Campos, R.; Kjems, J.; Malinowska, E.; Ferapontova, E. E. Electroanalysis of PM-Levels of Urokinase Plasminogen Activator in Serum

by Phosphorothioated RNA Aptamer. *The Analyst* **2015**, *140* (11), 3794–3802. https://doi.org/10.1039/C4AN02354D.

(63) Slavkovic, S.; Johnson, P. E. Isothermal Titration Calorimetry Studies of Aptamer-Small Molecule Inter- Actions: Practicalities and Pitfalls. *Aptamers* **2018**, *2*, 7.

(64) Shoara, A. A.; Reinstein, O.; Borhani, O. A.; Martin, T. R.; Slavkovic, S.; Churcher, Z. R.; Johnson, P. E. Development of a Thermal-Stable Structure-Switching Cocaine-Binding Aptamer. *Biochimie* **2018**, *145*, 137–144. https://doi.org/10.1016/j.biochi.2017.08.010.

(65) Cash, K. J.; Ricci, F.; Plaxco, K. W. A General Electrochemical Method for Label-Free Screening of Protein–Small Molecule Interactions. *Chem. Commun.* **2009**, No. 41, 6222. https://doi.org/10.1039/b911558g.

(66) Chen, W.; Liu, Y.-H.; Li, H.-N.; Liu, A.-L.; Lin, X.-H.; Chen, Y.-Z. Ultrasensitive and Facile Electrochemical Deoxyribonucleic Acid Biosensor Based on the Conformational Change of the Recognition Interface. *Anal. Chim. Acta* **2012**, *748*, 89–94. https://doi.org/10.1016/j.aca.2012.08.046.

(67) Ma, K.-S.; Zhou, H.; Zoval, J.; Madou, M. DNA Hybridization Detection by Label Free versus Impedance Amplifying Label with Impedance Spectroscopy. *Sens. Actuators B Chem.* **2006**, *114* (1), 58–64. https://doi.org/10.1016/j.snb.2005.04.038.

(68) Arroyo-Currás, N.; Dauphin-Ducharme, P.; Ortega, G.; Ploense, K. L.; Kippin, T. E.; Plaxco, K. W. Subsecond-Resolved Molecular Measurements in the Living Body Using Chronoamperometrically Interrogated Aptamer-Based Sensors. *ACS Sens.* **2018**, *3* (2), 360–366. https://doi.org/10.1021/acssensors.7b00787.

(69) Neves, M. A. D.; Slavkovic, S.; Churcher, Z. R.; Johnson, P. E. Salt-Mediated Two-Site Ligand Binding by the Cocaine-Binding Aptamer. *Nucleic Acids Res.* **2016**, gkw1294. https://doi.org/10.1093/nar/gkw1294.

(70) Jambrec, D.; Gebala, M.; La Mantia, F.; Schuhmann, W. Potential-Assisted DNA Immobilization as a Prerequisite for Fast and Controlled Formation of DNA Monolayers. *Angew. Chem. Int. Ed.* **2015**, *54* (50), 15064–15068. https://doi.org/10.1002/anie.201506672.

(71) Magriñá, I.; Ortiz, M.; Simonova, A.; Hocek, M.; O' Sullivan, C. K.; Forster, R. J. Ferrocene-Containing DNA Monolayers: Influence of Electrostatics on the Electron Transfer Dynamics. *Langmuir* **2021**, *37* (11), 3359–3369. https://doi.org/10.1021/acs.langmuir.0c03485.

CHAPTER 3: ON THE SIGNALING MECHANISM OF ELECTROCHEMICAL APTAMER-BASED BIOSENSORS

3.1. Author's note

The results of this chapter are part of a collaborative article titled "Redox reporter – ligand competition to support signaling in the cocaine-binding electrochemical aptamer-based biosensor" which was submitted on February 24, 2023, to *Chemistry – A European Journal*. We focus here on the electrochemical results obtained which we compare in this study to nuclear magnetic resonance, fluorescence spectroscopy and isothermal calorimetry titration. These latest results were obtained by our collaborators at York University in Prof. Philip Johnson's laboratory.

It should be noted that the references pertaining to this chapter are included in the bibliography at the end of this chapter.

Despite the ability of electrochemical impedance spectroscopy in reporting the lowest electrochemically binding affinity of the receptors toward their corresponding ligands in E-AB sensors, the results obtained through this method does not always align with results obtained in isothermal titration calorimetry. We observed this when comparing the K_D values measured via EIS and ITC for the MN4 aptamer (analogous to other aptamers we studied in Chapter 2, see secondary structure Figure 19A) that binds to cocaine and certain anti-malarial compounds (i.e., quinine, primaquine and chloroquine). In doing so we measured K_D values that were 1 – 3 orders of magnitude higher compared to previously reported ITC results by Slavkovic.[1] Using the Langmuir-Hill equation to fit the charge transfer resistance yields K_D values of 86.6 µM, 2180 µM, 1000 µM, and 134.2 µM for cocaine, quinine, primaquine, and chloroquine, respectively, while the ITC measurements report K_D values of 5.5 µM, 0.2 µM, 0.5 µM, and 0.037 µM for the same target molecules. Moreover, the ITC measurement was able to detect a second, low-affinity binding event between MN4 aptamer and chloroquine molecule with a K_D value of 1.6 µM, which we do not observed in the EIS results (Figure 19B).

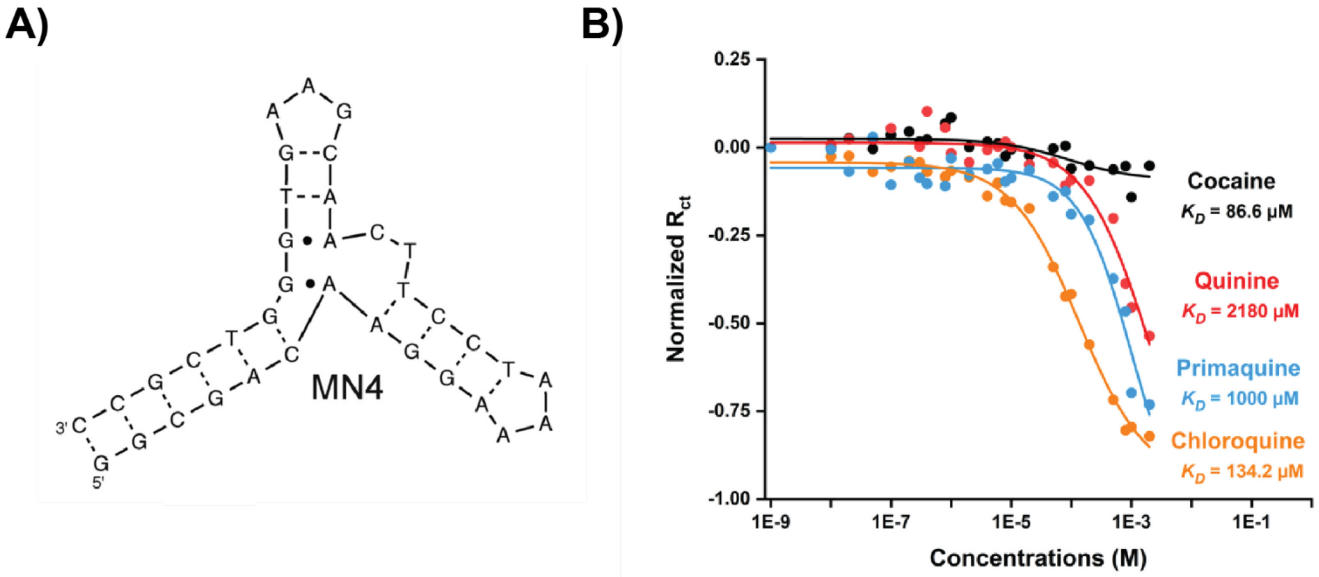

Figure 19. (**A**) The secondary structure of the MN4 cocaine-and-quinine binding aptamer is depicted. Watson-Crick base pairs are represented by dashes between nucleotides, while non-Watson-Crick base pairs are represented by dots. (**B**) The R_{ct} values of the MN4 aptamer E-AB sensor decreases upon the addition of the target molecules. By fitting the Langmuir-Hill equation to the charge transfer resistance curve, K_D values of 86.6 µM, 2180 µM, 1000 µM, and 134.2 µM for the detection of cocaine, quinine, primaquine, and chloroquine, were obtained, respectively. In the case of chloroquine, as is shown, the impedimetric interrogation is reporting a single binding event, while ITC measurement could recognize a second, low-affinity binding with a K_D value of 1.6 µM.[1]

We hypothesize that the different binding transduction mechanisms of ITC and EIS may account for the discrepancies in K_D values we measured. In ITC measurements, for example, the aptamer does not have to be labeled and binding is transduced as a result of heat released. In EIS, in contrast, the aptamer is modified with a redox reporter, methylene blue, which changes its electron transfer kinetics upon aptamer target binding. We thus envision that the redox reporter could influence the signal transduction mechanism of E-AB sensors. This is because methylene blue has the ability to bind with micromolar affinities to nucleic acids through intercalation with GC-rich portions of DNA duplexes in the minor and major grooves.[2,3] We foresee that methylene blue could compete for the same ligand binding site as opposed to being displaced as a result of the aptamer's conformational rearrangement.

Methylene blue when attached to the MN19 aptamer competes with its ligand binding site. We observed this through an electrochemical impedance spectroscopy study where we challenged MN19 E-AB sensors with increasing amounts of cocaine, quinine, primaquine and chloroquine. By measuring the phase shift of the AC current response in the frequency range of 0.1 Hz to 10 kHz while applying a fixed sinusoidally oscillating potential centered around the methylene blue redox potential, we observed that upon the addition of cocaine, the phase peak which was initially centered at less than 1 Hz began to shift gradually towards higher frequencies (Figure 20A). These results suggest the formation of different electron transfer states at each ligand concentration, which deviates from the commonly accepted two-state model (Figure 11) and instead supports a Langmuir-Hill-type model of electron transfer rate changes. We also observed that the maximal electrochemical response of the biosensors changed accordingly when titrated with different ligands (chloroquine, quinine, primaquine and cocaine) of varying affinities (Figure 20B). Specifically, the highest affinity ligand (chloroquine) resulted in the largest decrease in charge transfer resistance of the E-AB biosensor, whereas the lowest affinity ligand (cocaine) resulted in the lowest decrease in charge transfer resistance. The results obtained from the electrochemical impedance spectroscopy study indicate that the electrochemical properties of the biosensor are consistent with, in contrast to the vastly accepted signal transduction mechanism of conformational rearrangement, a new mechanism we coined « redox-reporter-ligand competition ».

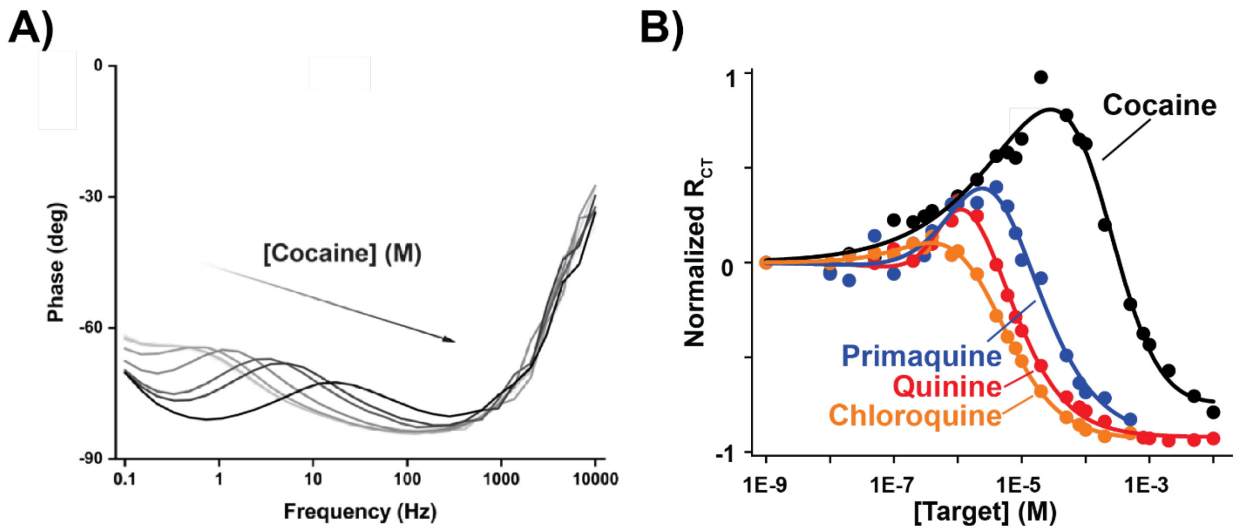

Figure 20. The methylene blue-labelled MN19 aptamer undergoes a redox reporter – ligand competition to support signaling in E-AB sensors. (**A**) Interrogation of the MN19 E-AB sensor using electrochemical impedance spectroscopy as a function of increasing amounts of cocaine reveals the formation of a concentration-dependent peak, which shifts towards higher interrogating frequencies as a function of ligand concentration. This is instead of measuring two distinct peaks in the phase response of the sensor that can be associated with the unbound and bound state. We attribute the formation of a single state at each target concentration to a competition between the redox reporter and the ligand for the MN19 aptamer. (**B**) We likewise observed this competition mechanism between the redox reporter and different ligands when the aptamer is immobilized on electrodes. By measuring the relative E-AB sensor response to various ligands with different affinities for the aptamer, we found that the normalized charge transfer resistance decreases the most when the aptamer is challenged with chloroquine, which has the highest binding affinity for this class of aptamer among the tested ligands.

The electrochemical aptamer-based biosensors employ a novel mechanism for sensing and signaling, whereby the redox reporter, methylene blue, covalently attached to the aptamer, competes with the ligand for the same binding site. Upon the introduction of the target molecule, the redox reporter is displaced from the binding site, leading to two potential outcomes. Firstly, methylene blue displacement can cause a shift in the redox reporter's relative position to the electrode surface, subsequently altering the electron transfer rate. Alternatively, displacement may result in a change in the medium surrounding the redox reporter, modifying its reorganizational energy, and thereby altering its charge transfer kinetics, as observed in the electrochemical impedance spectroscopy. This mechanism may arise from the target molecule's displacement of the redox reporter from the binding site or environmental changes impacting the redox reporter (Figure 21).

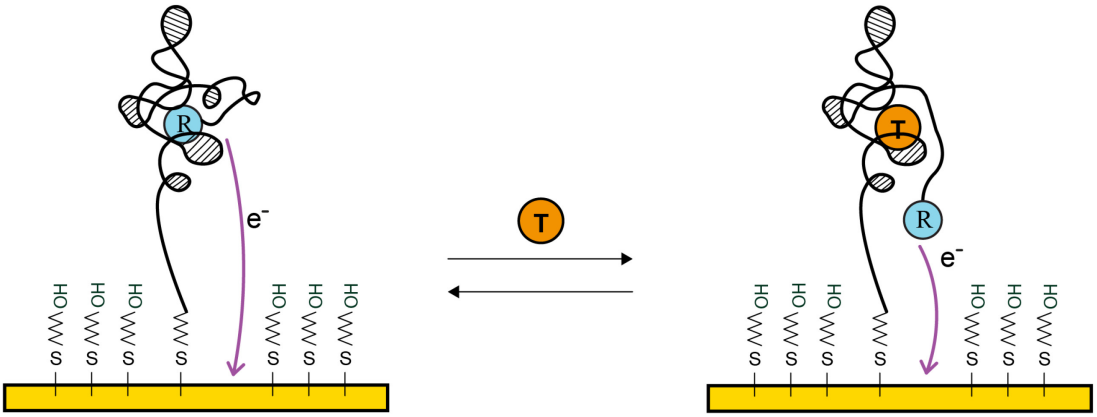

Figure 21. In the cocaine-binding E-AB sensor, the binding of the redox reporter in close proximity to the aptamer's ligand binding site is critical for generating a signal change. Methylene blue binds to this site, allowing the aptamer's structure to fold. The displacement of methylene blue from this site due to ligand binding alters its proximity to the electrode or its environment, leading to changes in its electron transfer rate. Our results indicate that the mechanism behind signaling in this E-AB sensor is driven by a competition between the redox reporter and the ligand, rather than the common mechanism of aptamers undergoing a binding-induced conformational change.

The "redox reporter – ligand competition" mechanism for the MN19 E-AB sensor could have limitations in detecting certain ligands. These limitations include difficulty in detecting ligands that have a binding affinity that is comparable to or lower than that of methylene blue for the aptamer, and ligands that bind in close proximity to methylene blue. Both factors are essential for the proper functioning of the sensor.

The proposed redox-reporter-ligand competition mechanism using the comprehensive analytical methodology to uncover it, have the potential to enhance the design of aptamers for electrochemical biosensors. A thorough comprehension of the structure-function of aptamers and the role of redox reporters in signal transduction could reduce the attrition rate in translating aptamers into electrochemical biosensors. The incorporation of DNA binding motifs for a redox reporter in the conserved regions of an aptamer could establish a redox reporter-ligand competition mechanism. This proposed mechanism is anticipated to be broadly applicable to other aptamer systems, and the introduction of intercalative redox reporters with DNA binding properties could expand the dynamic range of electrochemical biosensors. Moreover, the use of methylene blue in electrochemical biosensors must be taken into account when developing SELEX schemes for aptamers customized for E-AB sensing. By implementing these principles, it is expected that the design of aptamers for E-AB sensors' signaling would be improved, ultimately enhancing their translation into practical applications.

References

(1) Slavkovic, S.; Churcher, Z. R.; Johnson, P. E. Nanomolar Binding Affinity of Quinine-Based Antimalarial Compounds by the Cocaine-Binding Aptamer. *Bioorg. Med. Chem.* **2018**, *26* (20), 5427–5434. https://doi.org/10.1016/j.bmc.2018.09.017.

(2) Rohs, R.; Sklenar, H.; Lavery, R.; Röder, B. Methylene Blue Binding to DNA with Alternating GC Base Sequence: A Modeling Study. *J. Am. Chem. Soc.* **2000**, *122* (12), 2860–2866. https://doi.org/10.1021/ja992966k.

(3) Tuite, E.; Norden, B. Sequence-Specific Interactions of Methylene Blue with Polynucleotides and DNA: A Spectroscopic Study. *J. Am. Chem. Soc.* **1994**, *116* (17), 7548–7556. https://doi.org/10.1021/ja00096a011.

CHAPTER IV: CONCLUSION

In this study, we examined the effectiveness of square-wave voltammetry and electrochemical impedance spectroscopy, for interrogating the E-AB sensors to maximize their analytical performances. Despite being the widely used electrochemical interrogation technique, square-wave voltammetry returned aptamers' dissociation constants significantly departing ones measured using aptamers' gold standard characterization methods in solution. As a result, this leaves certain E-AB sensors unfit to measure the target for which they have been designed for in clinically relevant ranges further limiting their translability into real-world scenarios. Electrochemical impedance spectroscopy, in contrast, due to its ability to deconvolute interfacial resistive and capacitive contributions to the measured current can quantify the contributions associated with various electrochemical processes and measure dissociation constants with higher precision. We thus decided to utilize electrochemical impedance spectroscopy as the main electrochemical technique to interrogate E-AB sensors in our study.

Our findings demonstrate that electrochemical impedance spectroscopy enables measurements of dissociation constants of E-AB sensors close to ones measured using a gold standard method, isothermal calorimetry titration. Indeed, when using this electrochemical interrogation technique, we were able to measure dissociation constants within experimental errors or only 2−3-fold apart from those obtained using isothermal titration calorimetry, the technique used to determine aptamers' affinity in solution. In comparison, the dissociation constants obtained when interrogating using square-wave voltammetry varied greatly with respect to isothermal titration calorimetry. Therefore, our results suggest that electrochemical impedance spectroscopy is a more sensitive and accurate electrochemical technique compared to square-wave voltammetry for interrogating E-AB sensors.

Electrochemical impedance spectroscopy helped us reveal an alternative signal transduction mechanism in E-AB sensors. We show that methylene blue folds the cocaine-binding aptamer, and subsequently ligand can displace it from the aptamer's binding pocket in a competitive fashion. Our study thus suggests that the widely accepted "conformational change" signaling mechanism in E-AB sensors may need revision, and that for the cocaine-binding aptamer a "redox reporter-ligand competition" mechanism provides a more accurate description of its signal transduction. This discovery offers new insights into the fundamental mechanisms of E-AB sensors and highlights the importance of understanding their underlying physicochemical phenomenon. Specifically, by identifying the role of methylene blue in E-AB sensors' signal transduction mechanism we could improve aptamer design with improved selectivity, sensitivity, and detection limits. Furthermore, this discovery highlights the

importance of careful consideration of the choice of redox reporters in the design of E-AB sensors. For instance, one may select an alternate redox reporter to have minimal interference with ligand binding so that it could lead to improved sensor responses. Another potential research direction is to explore the role of conformational change and reorganizational energy on the redox reporter in the binding mechanism of the aptamer. By deconvoluting these two contributions, researchers can gain a deeper understanding of the fundamental chemistry and physics that govern the operation of E-AB sensors. Overall, this study contributes to the fundamental understanding of E-AB sensors and provides a basis for improving their performance, which has significant implications for biomedical and environmental monitoring applications.

The results of our studies highlight the importance of using appropriate electrochemical interrogation techniques for measuring the response and affinity of E-AB sensors. Our findings support that electrochemical impedance spectroscopy has the ability to improve the accuracy and precision of measurements in undiluted complex matrices and in turn lead to the development of more effective diagnostic tools for a wide range of applications. Given that E-AB sensors can be easily miniaturized, and that electrochemical impedance spectroscopy improves the measured sensitivity, one could foresee that E-AB sensors given that they can be readily in undiluted complex matrices could be developed into portable miniaturized device, enabling point-of-care testing in remote or resource-limited settings. The availability of a technology, capable of achieve this, as is the case of E-AB biosensors, along to high precision, real-time performance in complex, undiluted matrices may facilitate progress for biotechnology researchers and potentially revolutionize healthcare to solve the personalized medicine paradigm.

APPENDIX 1
Chapter 2 - Supporting information

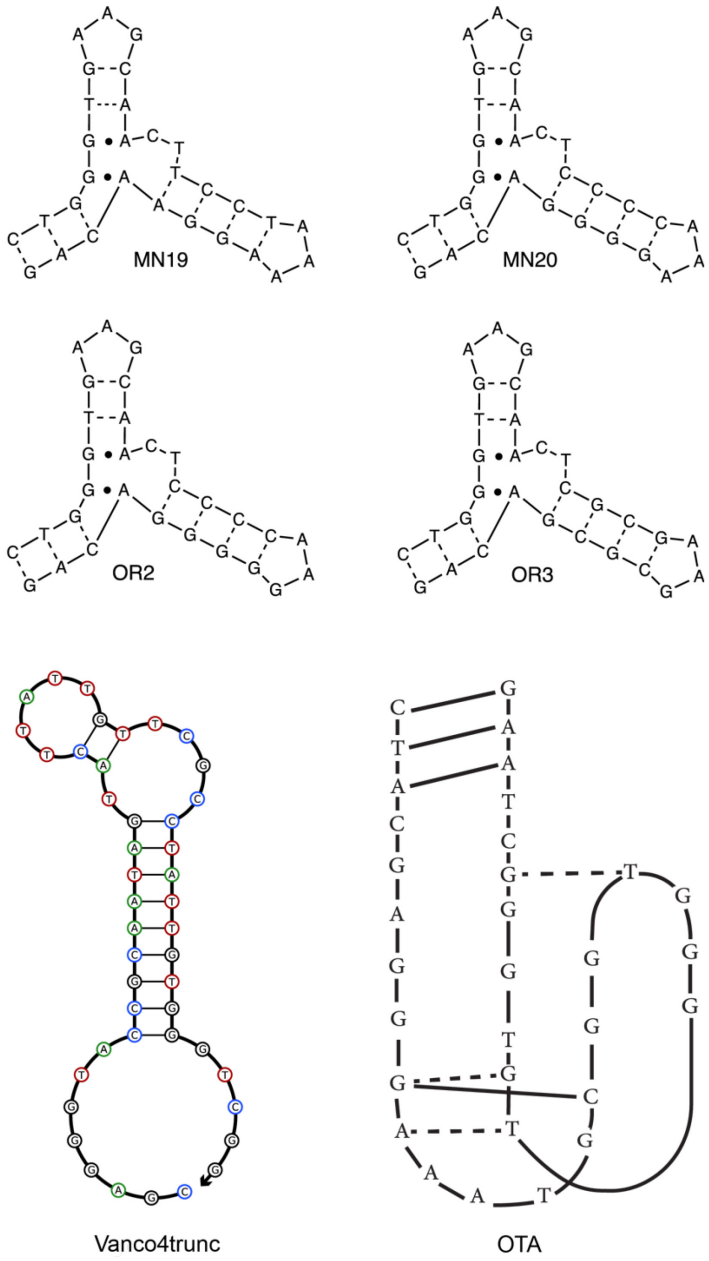

Figure S1. Quinine-binding aptamers (i.e., MN19, MN20, OR2 and OR3) possess similar binding motifs and structures thus offering close affinity with the target molecule quinine. Vancomycin-binding aptamer's (i.e., Vanco4trunc) structure is a computational prediction from NUPACK™.[1] The ochratoxin A-binding aptamer (i.e., OTA) structure was inspired from the literature.[2] We represent Watson-Crick base pairs with dashes between nucleotides, while we represent non-Watson-Crick base pairs with dots.

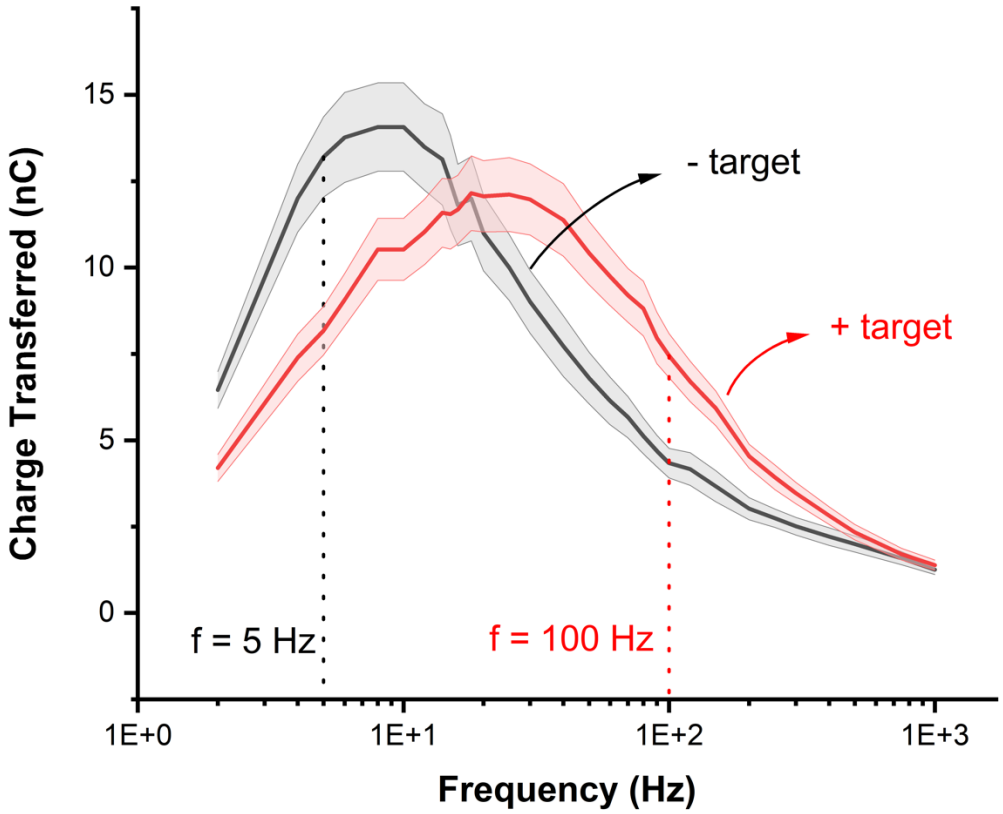

Figure S2. To determine the square-wave frequency to interrogate E-AB biosensors, we use Lovric formalism. Briefly, this involves measuring the peak current of square-wave voltammograms at increasing square-wave frequencies when biosensors are in the absence and presence of saturating amounts of the target. In dividing the peak current by the measured square-wave frequency we determine the amount of redox reporter able to transfer electrons at a given rate. We then select interrogating square-wave frequencies by determining square-wave frequencies at which charge transferred differences are maximized while minimizing the charge transferred when biosensors are in absence of the target. For the vancomycin-binding aptamer, for example, we determine that these frequencies be 5 and 100 Hz.

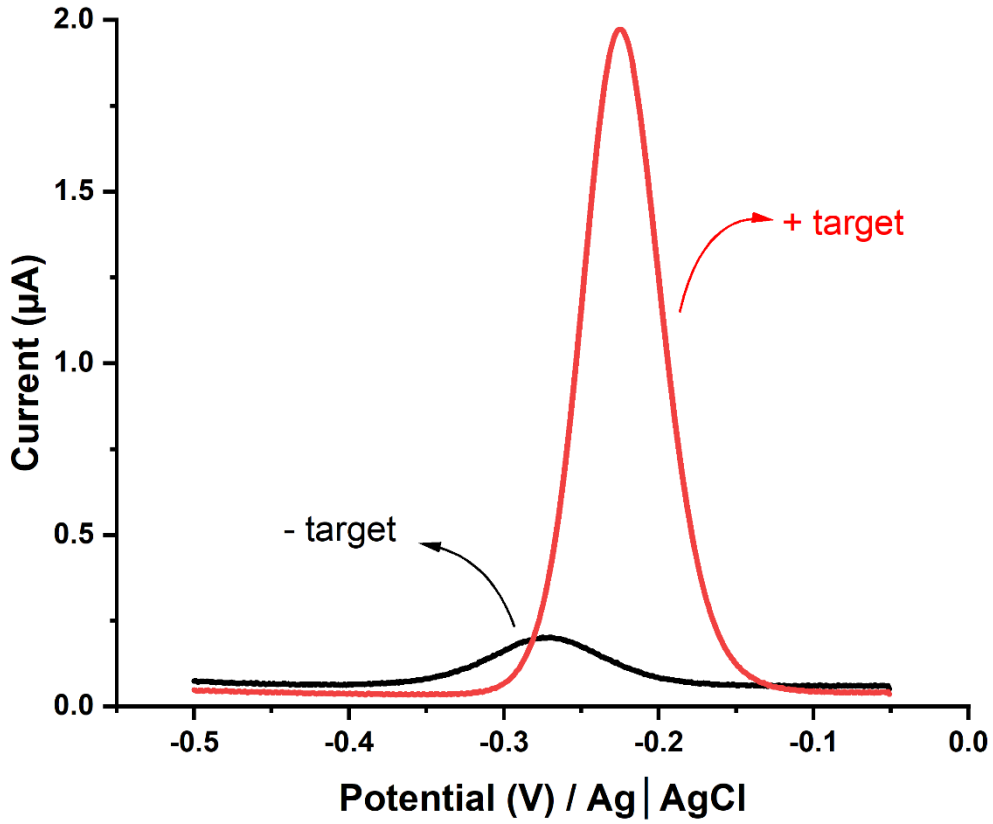

Figure S3. Representative square-wave voltammograms of the MN19 quinine-binding E-AB sensor in absence and presence of quinine (10 mM).

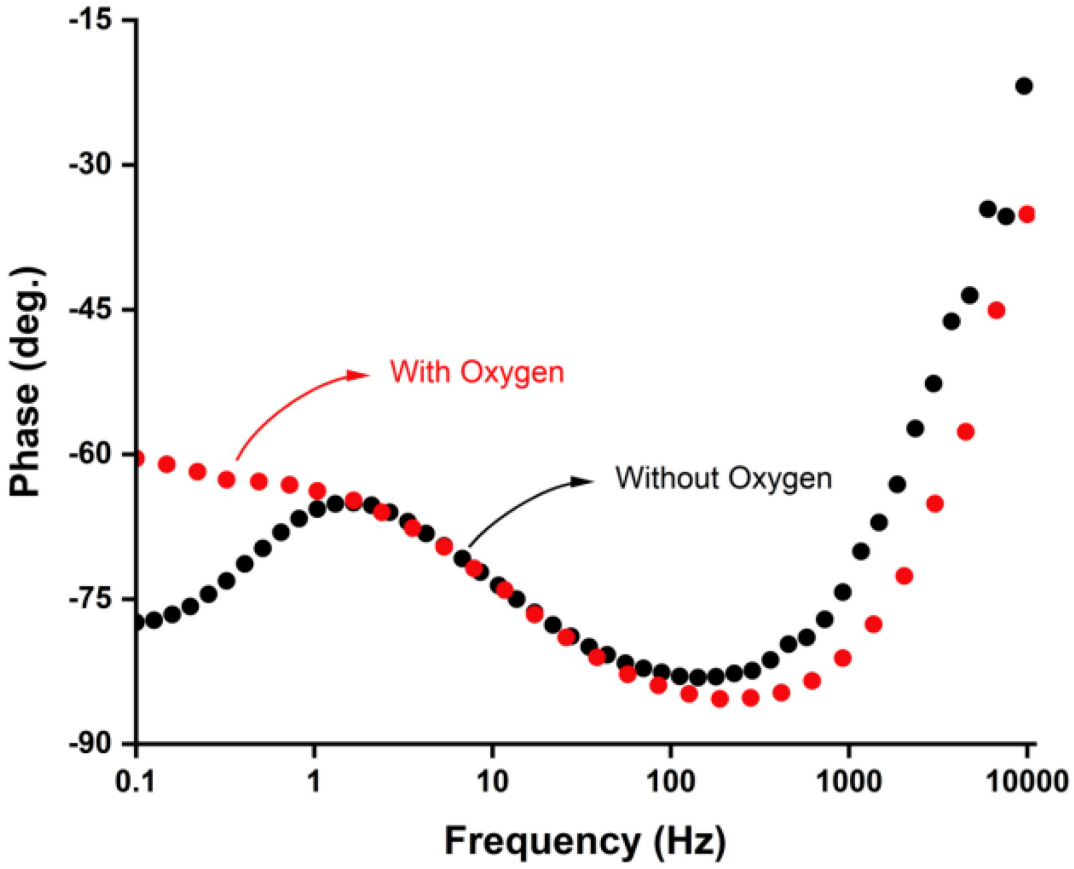

Figure S4. To fully resolve the electron transfer of the covalently attached aptamer's redox reporter (notably for the quinine-binding MN19, MN20, OR2 and OR3 aptamers), we degassed the electrochemical cell with a constant flow of Ar. In doing so, we observe a decrease in the measured phase at interrogating frequencies < 1 Hz, which we presume originates from a contribution to the measured current originating from the reduction of dissolved oxygen.

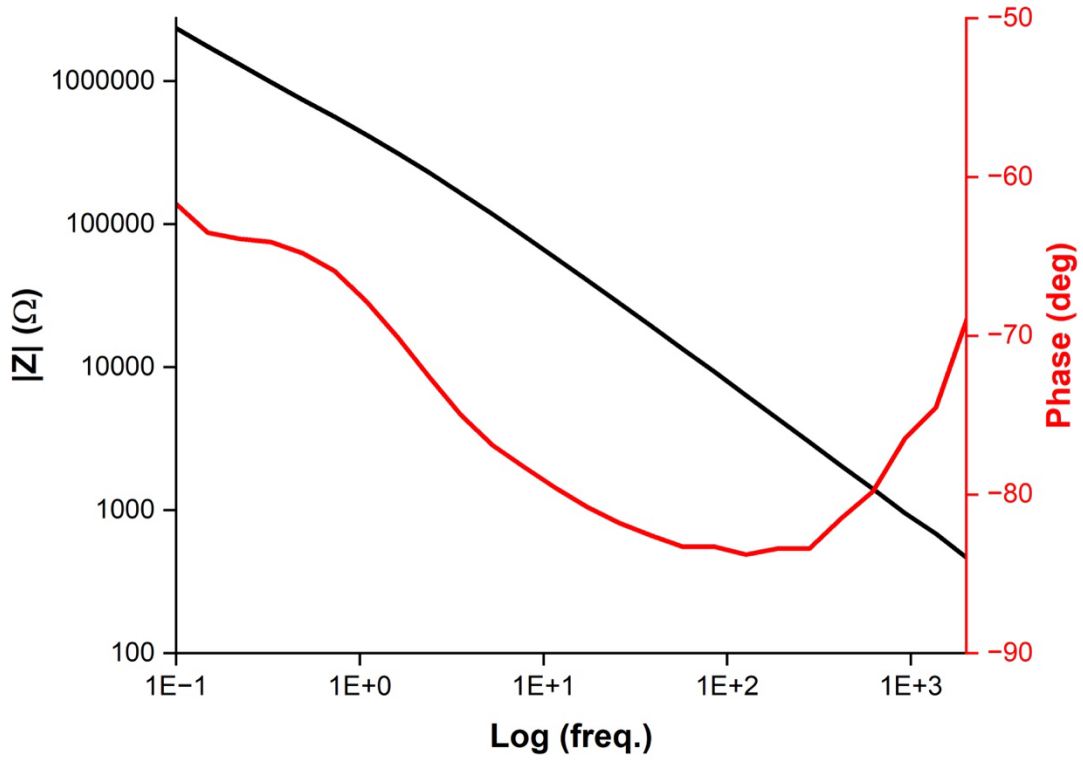

Figure S5. Representative electrochemical impedance spectroscopy results obtained for the MN19 quinine-binding aptamer in absence of quinine.

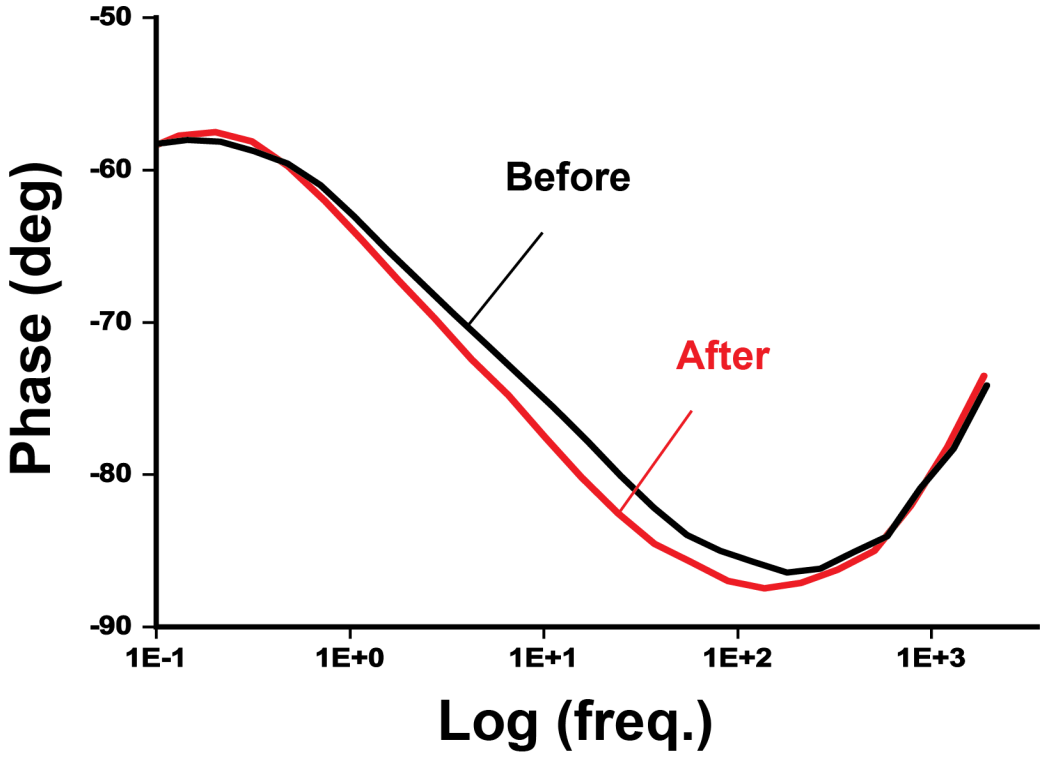

Figure S6. Phase response of the MN19 quinine-binding E-AB sensor prior to starting and after the completion of a binding curve experiment. This indicates that our sensors do not experience significant degradation as a result of interrogation or time.

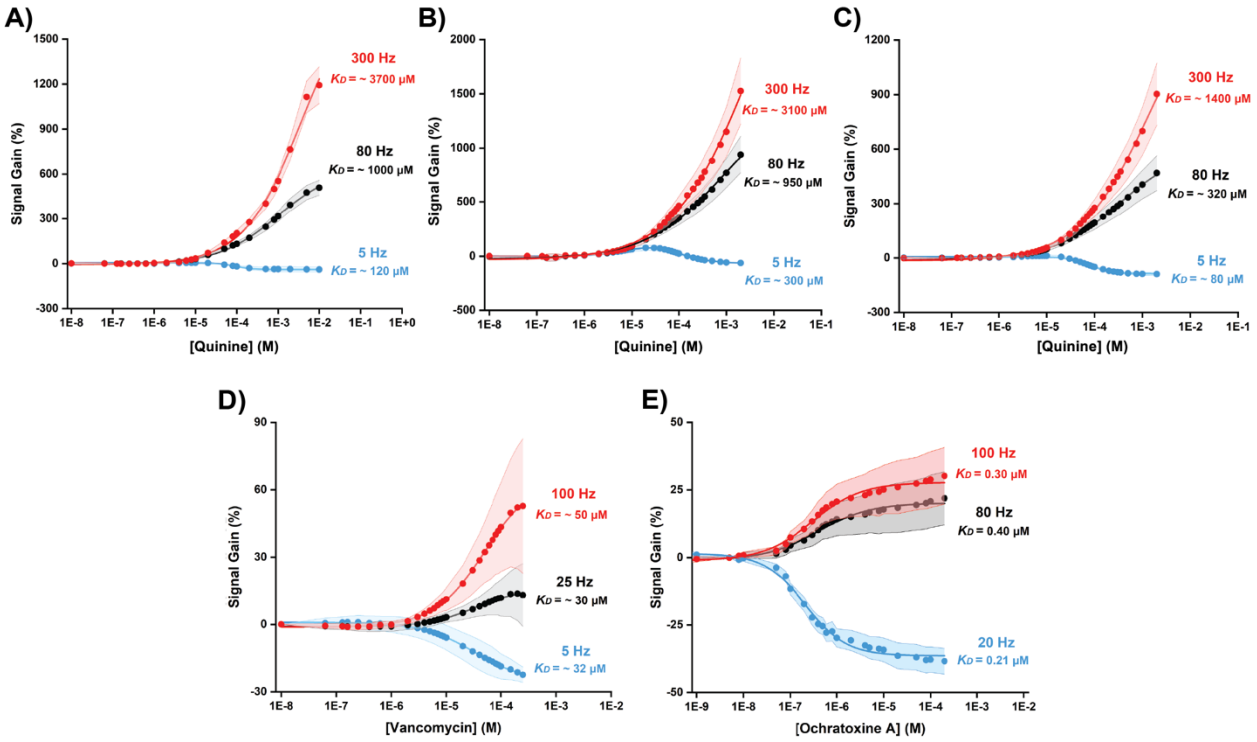

Figure S7. (**A**), (**B**), (**C**) When interrogating quinine-binding E-AB sensors aptamer variants, MN20, OR2 and OR3, respectively with increasing square-wave frequencies, we measure 1-2 orders of magnitude difference in the aptamer's K_D. We refer to these as "apparent" K_D values which are counter-intuitive given that an aptamer should possess a single K_D value for a given molecule. While we measure smaller variations for vancomycin or ochratoxin A-binding aptamers (2-3 fold), K_D values' frequency dependence in other E-AB biosensors holds. We obtained all our square-wave voltammetry results in 1X phosphate buffer solution at 20˚C except for our ochratoxin A measurement which we performed in 10 mM Tris (pH 8.0), 20 mM $CaCl_2$, 5 mM KCl, and 120 mM NaCl at 20 ˚C.

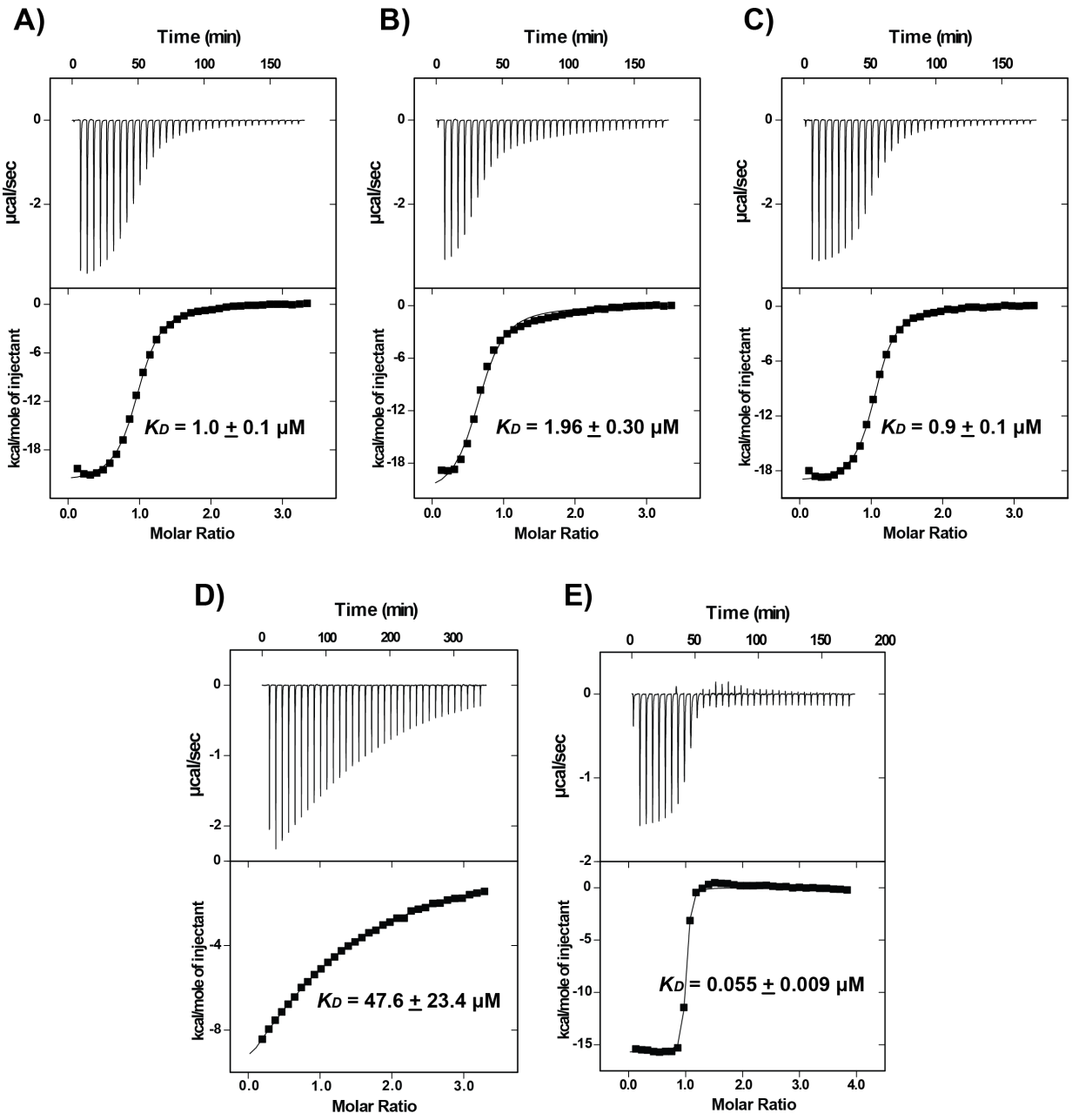

Figure S8. In interrogating the quinine-binding aptamers using isothermal calorimetry, (**A**) MN20, (**B**) OR2 and (**C**) OR3, we find K_D values several orders of magnitude (2-3) smaller than ones measured using the lowest square-wave voltammetry frequency. (**D**) While our vancomycin aptamer revealed indistinguishable differences from our square-wave voltammetry measurements, our thermograms for the (**E**) ochratoxin A-binding aptamer show a 4-8 fold tighter binding. We obtained all our square-wave voltammetry results in 1X phosphate buffer solution at 20 ˚C except for our ochratoxin A measurement which we performed in 10 mM Tris (pH 8.0), 20 mM $CaCl_2$, 5 mM KCl, and 120 mM NaCl at 20 ˚C.

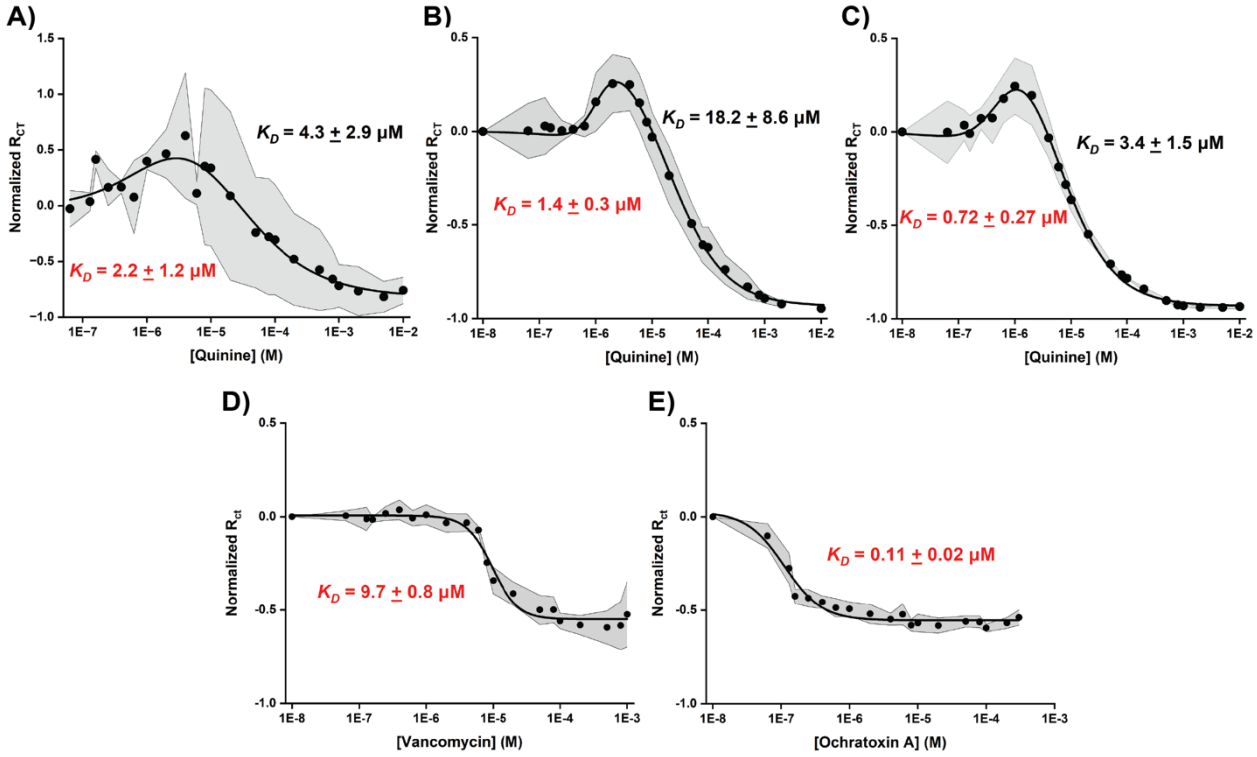

Figure S9. When interrogating E-AB biosensors using electrochemical impedance spectroscopy we measure K_D values experimentally equivalent to ones measured with isothermal calorimetry. (**A**), (**B**), (**C**) This is the case when interrogating quinine-binding E-AB sensors aptamer variants, MN20, OR2 and OR3, respectively, and looking at the initial positive increase in charge transfer resistance at lower quinine concentrations which we associate with binding to the aptamer's high-affinity binding site. We hypothesized that the further decrease in charge transfer we measure at higher quinine concentrations is rather associated with binding to a low-affinity binding site. The K_D values we measure using electrochemical impedance spectroscopy are also several folds lower than the ones measured using square-wave voltammetry. Such observation holds for other E-AB biosensors binding vancomycin or ochratoxin A-binding. We obtained all our electrochemical impedance spectroscopy results in 1X phosphate buffer solution at 20 ˚C except for our ochratoxin A measurement which we performed in 10 mM Tris (pH 8.0), 20 mM $CaCl_2$, 5 mM KCl, and 120 mM NaCl at 20 ˚C.

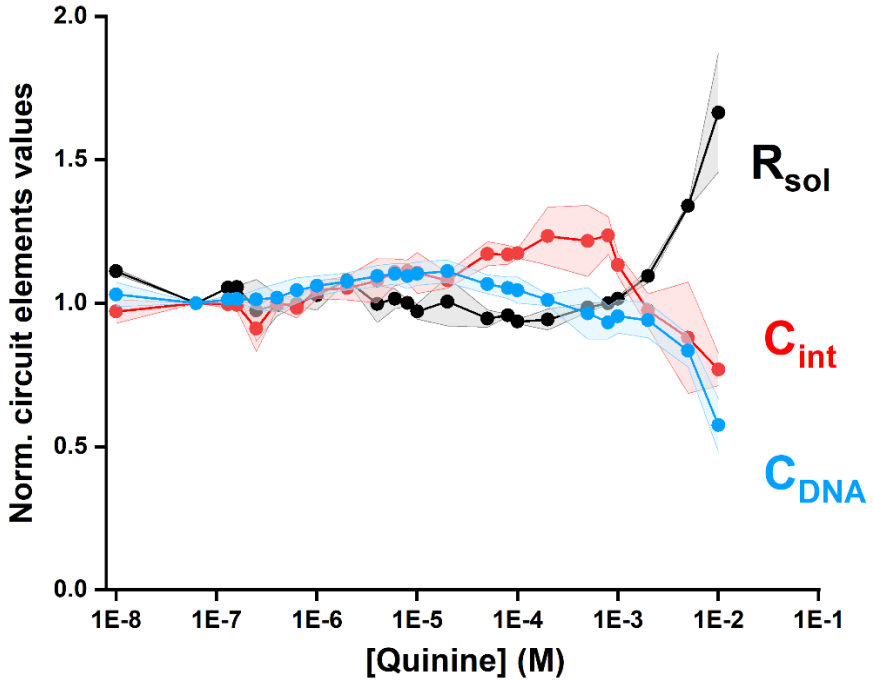

Figure S10. To illustrate that the charge transfer resistance remains the sole parameter influenced by the addition of the target, we quantified other circuit element values as a function of increasing amounts of quinine for the MN19 E-AB biosensor. In doing so we found that all circuit elements (i.e., solution resistance (R_{sol}), formation of the electrical double layer (C_{int}) and the redox reporter pseudocapacitance (C_{DNA})) remain constant where we monitor changes in charge transfer resistance (< 1 mM). It is only after reaching concentrations > 5 mM that we monitor changes in R_{sol}, C_{int} and C_{DNA} which are concentrations that fall outside clinically relevant ranges for quinine.

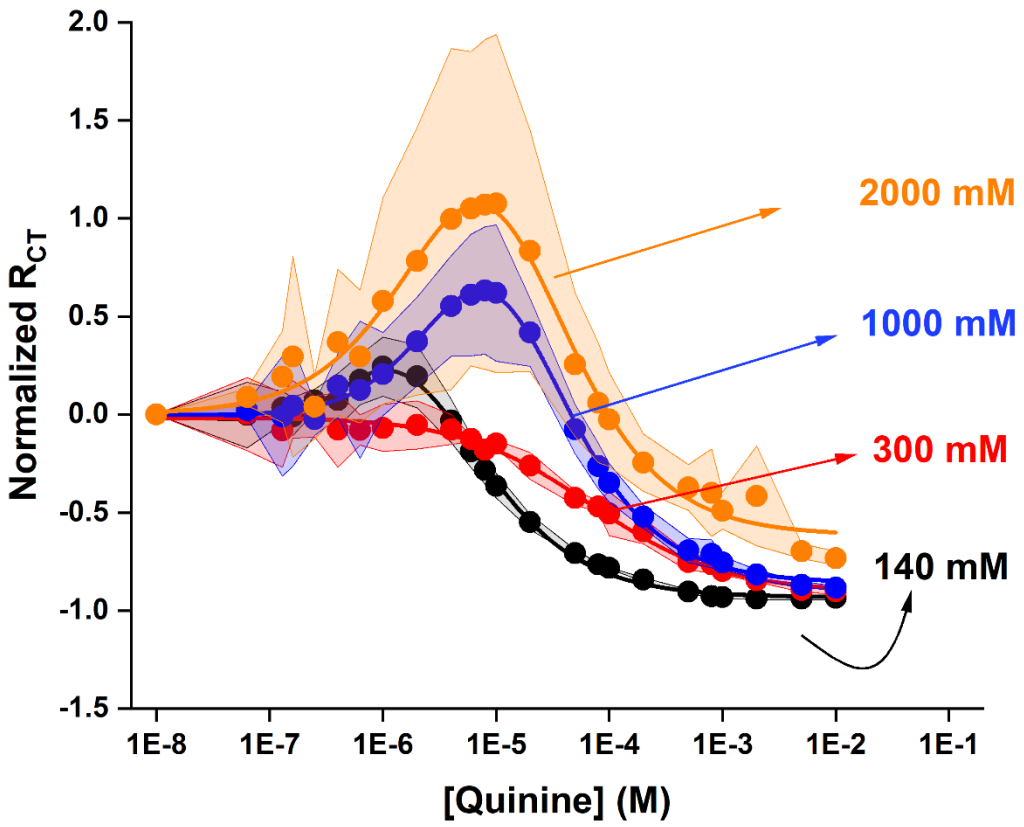

Figure S6. Given that the OR3 quinine-binding aptamer variant has been reported to possess two binding sites which are salt dependent, we decided to further explore this when the aptamer is adapted in an E-AB biosensor. For this, we exposed OR3 quinine-binding E-AB biosensors to increasing amounts of quinine and monitored the resulting changes in charge transfer resistance and this as a function of buffer NaCl concentrations (i.e., 140 mM, 300 mM, 1 M and 2 M). In doing so we found that the initial positive increase in charge transfer resistance which we associated with the high affinity binding site of the aptamer started to increase in intensity. This is in accordance with previous results where this binding site appeared to be sensitive to salt concentration.

References

(1) Zadeh, J. N.; Steenberg, C. D.; Bois, J. S.; Wolfe, B. R.; Pierce, M. B.; Khan, A. R.; Dirks, R. M.; Pierce, N. A. NUPACK: Analysis and Design of Nucleic Acid Systems. *J. Comput. Chem.* **2011**, *32* (1), 170–173. https://doi.org/10.1002/jcc.21596.

(2) Xu, G.; Zhao, J.; Yu, H.; Wang, C.; Huang, Y.; Zhao, Q.; Zhou, X.; Li, C.; Liu, M. Structural Insights into the Mechanism of High-Affinity Binding of Ochratoxin A by a DNA Aptamer. *J. Am. Chem. Soc.* **2022**, *144* (17), 7731–7740. https://doi.org/10.1021/jacs.2c00478.